รายงานวิจัยฉบับสมบูรณ์

โครงการ “การสังเคราะห์ พิสูจน์เอกลักษณ์ สมบัติเชิงความร้อน
และฟังก์ชันของโครงข่ายโลหะอินทรีย์”

โดย รศ.ดร. สุจิตรา ยังมี และคณะ

กรกฎาคม 2555

สัญญาเลขที่ BRG5280012

รายงานวิจัยฉบับสมบูรณ์

โครงการ“การสังเคราะห์ พิสูจน์เอกลักษณ์ สมบัติเชิงความร้อน และฟังก์ชันของโครงข่ายโลหะอินทรีย์”

คณะผู้วิจัย

1. รศ.ดร.สุจิตรา ยังมี	มหาวิทยาลัยขอนแก่น
2. ผศ.ดร.เชวง ภควัตชัย	มหาวิทยาลัยสงขลานครินทร์
3. รศ.ดร.ณรงค์ศักดิ์ ชัยชิต	มหาวิทยาลัยธรรมศาสตร์
4. Prof. Jan Reedijk	Leiden University, The Netherlands

สนับสนุนโดยสำนักงานกองทุนสนับสนุนการวิจัย
(ความเห็นในรายงานนี้เป็นของผู้วิจัย สกว.ไม่จำเป็นต้องเห็นด้วยเสมอไป)

สัญญาเลขที่ BRG5280012

โครงการ “การสังเคราะห์ พิสูจน์เอกลักษณ์ สมบัติเชิงความร้อน และฟังก์ชันของโครงข่ายโลหะอินทรีย์”

รายงานวิจัยฉบับสมบูรณ์

Abstract

Porous coordination polymers (PCPs), also known as metal organic frameworks (MOFs) recently have received great attention because of their diverse and fascinating architectures with promising functional properties such as molecular adsorption and separation processes, ion-exchange, catalyst, sensor technology, optoelectronics and magnetism. Particularly, the guest removal and re-adsorption in flexible and dynamic molecular solids are of interest for many potential applications especially in the areas of gas storage and sensors. This research discusses functional properties toward catalysis, anion-exchange and dynamic behaviors in Zn(II)-4,4′-bipyridine-carboxylato compounds exhibiting 1D, 2D and 3D structural frameworks. More recently, we have synthesized the flexible and dynamic non-coordination supramolecular Co(II)/Fe(II)-2-aminopyrazine-sulfate frameworks supported by weak molecular interactions such as hydrogen bonds and π-π stacking. These compounds exhibit water-induced reversible crystal-to-amorphous transformations with chromotropism which is uncommon for the non-coordination frameworks to maintain their structures. Contradictory, a related coordination polymer is obtained for Cd(II) which also shows water-induced reversible structural phase transition. Furthermore, the azido Co(II) complex system yielded four coordination polymers with interesting molecular magnetic phenomena.

สัญญาเลขที่ BRG5280012

โครงการ “การสังเคราะห์ พิสูจน์เอกลักษณ์ สมบัติเชิงความร้อน และฟังก์ชันของโครงข่ายโลหะอินทรีย์”

รายงานวิจัยฉบับสมบูรณ์

บทคัดย่อ

สารประกอบโคออร์ดิเนชันพอลิเมอร์ที่มีรูพรุน (PCP) หรือโครงข่ายโลหะอินทรีย์ (MOF) ได้รับความสนใจเป็นอย่างยิ่งในปัจจุบัน เนื่องจากมีโครงสร้างที่หลากหลายและน่าทึ่ง ร่วมกับแสดงสมบัติหน้าที่ที่ดี ได้แก่ การดูดซับและกระบวนการแยกเชิงโมเลกุล การแลกเปลี่ยนไอออน การเร่งปฏิกิริยา เทคโนโลยีเซนเซอร์ ออฟโตอิเล็กทรอนิกส์ และสมบัติทางแม่เหล็ก โดยเฉพาะอย่างยิ่งในกระบวนการกำจัดและดูดซับกลับคืนของเกสต์ในโครงข่ายโลหะอินทรีย์ที่มีความยืดหยุ่นและมีสมบัติเชิงพลวัตินั้น กำลังได้รับความสนใจอย่างมาก ซึ่งเหมาะแก่การประยุกต์ในการกักเก็บแก๊สและเซนเซอร์ ในงานวิจัยฉบับนี้อภิปรายสมบัติหน้าที่ของโครงข่ายโลหะอินทรีย์ ได้แก่ การเร่งปฏิกิริยา การแลกเปลี่ยนไอออนลบ และพฤติกรรมเชิงพลวัติของสารเชิงซ้อน Zn(II)-4,4′-bipyridine-carboxylato ซึ่งแสดงโครงข่ายตั้งแต่หนึ่งมิติ สองมิติ และสามมิติ และสามารถสังเคราะห์โครงข่ายซุปปราโมเลกุลที่ไม่มีการโคออร์ดิเนชันในระบบ Co(II)/Fe(II)-2-aminopyrazine-sulfate ซึ่งประกอบขึ้นมาจากอันตรกิริยาแบบอ่อน ได้แก่ พันธะไฮโดรเจนและอันตรกิริยา π-π และสารกลุ่มนี้แสดงการเปลี่ยนแปลงเฟสโครงสร้างแบบผันกลับได้จากโครงร่างผลึกเป็นอสัณฐานเมื่อถูกเหนี่ยวนำโดยโมเลกุลน้ำร่วมกับการเปลี่ยนแปลงสี ซึ่งพฤติกรรมนี้พบได้ยากในโครงข่ายที่ไม่มีการโคออร์ดิเนชัน ขณะที่เปลี่ยนชนิดโลหะเป็น Cd(II) ทำให้เกิดโคออร์ดิเนชันพอลิเมอร์สองมิติและแสดงการเปลี่ยนเฟสโครงสร้างผลึกแบบผันกลับได้เมื่อถูกเหนี่ยวนำโดยโมเลกุลน้ำ นอกจากนั้น ในระบบสารเชิงซ้อน Co(II) azido ทำให้ได้โคออร์ดิเนชันพอลิเมอร์ 4 ชนิดที่มีปรากฏการณ์ทางแม่เหล็กเชิงโมเลกุลที่น่าสนใจ

สัญญาเลขที่ BRG5280012

โครงการ "การสังเคราะห์ พิสูจน์เอกลักษณ์ สมบัติเชิงความร้อน และฟังก์ชันของโครงข่ายโลหะอินทรีย์"

รายงานสรุปความก้าวหน้าของโครงการประจำปี

Executive Summary

Metal-organic frameworks (MOFs) have attracted intensive attention for the past decade owing to their diverse topologies and enormous potential applications for molecular adsorption and separation, catalysis, ion exchange, optoelectronics and sensor technology. MOFs have advantages in that they provide not only light materials with high porosity, but also desirable regular networks. One of the more prominent applications pursued for these materials has been their possible use in high-density hydrogen storage. The field of metal-organic frameworks has been extensively investigated with a focus on functional material research and crystal engineering. In material research, the coordination networks with interesting properties are constructed for fine-tuning the properties and creating new functional materials. On the other hand, crystal engineering is attracting interest from both the synthetic routes and the art of structural design.

The present research deals with the systematic synthesis, structural characterization and magnetic properties of novel metal-organic framework materials based on the coordination chemistry of carboxylates, sulfate, azide and *N*,*N*′-ditopic organic spacers. The central aim is to generate new compounds of this interesting family which is focused on the core features of crystal engineering and their functions toward anion-exchange, catalysis, dynamic structural transformation with chromotropism and molecular magnetism. An emphasis is therefore given to the analysis of the crystal structures and functional properties of many product systems. This research can be separated into two parts:

Part I addresses the syntheses, structural characterization, anion exchange and catalytic properties of a series of 4,4'-bpy-carboxylato metal-organic frameworks. The combination of framework-builder coordination moiety (zinc(II)–4,4'-bpy and copper(II)–4,4'-bpy) with respectively formato, acetato and propionato ligands provides two series of novel metal organic frameworks. Eleven zinc(II)-4,4'-bpy-carboxylato coordination polymers, i.e. the 3D frameworks $\{[Zn_3(4,4'\text{-bpy})_{3.5}(\mu\text{-OOCH})_4(H_2O)_2](X)_2\}_n$ when X = $ClO_4^-\bullet H_2O$ (**1**), PF_6^- (**2**), $BF_4^-\bullet H_2O$ (**3**), the 2D layer $\{[Zn(4,4'\text{-bpy})(\mu\text{-OOCH})(H_2O)_2](CF_3SO_3)(H_2O)\}_n$ (**4**), the 2D zig zag layer $\{[Zn_4(4,4'\text{-bpy})_4(\mu\text{-OOCH})_5(H_2O)_5](NO_3)_3(4,4'\text{-bpy})_2(H_2O)_3\}_n$ (**5**), the 1D three-leg ladder $\{[Zn_3(4,4'\text{-bpy})_3(\mu\text{-OOCCH}_3)_4(H_2O)_2](PF_6)_2(H_2O)_2\}_n$ (**6**), the 2D layer $\{[Zn_3(4,4'\text{-bpy})_4(\mu\text{-OOCCH}_2CH_3)_4](ClO_4)_2(4,4'\text{-bpy})_2(H_2O)_4\}_n$ (**7**), the double-stranded zig zag chain $\{[Zn_3(4,4'\text{-bpy})_4(\mu\text{-OOCC}_2H_5)_4(H_2O)_2](PF_6)_2(H_2O)_2\}_n$ (**8**), the 2D layer $\{[Zn_2(4,4'\text{-bpy})_2(\mu\text{-OOCC}_2H_5)_2(OH)(H_2O)](BF_4)(H_2O)_2\}_n$ (**9**), the double ladders chain $\{[Zn_2(4,4'\text{-bpy})_2(\mu\text{-OOCC}_2H_5)_2(H_2O)_2]$

$(CF_3SO_3)_2\}_n$ (**10**) the double-stranded zig zag chain $\{[Zn_3(4,4'\text{-bpy})_4(\mu\text{-}OOCC_2H_5)_4(H_2O)_2](NO_3)_2(H_2O)_3\}_n$ (**11**) and nine cooper(II)-4,4'-bpy-carboxylato coordination polymers, the triple-stranded layers $\{[Cu_3(4,4'\text{-bpy})_2(\mu\text{-}OOCH)_4(H_2O)_2](X)_2(H_2O)_6\}_n$ when X = ClO_4^- (**12**), PF_6^- (**13**), BF_4^- (**14**), $CF_3SO_3^-$ (**15**), the zig zag 2D layer $\{[Cu(4,4'\text{-bpy})(\mu\text{-}OOCH)\ (NO_3)]\}_n$ (**16**), the quadruple-stranded layers $\{[Cu_2(4,4'\text{-bpy})_2(\mu\text{-}OOCCH_3)_3](X)\ (H_2O)\}_n$ when X = ClO_4^- (**17**), PF_6^- (**18**), BF_4^- (**19**), $CF_3SO_3^-$ (**20**) are obtained and have been crystallographically characterized. This study shows that the change from a formato ligand to an acetato and a propionato ligand gives rise to the formation of drastically distinct metal organic frameworks, as the result of the different steric bulk of the carboxylato unit involved.

The thermal and optical properties, ion-exchange with structure retention and catalytic reactivity, as well as dynamic structural transformation have been investigated. Compounds **6-9** and **11** show a crystalline-to-crystalline structural transformation up on removal/reintroduction of water guest molecules. The anion exchange among zinc(II) and copper(II) compounds is found to be highly selective while anion-sensing properties in an aqueous solution is found only in **1**. Interestingly, these zinc(II) compounds are effective heterogeneous catalysts for the high-yielding cyanosilylation of acetaldehyde in dichloromethane with size-selective. Contradictory, all copper(II) compounds are less active and less selective catalysts for cyanosilylation of aldehydes.

Part II addresses the syntheses, structural characterization and their functional properties toward dynamic structural transformation with chromotropism and magnetism. Novel fifteen metal(II) polymeric complexes were successfully synthesized and structurally characterized, as following: firstly, five Cu^{II} coordination networks containing 2-aminopyrazine and various carboxylate anions, 2D wavy sheet $[Cu(ampyz)(O_2CH)_2]_n$ (**III-1**), 1D chains $[Cu_2(ampyz)(O_2C_2H_3)_4]_n$ (**III-2**) and $[Cu_2(ampyz)(O_2C_3H_5)_4]_n$ (**III-3**), 2D layer $[Cu_2(ampyz)(O_4C_4H_4)_2]_n(H_2O)_n$ (**III-4**) and 2D stairlike layer $[Cu(ampyz)(O_4C_3H_2)]_n(H_2O)_{2n}$ (**III-5**), secondly, three isostructural flexible metal-supramolecular architectures $[M(H_2O)_4(ampyz)_2][M(H_2O)_6](SO_4)_2(H_2O)_2$ (M are Co^{II} (**IV-1**), Fe^{II} (**IV-2**) and Co^{II}/Fe^{II} (**IV-3**)) and a flexible 2D Cd^{II} coordination network $[Cd(ampyz)(H_2O)_2(SO_4)]_n(H_2O)_n$ (**IV-4**), thirdly, two flexible metal-organic frameworks $[Co(pydc)(H_2O)_2]_n$ (**IV-5**) and $[Co(pydc)(H_2O)_4]_n(H_2O)_n$ (**IV-6**), (pydc = 3,5-pyridinedicarboxylate) and lastly, four azido Co^{II} magnetic hybrid frameworks, *i.e.* 1D chain of $[Co_3(N_3)_6(OH_2)_2(2,2'\text{-bpe})_2]_n(2,2'\text{-bpe})_n$ (**V-1**), 2D layer $[Co(N_3)_2(2,2'\text{-bpe})]_n$ (**V-2**) and 2D sheet $[Co(N_3)_2(ampyz)]_n$ (**V-3**) and 3D framework $[Co(N_3)_2(ampyz)]_n$ (**V-4**) of $[Co(N_3)_2(ampyz)]_n$.

Compound **III-1** reveals a 2D wavy sheet structure. Both **III-2** and **III-3** consist of polymeric chains constructed from paddle-wheel $(CuNO_4)_2$ chromophores. The structure of **III-4** consists of a 2D layer built from double-stranded chain of paddle-wheel units connecting ampyz spacers. Compound **III-5** exhibits a 2D stairlike layer built from malonate anions and μ_2–ampyz. Beside the various coordinative modes of carboxylates, the ampyz spacer has an influence on the molecular structures *via* either the ditopic bridging mode, or by other weaker interactions, such as hydrogen bonding and π–π stacking, which mainly

contribute to the stabilization of the overall supramolecular structures. All compounds emphasize the effect of the ampyz spacer in building the copper(II) networks and are compared with the same carboxylate coligands in the μ_2–pyz Cu^{II} systems. Magnetic properties of **III-1** and **III-5** reveal weak ferromagnetic and weak antiferromagnetic spin exchange interactions between adjacent Cu^{II} ions *via* μ_2-*syn-anti* carboxylates and μ_2-ampyz with the spin exchange parameters of J_{inter}/k = +6.9 K and J_{intra}/k = –2.3 K, for **III-1** and J_{inter}/k = +7.4 K and J_{intra}/k = –2.2 K for **III-5**, respectively. Magnetic behaviors of **III-2-4** exhibit very strong antiferromagnetic interactions *via* four μ_2-*syn-syn* carboxylates bridging between Cu^{II} ions which is well-known for the classical paddle-wheel Cu^{II} complexes.

Compounds **IV-1-3** are isomorphous series. Monomeric complex units $[M(H_2O)_4(ampyz)_2]^{2+}$ are assembled by intermolecular hydrogen bonding and π-π stacking *via* ampyz moieties to build 2D sheets. These layers are linked by intermolecular hydrogen bonding *via* ampyz ligand, $[M(H_2O)_6]^{2+}$ unit, sulfate anion and lattice and coordinated water molecules to stabilize 3D supramolecular structure. Whereas **IV-4** shows a 2D coordination network where the sulfato connector and the bridging ampyz link Cd^{II} ions. Lattice water molecules are filled in between the layers *via* the hydrogen bonds stabilizing 3D supramolecular network of **IV-4**. Interestingly, compounds **IV-1-3** exhibit water-induced reversible crystal-to-amorphous transformations with chromotropism and compound **IV-4** also shows water-induced reversible structural phase transformation confirmed by spectroscopic techniques, elemental analyses, TGA, and XRPD. These results demonstrate the significant role between coordination bridges and weaker intermolecular interactions for the structural conversion even though **IV-1-3** are lack of coordination bridges for maintenance of their structures, however, the weak intermolecular interactions, especially hydrogen bonding, play a key role to the recovery of the crystalline phase. Moreover, the selective methanol accommodation with chromotropism in dehydrated **IV-1A** is observed which could be attributed to the proper size of methanol and weak host-guest interactions causing the changes of the *d*-orbital energy in distorted octahedral geometry. However the **IV-1A·MeOH** is unstable in air. The original crystalline phase **IV-1″** is easily recovered after the evaporation of methanol at room temperature which is indication of high selective recognition of **IV-1A** to water molecules. This work is beneficial to expand the field of the crystal engineering by controlling the weak interaction of coordination moieties.

By utilizing a flexible coligand 1,2-bis(2-pyridyl)ethylene (2,2′-bpe), two new azido-bridged cobalt(II) coordination networks **V-1** and **V-2** have been obtained. Compound **V-1** shows uncommon 1D chain comprised of double EO azido bridged five- and six-coordinated Co^{II} geometries in a unique $(-5-5-6-)_n$ sequence of the coordination number. The 2,2′-bpe acts as terminal co-ligand and uncoordination molecule in the crystal lattice. Moreover the adjacent 1D chain is assembled by C–H···π interactions and the intermolecular hydrogen bonding between uncoordination 2,2′-bpe and coordination water molecules building 2D layer. Whereas compound **V-2** is 2D coordination network containing the alternating double EO and double EE bridging modes of azides and ditopic 2,2′-bpe bridges. The magnetic

investigation of **V-1** reveals dominant intrachain ferromagnetic interactions with double EO azide-bridge and weak interchain antiferromagnetic interactions with overall metamagnetic behavior having magnetic ordering at 6 K. The magnetic behavior of **V-2** shows spin-canted antiferromagnetism below T_N of 12 K. In case of the versatile ampyz spacer, two high dimensional cobalt(II) azido inorganic-organic hybrid frameworks, which contain similarly alternating double EO and double EE azido-bridged Co^{II} chain were obtained from the different preparative methods. The high symmetric square-grid structure of **V-3** from layer diffusion method which consists of *trans*-ampyz bridging between octahedral Co^{II} centers in axial positions, presents the coexistence of a big spin canting angle and metamagnetism below 10 K. The canting angle is estimated to be 7.7° and the critical field for metamagnetic phase transition is ≈ 600 Oe at 2 K. The interlayer hydrogen bonding between amino group of ampyz spacer and symmetric double EE azido bridges plays an important role on the field-induce metamagnetic phase transition. The spin canting of **V-3** could be attributed to the significant antisymmetric exchange arising from the structure phase transition at low temperature and the great role of magnetic anisotropy of Co^{II} ion. Whereas 3D framework containing *cis*-ampyz bridging among Co^{II} centers of **V-4** was synthesized from hydrothermal technique. It was crystallized in lower space group and exhibited only small spin-canted antiferromagnetism below 16 K. It is suggests that the large magnetic anisotropy in **V-4** might contribute a spin canting together with small antisymmetric coupling between Co^{II} ions, arising from a distortion in the crystal net at low temperature, which is frequently found in the related complexes containing the same bridging mode of azide. These results will provide the merit for future investigations and demonstrate the importance of the crystal engineering of inorganic-organic hybrid framework in the field of molecular-based magnetic materials.

TABLE OF CONTENTS

LIST OF ABBREVIATIONS

ampyz	2-aminopyrazine
bpy	4,4′-bipyridine
dpe	1,2-di(4-pyridyl)ethylene
MeOH	Methanol
EtOH	Ethanol
DMF	Dimethylformamide
DMSO	Dimethylsulfoxide
EPR	Electron paramagnetic resonance
pyz	pyrazine
T	Tesla
G	Gauss
FC	field-cooled
SBU	secondary building unit
ZFC	zero-field cooled
kK	KiloKeyser (1000 cm^{-1})
χ_m	Molar magnetic susceptibility
J	exchange energy
h	Plank's constant
β, μ_B	Bohr magneton
N	Avogadro's number
k	Boltzmann constant
H	the magnetic field strength
g	Lande´ splitting factor
θ	Weiss constant
α	canting angle

Part II

Metal-Organic Frameworks and Their Functions
Toward Dynamic Structural Transformation
with Chromotropism and Magnetism

2

Metal-Organic Frameworks and Their Functions Toward Dynamic Structural Transformation with Chromotropism and Magnetism

1. Introduction

A great interest of transition metal complex-assemblies in inorganic-organic hybrid framework materials has recently been devoted to the development of rational synthetic routes to novel one-, two- and three-dimensional crystal frameworks, due to their potential applications in many areas. The molecule-based crystal is a characteristic of the assemblage which is dissimilar to inorganic assemblage. This is ascribed to a variety of coordination geometries of building blocks and the coordination numbers. Furthermore, the functionality of organic and inorganic ligands as a connector is essential for the formation of coordination network structures and the intermolecular interactions involving hydrogen bonding and π-π stacking which all are necessary to rational design of crystal frameworks together with the fine tuning their functional properties.

The work described in this topic was started with the intention of developing in a field of crystal engineering of inorganic-organic hybrid framework materials as well as expanding and learning the insights of fundamental molecule-based magnetic materials. The three main purposes of this work are described in the terms of "*structural diversity*", "*structural dynamic*" and "*magnetic ordering*". In the diversity of structural frameworks the influences of flexibility, functional group and versatile coordination modes of bridging ligands on the structural architectures are demonstrated in all compounds. In addition, the effects of metal ions and reaction temperature are also observed. In the feature of structural dynamic behaviors, by employing the versatile aminopyrazine spacer with sulfate anion, the reversible structural phase transformations with chromotropism in the characteristic 3rd generation flexible metal-supramolecular frameworks and coordination polymer are demonstrated, in which all compounds are supported by weak intermolecular interactions, such as hydrogen bonds, π–π stacking, and electrostatic forces. It is interesting that these phenomena are not common in non-coordination supramolecular systems. Furthermore, this behavior with the color change is also found in the 1D and 2D coordination polymers of the Co(II)-3,5-pyridinedicarboxylate system. Lastly, the crystal engineering of molecular magnetism which aims to control the spins in molecules and molecular assemblies has been developed. The final part mainly deals with the investigation of long-range magnetic orders in extended inorganic hybrids of cobalt(II) azido complexes. This part various interesting molecule-based magnetic phenomena (ferromagnetism, canted antiferromagnetism and metamagnetism) in highly anisotropic Co^{II} complexes along with their diversity of structural dimensions and coordination geometries are studied.

First part, the structural characterization and magnetic measurement in series of Cu^{II} coordination polymers containing 2-aminopyrazine (ampyz) and different carboxylato ligands are presented. It has been known that crystal engineering is attracting much interest from both the synthetic routes and the state of art in structural design. This chapter focuses on the structural diversity of Cu^{II} coordination polymers caused by the effect of functional group (amine) in ampyz spacer and versatile coordination modes of carboxylate bridges. No compounds in this system have been reported as yet. Thus five new Cu^{II} coordination networks containing both μ_2-ampyz and the bridging carboxylate anion, *i.e.* 2D layer $[Cu(ampyz)(O_2CH)_2]_n$ (**III-1**), 1D chains $[Cu_2(ampyz)(O_2C_2H_3)_4]_n$ (**III-2**) and $[Cu_2(ampyz)(O_2C_3H_5)_4]_n$ (**III-3**), 2D layer $[Cu_2(ampyz)(O_4C_4H_4)_2]_n(H_2O)_n$ (**III-4**), 2D layer $[Cu(ampyz)(O_4C_3H_2)]_n(H_2O)_{2n}$ (**III-5**) were reported (when HCO_2^- = formate, $CH_3CO_2^-$ = acetate, $C_2H_5CO_2^-$ = propionate, $CH_2C_2O_4^{2-}$ = malonate and $C_2H_4C_2O_4^{2-}$ = succinate anions). The structures of all compounds are compared with compounds containing the same carboxylate ligands in the μ_2-pyrazine Cu^{II} systems. The EPR and magnetic measurements at low temperature of all the compounds have also been investigated and briefly discussed.

The second deals with the structural dynamics with chromotropism in metal supramolecular frameworks and coordination polymer. Since the role of many interaction sites of ampyz spacer was observed from previous chapter and the structural diversity in metal sulfate chemistry was known, therefore, series of metal(II) supramolecular structures and Cd^{II} coordination polymer containing ampyz and sulfate anions, which exhibit significant chromotropism associated with reversible water-induced structural phase transformations, have been studied. The effect of 3*d*- and 4*d*- transition metal centers on the molecular assembles were observed, leading to the differences in structural dynamics behaviors. Many techniques (thermal analysis, X-ray powder diffraction, elemental analysis, IR and UV-vis spectroscopic techniques) have been employed to study the reversible structural phase transformations. In this series three new supramolecular metal-coordination architectures $[M(H_2O)_4(ampyz)_2][M(H_2O)_6](SO_4)_2\,(H_2O)_2$ (M = Co (**IV-1**), Fe (**IV-2**), and mixed Co/Fe (**IV-3**) and a Cd^{II} coordination polymer $[Cd(ampyz)(H_2O)_2(SO_4)]_n(H_2O)_n$ (**IV-4**) are demonstrated. In addition this behavior with the color change is also found in the 1D and 2D coordination polymers of the Co(II)-3,5-pyridinedicarboxylate system. The 3,5-pyridinedicarboxylate (pydc) is chosen as an organic spacer since this molecule has proven to be able to establish a bridge between metal centers. Therefore $[Co(pydc)(H_2O)_2]_n$ (**IV-5**) and $[Co(pydc)(H_2O)_4]_n(H_2O)_n$ (**IV-6**), (pydc = 3,5-pyridinedicarboxylate) are reported, which exhibit significant chromotropism associated with water-induced crystal-to-amorphous phase transformations.

Last part demonstrates the importance of the crystal engineering of inorganic-organic hybrid framework in the field of molecular-based magnetic materials. The structural diversity and the comprehensive study of long-range magnetic orders of four new azido cobalt(II) extended inorganic hybrids are described, which show various structural dimensionalities from 1D chain, 2D layer to 3D framework structures. In this chapter, two compound systems are divided according to the organic coligands. The former shows two

azido Co^{II} complexes with 1,2-bis(2-pyridyl)ethylene (2,2′-bpe), *i.e.* 1D chain $[Co_3(N_3)_6(OH_2)_2(2,2'\text{-bpe})_2]_n(2,2'\text{-bpe})_n$ (**V-1**) and 2D layer $[Co(N_3)_2(2,2'\text{-bpe})]_n$ (**V-2**). This work is the first report of azido complexes containing 2,2′-bpe flexible coligand. The last part presents two azido Co^{II} complexes with ampyz spacer, *i.e.* 2D sheet $[Co(N_3)_2(ampyz)]_n$ (**V-3**) and 3D framework $[Co(N_3)_2(ampyz)]_n$ (**V-4**). It is interesting that they were obtained from the different preparative methods and similarly contain alternating double EO and double EE azido-bridged Co^{II} chain. The magnetic properties of **V-1-4** are discussed and compared with the related azido complex systems.

2. Experimental

2.1 Series of copper(II) coordination polymers containing ampyz and different carboxylato ligands

$[Cu(ampyz)(O_2CH)_2]_n$ (III-1). An ethanolic solution (5 mL) of ampyz (0.5 mmol, 48 mg) was carefully layered on an aqueous solution (5 mL) of $Cu(HCO_2)_2$ (0.5 mmol, 76 mg) with 0.1 mL (2.6 mmol) of formic acid in 20 mL of glass vial. This vial was sealed and allowed to stand undisturbed at room temperature. After four days, blue-green rod-shaped crystals of **III-1** were obtained. Yield 84 mg (68%) based on copper salt. Anal. Calcd for $CuC_6H_7N_3O_4$: C, 28.98; H, 2.82; N, 16.90 %.Found: C, 28.81; H, 2.91; N, 16.89 %. IR (KBr, cm^{-1}): 3364w, 3127w, 1639m, 1587s, 1329m, 1236w, 1076w, 1030w, 811w, 572w. UV–vis (diffuse reflectance, cm^{-1}): 15670.

$[Cu_2(ampyz)(O_2C_2H_3)_4]_n$ (III-2) was synthesized similarly to compound **III-1** using $Cu(CH_3CO_2)_2$ (0.5 mmol, 91 mg) instead of $Cu(HCO_2)_2$ with 0.1 mL (1.7 mmol) of acetic acid. After three days, green rod-shaped crystals of **III-2** were obtained. Yield 190 mg (83%) based on copper salt. Anal. Calcd for $Cu_2C_{12}H_{17}N_3O_8$: C, 31.45; H, 3.71; N, 9.17 %. Found: C, 31.33; H, 3.77; N, 9.18 %. IR (KBr, cm^{-1}): 3387w, 3342w, 3224w, 1655m, 1608s, 1435m, 1349w, 1219w, 1017w, 685w, 628w. UV-vis (diffuse reflectance, cm^{-1}): 14270.

$[Cu_2(ampyz)(O_2C_3H_5)_4]_n$ (III-3). An ethanolic solution (5 mL) of ampyz (0.5 mmol, 48 mg) was added to a stirring 5 mL of aqueous solution containing $Cu(OH)_2$ (0.5 mmol, 49 mg) and propionic acid (1 mL, 13 mmol). The resulted solution was stirred at 50 °C for an hour and then a small amount of precipitates was filtered off. The green filtrate was allowed to stand for four days at room temperature to yield green rod-shaped crystals of **III-3**. Yield 132 mg (51%) based on copper salt. Anal. Calcd for $Cu_2C_{16}H_{25}N_3O_8$: C, 37.36; H, 4.86; N, 8.17 %. Found: C, 37.13; H, 4.96; N, 8.17 %. IR (KBr, cm^{-1}): 3427w, 3229w, 1645m, 1602s, 1541w, 1427m, 1381w, 1301w, 1217w, 1070w, 1018w, 813w. UV-vis (diffuse reflectance, cm^{-1}): 14280.

$[Cu_2(ampyz)(O_4C_4H_4)_2]_n(H_2O)_n$ (III-4). An ethanolic solution (3 mL) of ampyz (0.5 mmol, 48 mg) was carefully layered on a solution containing $Cu(NO_3)_2{\cdot}3H_2O$ (0.5 mmol, 121 mg) and succinic acid (0.5 mmol, 59 mg) in a mixture of water (4 mL) and ethanol (1 mL). The vial was sealed and allowed to stand

undisturbed at room temperature. After four days, blue-green rod-shaped crystals of **III-4** were obtained. Yield 79 mg (34%) based on copper salt. Anal. Calcd for $Cu_2C_{12}H_{15}N_3O_9$: C, 30.52; H, 3.18; N, 8.90 %. Found: C, 30.68; H, 3.32; N, 8.85 %. IR (KBr, cm^{-1}): 3368br, 3172w, 1624s, 1544w, 1428s, 1403w, 1301w, 1219w, 1070w, 1021w, 577w. UV-vis (diffuse reflectance, cm^{-1}): 14450.

$[Cu(ampyz)(O_4C_3H_2)]_n(H_2O)_{2n}$ (III-5) was synthesized similarly to compound **III-4** using disodium malonate monohydrate (0.5 mmol, 83 mg) instead of succinic acid. After four days, green rod-shaped crystals of **III-5** were obtained. Yield 44 mg (15%) based on copper salt. Anal. Calcd for $Cu_2C_{14}H_{22}N_6O_{12}$: C, 28.34; H, 3.74; N, 14.16 %. Found: C, 29.06; H, 3.02; N, 14.45 %. The microanalysis is slightly deviated. Presumably this is from the loss of solvent. IR (KBr, cm^{-1}): 3342br, 3220w, 1665m, 1578s, 1547m, 1421m, 1362m, 1270w, 1229w, 1081w, 1031w, 810w, 744w. UV-vis (diffuse reflectance, cm^{-1}): 15675.

2.2 Series of metal(II) supramolecular frameworks containing ampyz and sulfate anions

$[Co(H_2O)_4(ampyz)_2][Co(H_2O)_6](SO_4)_2(H_2O)_2$ (IV-1). An ethanolic solution (5 mL) of ampyz (1.0 mmol, 96 mg) was carefully layered on an aqueous solution (5 mL) of $CoSO_4{\cdot}7H_2O$ (0.5 mmol, 141 mg) in a glass vial (20 mL). This vial was sealed and allowed to stand undisturbed at room temperature. After four days, orange crystals of **IV-1** were obtained. Yield 92 mg (26%) based on metal salt. Anal. Calcd for $Co_2C_8H_{34}N_6O_{20}S_2$: C, 13.41; H, 4.78; N, 11.73%. Found: C,13.48; H, 4.39; N, 11.79%. IR (KBr, cm^{-1}): 3450s, 3335s, 3257s, 1644m, 1603w, 1540m, 1444m, 1216w, 1108s, 1074s, 1022m, 983w, 825w, 642m. UV–vis (diffuse reflectance, cm^{-1}): 31000, 22300, 19800, less than 9000.

$[Fe(H_2O)_4(ampyz)_2][Fe(H_2O)_6](SO_4)_2(H_2O)_2$ (IV-2) was synthesized in a similar manner to that of compound **IV-1** by using $FeSO_4{\cdot}7H_2O$ (0.5 mmol, 139 mg) instead. After four days, yellow crystals of **IV-2** were obtained. Yield 80 mg (23%) based on metal salt. Anal. Calcd for $Fe_2C_8H_{34}N_6O_{20}S_2$: C, 13.53; H, 4.83; N, 11.83%. Found: C,13.49; H, 4.41; N, 11.84%. IR (KBr, cm^{-1}): 3451s, 3335s, 3255s, 1645m, 1602w, 1540m, 1444m, 1216w, 1107s, 1074s, 1021m, 982w, 825w, 655m. UV–vis (diffuse reflectance, cm^{-1}): 29000, 24500sh, 11700.

$[Co(H_2O)_4(ampyz)_2][Fe(H_2O)_6](SO_4)_2(H_2O)_2$ (IV-3) was synthesized in a similar manner to that of compound **IV-1** by using $CoSO_4{\cdot}7H_2O$ (0.25 mmol, 70 mg) and $FeSO_4{\cdot}7H_2O$ (0.25 mmol, 70 mg) instead. After four days, yellowish orange crystals of **IV-3** were obtained. Yield 72 mg (20%) based on metal salt. Anal. Calcd for $CoFeC_8H_{34}N_6O_{20}S_2$: C, 13.47; H, 4.80; N, 11.78%. Found: C, 13.48: H, 4.28; N, 11.80%. IR (KBr, cm^{-1}): 3450s, 3337s, 3257s, 1644m, 1540m, 1444w, 1216w, 1109s, 1075s, 1022m, 982w, 824w, 655m. UV–vis (diffuse reflectance, cm^{-1}): 31600, 24300sh, 19200sh, 11100br.

$[Cd(ampyz)(H_2O)_2(SO_4)]_n(H_2O)_n$ (IV-4) was synthesized in a similar manner to that of compound **IV-1** by using $CdSO_4{\cdot}8/3H_2O$ (0.5 mmol, 385 mg) instead. After four days, colorless crystals of **IV-4** were obtained. Yield 90 mg (53%) based on metal salt. Anal. Calcd for $CdC_4H_{10}N_3O_6S$: C, 14.10; H, 2.96; N,

12.34%. Found: C, 14.09; H, 2.34; N, 12.33%. IR (KBr, cm^{-1}): 3426m, 3328m, 3223m, 1634m, 1542m, 1474w, 1444m, 1360w, 1327w, 1218m, 1114s, 1075m, 1017m, 814w, 617s. UV–vis (diffuse reflectance, cm^{-1}): 27700.

2.3 Co(II) 3,5-Pyridinedicarboxylate Frameworks

$[Co(pydc)(H_2O)_2]_n$ (IV-5)

A methanol solution (1 mL) of $Co(NO_3)\cdot 6H_2O$ (0.2 mmol, 58 mg) was carefully layered on a mixed DMF/H_2O solution (2 mL) of H_2pydc (0.1 mmol, 17 mg) and KOH (0.4 mmol, 23 mg) in a glass tube. This tube was sealed and allowed to stand undisturbed at room temperature. After three weeks, deep pink rod-shaped crystals of **1** were obtained. Yield: 76 mg (77%) based on cobalt salt. Anal. Calcd for $CoC_7H_7NO_6$: C, 32.33; H, 2.71 ; N, 5.39%. Found: C, 32.24; H, 2.42; N, 5.78 %. IR (KBr, cm^{-1}): 3316m, 3110m, 1615m, 1557s, 1456m, 1439m, 1401w, 1128w, 1034w, 852w, 763m. 753m, 589m. UV-vis (diffuse reflectance, cm^{-1}): 34 100, 19 220, 16 610sh, 11 780, less than 9 000.

$[Co(pydc)(H_2O)_4]_n(H_2O)_n$ (IV-6)

An aqueous solution (5 mL) of $Co(NO_3)\cdot 6H_2O$ (1 mmol, 291 mg) was carefully layered on a DMF solution (5 mL) of H_2pydc (0.5 mmol, 84 mg) in a glass vial (15 mL). This vial was sealed and allowed to stand undisturbed at room temperature. After two weeks, orange crystals of **2** were obtained. Yield: 318 mg (85%) based on cobalt salt. Anal. Calcd for $CoC_7H_{13}NO_9$: C, 26.77; H, 4.17; N, 4.46%. Found: C, 26.78; H, 4.01; N, 4.52%. IR (KBr, cm^{-1}): 3346m, 3203m, 1606s, 1557s, 1445w, 1403m, 1381m, 1125w, 832w, 772m. 737m, 619w. UV-vis (diffuse reflectance, cm^{-1}): 33 910, 20 270, less than 9 000.

2.3. Series of azido cobalt(II) hybrid frameworks (CompoundsV-1-4)

$[Co_3(N_3)_6(OH_2)_2(2,2'\text{-bpe})_2]_n(2,2'\text{-bpe})_n$ (V-1) and $[Co(N_3)_2(2,2'\text{-bpe})]_n$ (V-2). A solution containing $CoCl_2\cdot 6H_2O$ (0.5 mmol, 119 mg) and 2,2′-bpe (0.5 mmol, 91mg) in a mixture of water (2 mL) and ethanol (2 mL) was carefully layered on an aqueous solution (2 mL) of NaN_3 (1 mmol, 65 mg) in 18 mL of glass vial. The vial was sealed and allowed to stand undisturbed at room temperature. After five days, long blue rod-shaped crystals of **V-1** and small pink square-shaped crystals of **V-2** were obtained. These crystals were manually separated, washed with water, and dried in air. Yield for **V-1**: 26 mg (5%) based on metal salt. Anal. Calcd for $Co_3C_{36}H_{34}N_{24}O_2$: C, 42.74; H, 3.39; N, 33.23%. Found: C, 42.49; H, 3.10; N, 32.98%. IR (KBr, cm^{-1}): 3200br, 2089vs, 2050m, 1592m, 1479m, 1296m, 1158w, 974m, 780m. UV–vis (diffuse reflectance, cm^{-1}): 18500sh, 16500, 12500sh, 9800. Yield for **V-2**: 56 mg (34%) based on metal salt. Anal. Calcd for $CoC_{12}H_{10}N_8$: C, 44.32; H, 3.10; N, 34.46%. Found: C, 44.04; H, 2.98; N, 34.51%. IR (KBr, cm^{-1}): 3397w, 3091w, 2097vs, 2072vs, 1599m, 1480m, 1298w, 1160m, 970m, 779m, 743m, 542w. UV–vis (diffuse reflectance, cm^{-1}): 18000, 16500, less than 9000. The single-crystals of **V-2** were prepared in a U-shaped tube. An aqueous solution (2 mL) of NaN_3 (1 mmol) was filled into the one branch of U-tube that contains distilled water 1 mL. Another branch was filled with a solution containing

$CoCl_2 \cdot 6H_2O$ (0.5 mmol) and 2,2′-bpe (0.5 mmol) in a mixture of water (1 mL) and ethanol (2 mL). After one week, the suitable single-crystals of **V-2** for X-ray diffraction study were obtained.

2D layer of $[Co(N_3)_2(ampyz)]_n$ (V-3). A mixture solution of water (1 mL) and ethanol (2 mL) of $Co(NO_3)_2 \cdot 6H_2O$ (0.5 mmol, 145 mg) was carefully layered on an aqueous solution (3 mL) of NaN_3 (1 mmol, 65 mg) in a glass vial (20 mL). Then an ethanolic solution (3 mL) of ampyz (1 mmol, 95 mg) was layered on this mixture. The vial was sealed and allowed to stand undisturbed at room temperature. After one week, orange rectangular crystals of **V-3** were obtained and then washed with water and filtered. Yield 36 mg (30%) based on metal salt. Anal. Calcd for $CoC_4H_5N_9$: C, 20.18; H, 2.12; N, 52.95%. Found: C,20.62; H, 2.05; N, 53.27%. IR (KBr, cm^{-1}): 3407m, 3326m, 2100vs, 2080vs, 1629m, 1541m, 1443m, 1354w, 1298w, 1220m, 1079w, 1025m, 804m. UV–vis (diffuse reflectance, cm^{-1}): 18400, less than 9000. The single-crystals of **V-3** were prepared in a U-shaped tube. An ethanolic solution (1 mL) of ampyz (1 mmol) was filled into the one branch of U-tube that contains distilled water (1 mL). Another branch was filled with an aqueous solution (1 mL) containing $Co(NO_3)_2 \cdot 6H_2O$ (0.5 mmol) and NaN_3 (1 mmol). After one week, the suitable single-crystals of **V-3** for X-ray diffraction study were obtained.

3D framework of $[Co(N_3)_2(ampyz)]_n$ (V-4). A mixture of $Co(NO_3)_2 \cdot 6H_2O$ (0.5 mmol, 145 mg), NaN_3 (1 mmol, 65 mg) and ampyz (1 mmol, 95 mg) in water (2 mL) and ethanol (2 mL) was sealed in a Pyrex tube (7 mL), then heated to 90 °C (temperature increase rate of 18°C/min), allowed to stay for 24 h, and cooled to 30°C (temperature decrease rate of 0.04°C/min). The red-orange polygonal crystals of **V-4** were obtained in a major phase together with unidentified purple powder phase. The crystals were washed with water and filtered to give pure crystals of **V-4**. Yield 53 mg (45%) based on metal salt. Anal. Calcd for $CoC_4H_5N_9$: C, 20.18; H, 2.12; N, 52.95%. Found: C,19.80; H, 2.15; N, 52.00%. IR (KBr, cm^{-1}): 3415m, 3307m, 2105vs, 2068vs, 1624m, 1540m, 1438m, 1322w, 1298w, 1218m, 1026w, 821w. UV–vis (diffuse reflectance, cm^{-1}): 18400, 9300.

3. Results and Discussion

3.1 Structural diversity and magnetic properties of copper(II) coordination polymers containing aminopyrazine and different carboxylato bridges

The field of coordination polymers has been extensively investigated over the past few decades with a focus on functional material research and crystal engineering. In material research, the coordination networks with interesting properties in areas such as molecular adsorption, catalysis, photoluminescence, magnetism and so on, are constructed for fine-tuning the properties and creating new functional materials.[1-7] On the other hand, crystal engineering is attracting interest from both the synthetic routes and the art of structural design.[8-14] One of the challenges in this field is to forecast the crystal structure from the building units. It is well-known that the chemistry of metal carboxylates shows various structural diversities beginning from a simple mononuclear complex to 3D frameworks with functional properties.[15-18] This

diversity results from the fact that the carboxylate groups can coordinate metal centers in various ways, such as monodentate, chelate, monatomic bridge, bridging bi- and tridentate, and also less common multiple bridges.[18-21] Therefore, the combination of metal carboxylates and other coligands, either bridging or terminal coligands, has a large potential to construct novel coordination networks. Consequently, this field has become a popular research area in recent decades.[15, 22-24]

The short rigid rodlike spacer pyrazine (pyz) is a *N*,*N*′-ditopic diimine which is widely used for constructing many metal-organic frameworks.[8, 25-27] It is well known that the pyz spacer is a good electron transfer agent in the superexchange pathways between connected metal centers showing antiferromagnetic routes. Several compounds with mixed pyz spacer ligands and metal carboxylates exhibiting various structural topologies together with interesting magnetic phenomena have been extensively investigated.[28-33] With Cu^{II} ion, both pyz and carboxylates play a key role for building Cu^{II} coordination polymers, and interesting compounds have been observed. For instance, the 2D layered structure of $[Cu(HCO_2)(NO_3)(pyz)]_n$ presents a long-range magnetic ordering below 3.7 K,[28] while $[Cu_2(pyz)(O_4C_3H_2)_2]_n(H_2O)_{2n}$ (in which $H_2C_3O_4^{2-}$ is the malonate anion) shows a unique 3D framework displaying metamagnetism.[29, 30]

The ligand 2-aminopyrazine (ampyz) is a substituted pyz containing an electron withdrawing amine group attached at the pyz ring and it also effectively acts as an organic spacer in many metal-organic frameworks.[34-37] However, no compounds containing both the ampyz spacer and bridging carboxylate groups have been reported as yet. Consequently, the present work demonstrates the use of ampyz as a rigid ditopic spacer in combination with either mono- or dicarboxylate anions. Formate (HCO_2^-), acetate ($CH_3CO_2^-$), propionate ($C_2H_5CO_2^-$), malonate ($CH_2C_2O_4^{2-}$), and succinate ($C_2H_4C_2O_4^{2-}$) anions have been used to construct a variety of Cu^{II} coordination polymers.

3.1.1 General observations and spectroscopic characterizations

In the present work, reaction of copper(II) and carboxylate anion with ampyz in a mixture of ethanol and aqueous media gives various copper(II) coordination polymers containing ampyz spacer together with carboxylato bridges. The different types of carboxylates can lead to structural diversities due to their coordination modes, steric effect, and flexibility. For the simplest carboxylate with the smallest steric effect, formate anion gives a 2D wavy sheet structure, whereas the larger sterically crowded carboxylates, acetate and propionate anions, give a polymeric chain, constructed from paddle-wheel $CuNO_4$ chromophores. On the other hand, the dicarboxylates can provide more opportunity to bind with metal centers in particular the flexible dicarboxylates, such as malonate and succinate anions mostly constructing unpredictable crystal frameworks.[29, 38-41] For this study, a 2D layer which contains the double-stranded chain of paddle-wheel units is built from succinate anions as well as 2D stairlike layer built from malonate anions. The description of the structures **III-1-5** is discussed in the following topics, together with the

comparison with the bridging pyrazine spacer in the similar Cu^{II} systems with their spectroscopic and magnetic properties.

The solid-state IR spectra of **III-1-5** in the region 4000-450 cm^{-1} exhibit characteristic bands for carboxylates and ampyz ligand (Figure 1). Compounds **III-1-3** show two narrow weak bands in the region 3400-3300 cm^{-1} and 3100-3200 cm^{-1}, which can be assigned to asymmetric and symmetric stretching of the primary amine in the ampyz ligand. Compounds **III-4** and **III-5** show broadbands in the region 3100-3400 cm^{-1} due to the bands overlapping of the ν(O–H) of water molecule. The NH_2 scissoring mode shows medium bands around 1640-1660 cm^{-1} which overlap with the ν_{as}(OCO) of carboxylate appearing strong bands in the range of 1620-1570 cm^{-1}. The ν_s(OCO) shows medium bands in the region 1320-1430 cm^{-1}. The weak, sharp band around 1070-1080 cm^{-1} can be assigned to the ν(C–N) of ampyz. The solid-state UV-visible diffuse reflectance spectra (Figure 2) show a single broadband around 14,270-14,450 cm^{-1} for compounds **III-2-4,** which are in agreement with those of common Cu^{II} paddle-wheel complexes with a square-pyramidal geometry (d_{xy}, d_{xz},d_{yz}, $d_{z2} \rightarrow d_{x2-y2}$ transition).[42]

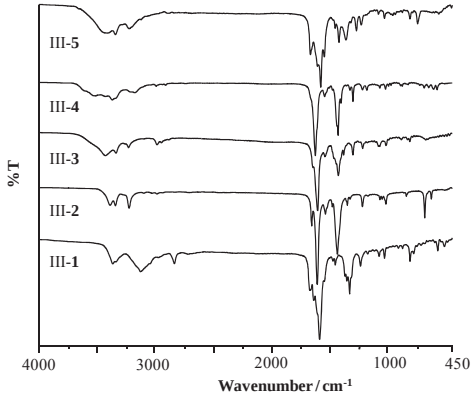

Figure 1 Infrared spectra for compounds **III-1-5**.

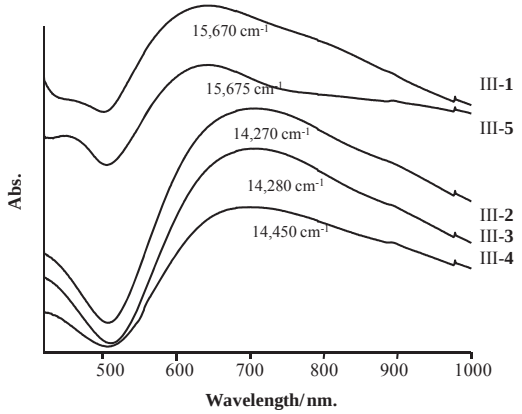

Figure 2 Solid-state UV-visible diffuse reflectance spectra for compounds **III-1-5**.

Compounds **III-1** and **III-5** show a single broadband at a higher energy, *i.e.* around 15,670 cm^{-1}, corresponding to the further structural distortion toward an elongated octahedral geometry with the sixth off-the-axis weakly interacting to Cu^{II} center. In fact these values of the transition energy (14,270 to 15,670 cm^{-1}) are all in the range usually found for the distorted square-pyramidal geometry of Cu^{II} centers (d_{xy}, d_{xz},d_{yz}, $d_{z2} \rightarrow d_{x2-y2}$ transition).[43]

3.1.2 Description of crystal structures

$[Cu(ampyz)(O_2CH)_2]_n$ (III-1)

The coordination environment of the Cu^{II} center is shown in Figure 3. Each Cu^{II} ion is five-coordinated showing a distorted square-pyramidal CuN_2O_3 chromophore with a τ value of 0.011 (τ = 0 for square pyramid and τ = 1 for trigonal bipyramid).[44] The equatorial plane around the copper atom is composed of two formate oxygen atoms (O1 and O3A) with the average Cu–O distance of 1.965(5) Å and two ampyz-nitrogen atoms with the Cu–N distances of 2.039(4) Å. The apical position is occupied by an oxygen from a formato bridge (Cu–O2′ = 2.300(5) Å). The CuN_2O_2 square base is not perfectly planar with tetrahedral twists between the O1–Cu–N1 and O3A–Cu–N1′ planes of 13.57°. The copper atoms are slightly shifted by 0.007 Å from the mean basal plane toward the apical position. This value is too small for the typically found square-pyramidal geometry which is attributed to the semicoordinated O2 atom of formate group weakly interacting to Cu center in off-the-axis position of an elongated octahedral geometry with the longest Cu–O2 distance of 2.718(5) Å.

The formato bridges exhibit a *syn*,*anti*–η^1:η^1:μ_2 coordinative mode bridging between adjacent Cu^{II} centers along the *a* axis with Cu···Cu separations of 4.7807(10) Å resulting a wavy polymeric chain structure as shown in Figure 4(a). The ditopic ampyz spacers link the Cu–HCO_2–Cu wavy chains parallel to the *b* axis with Cu···Cu separation of 6.8558(6) Å *via* ampyz.

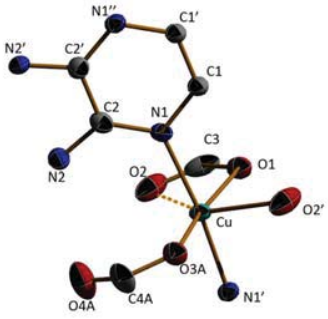

Figure 3 Asymmetric unit and atom labeling scheme of **III-1**. The ellipsoids are shown at 35% probability level, and the disordered O3B, C4B, O4B and hydrogen atoms are omitted for clarity. Both disordered positions of N2 are shown. The dashed line represents weak interaction in the off-the-axis position.

The N1–Cu–N1′ angle slightly deviates from linearity (9.5°). Consequently, the wavy 2D network is constructed from μ_2-HCO_2^- and μ_2-ampyz with the square grid dimension of ca. 4.781×6.856 Å in the *ab* plane (Figure 4(b)). In addition, the layer of **III-1** is stabilized by hydrogen bonding and π-π stacking interactions within the layer. The intralayer hydrogen bonds are built from the amine hydrogen of ampyz and two formate oxygen atoms forming a rhomboid hydrogen bonding array throughout the layer [N2H···O4A^{i} = 2.25 Å (124°), N2···O4A^{i} = 2.824(9) Å, (i) = *x*, 3/2–*y*, *z*; N2H···O3A^{i} = 2.32 Å (134°), N2···O3A^{i} = 2.979(9) Å, (i) = –1+*x*, *y*, *z*]. The lattice is further stabilized by π-π stacking between adjacent ampyz ligands merely overlayering at the edges of the rings with the separation of 3.632(3) Å.[45]

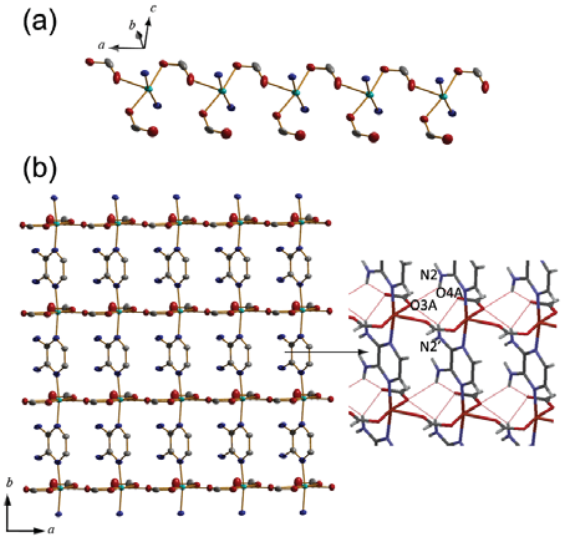

Figure 4 Segment of a wavy polymeric chain in **III-1** constructed from *syn-anti* formato bridges along *a* axis. Ampyz rings are omitted for the sake of clarity (a). Two-dimensional sheet structure of **III-1** in the *ab* plane; the inset presents the intralayered hydrogen bonds. Both disordered positions of amino group are shown. Cu atoms are represented in green, N in blue, O in red, and C in gray (b).

Interestingly, the crystal packing of these wavy sheets reveals the alternated ampyz arrangement in the *bc* plane (Figure 5), because of the 2_1-fold screw axis lined between the layers and the steric nature of ampyz ligands. Moreover, the interlayer hydrogen bonding between the hydrogen atoms of ampyz and the terminal formate oxygen atoms of the adjacent layer [N2H···O4A^{i} = 2.06 Å (152°), N2···O4A^{i} = 2.848(10) Å, (i) = –*x*, 1–*y*, –*z*] stabilizes the double sheet of **III-1** with the closest interlayer Cu···Cu separation of 6.7695(9) Å (inset of Figure 5).

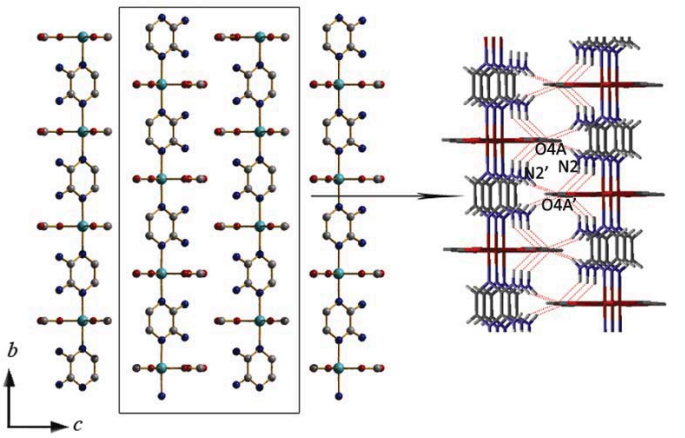

Figure 5 Packing diagram of the sheets in **III-1** showing the alternating ampyz ring arrangements in the *bc* plane. The inset shows hydrogen bonds stabilizing the double sheets of **III-1**. Both disordered positions of amino group are shown.

In comparison with mixed bridging pyrazine and formate in Cu^{II} complexes, the structure of compound **III-1** is close to the 2D sheet of $[Cu(HCO_2)(NO_3)(pyz)]_n$,[28] which crystallizes in the orthorhombic space group (*Pnma*) with the coordinated nitrate (Figure 6), whereas **III-1** crystallizes in the monoclinic space group ($P2_1/m$) with a monodentate formate instead of a nitrate group. In contrast $[Cu(HCO_2)_2(pyz)]_n$[31] reveals a 3D framework which consists of tetragonally elongated CuN_2O_4 octahedra made up of four bridging formate anions and two neutral pyz ligands (Figure 7).

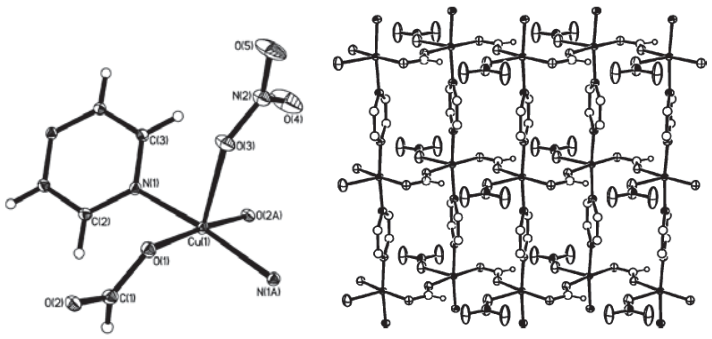

(a) **(b)**

Figure 6 Crystal structure (a) and 2D corrugated layer of $[Cu(HCO_2)(NO_3)(pyz)]_n$ (b).[28]

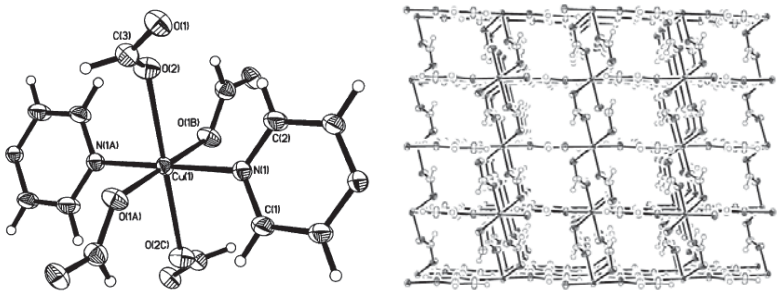

(a) **(b)**

Figure 7 Crystal structure (a) and 3D scaffold structure of $[Cu(HCO_2)_2(pyz)]_n$ (b).[31]

$[Cu_2(ampyz)(O_2C_2H_3)_4]_n$ (III-2) and $[Cu_2(ampyz)(O_2C_3H_5)_4]_n$ (III-3)

Both compounds **III-2** and **III-3** consist of a polymeric chain structure built up from bridging ampyz spacers connecting the paddle-wheel units of $[Cu_2(\mu_2\text{–}O_2C_2H_3)_4]$ or $[Cu_2(\mu_2\text{–}O_2C_3H_5)_4]$ for **III-2** and **III-3**, respectively. Their structures with atom numbering scheme are shown in Figure 8. Each Cu^{II} ion is five-coordinate showing a distorted square pyramidal $CuNO_4$ chromophore with $\tau = 0.002$ (for **III-2**) and 0.004 (for **III-3**). The basal position of the square pyramid is occupied by four oxygen atoms from four different carboxylate groups with mean distance of 1.967(2) and 1.966(3) Å for **III-2** and **III-3**, respectively. The apical position is occupied by a nitrogen atom from ampyz with Cu–N = 2.229(2) and 2.230(2) Å for **III-2** and **III-3**, respectively. The basal plane is nonplanar with tetrahedral twist of 16.59° for **III-2** and 16.89° for **III-3**. The copper atom lies 0.202 Å (for **III-2**) and 0.207 Å (for **III-3**) above the mean basal plane toward the axial site.

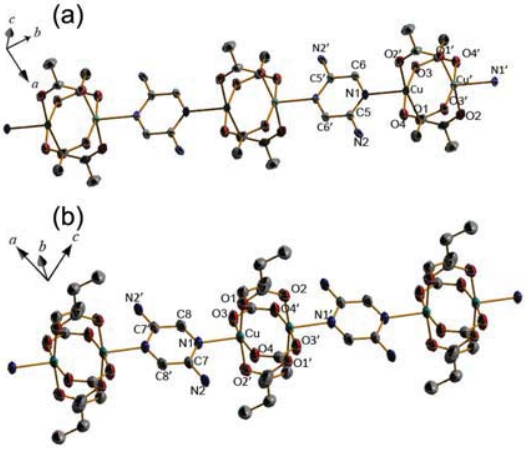

Figure 8 Part of a 1D chain structure of **III-2** (a) and **III-3** (b) with used atom labeling. The ellipsoids are shown at 35% probability level, and hydrogen atoms are omitted for clarity. Both disordered positions of N2 are shown.

Both acetate and propionate anion acts as a bidentate bridge in *syn*,*syn*–η^1:η^1:μ_2 coordinative mode bridging between Cu^{II} centers forming a paddle-wheel secondary building unit (SBU). The Cu···Cu separation in each dinuclear unit is 2.6286(4) Å for **III-2** and 2.6322(7) Å for **III-3**, which indicates a metal-metal interaction, and it agrees well with those reported for Cu^{II} paddle-wheel complexes of acetate and propionate.[42, 46, 47] The paddle-wheel SBUs are connected by μ_2-ampyz giving rise to the polymeric chain structure with Cu···Cu separation *via* ampyz of 7.2377(3) and 7.2498(5) Å for **III-2** and **III-3**, respectively. In the packing motif (Figure 9), both 1D chains of **III-2** and **III-3** are assembled alternatively *via* hydrogen bonding between amine hydrogen of ampyz and a carboxylato oxygen [for **III-2**: N2H···O4 = 1.96 Å (159°), N2···O4 = 2.774(4) Å; N2H···$O1^i$ = 2.13 Å (166°), N2···$O1^i$ = 2.973(5) Å, (i) = *–x*, 2 *–y*, 1 *–z*; for **III-3**: N2H···O4 = 2.12 Å (146°), N2···O4 = 2.875(6) Å; N2H···$O2^i$ = 2.46 Å (160°), N2···$O2^i$ = 3.285(7) Å, (i) = *x, y,* −1+*z*] to construct the 2D sheets with the closest Cu···Cu interchain distance of 6.3693(4) Å for **III-2** and 6.9001(7) Å for **III-3** corresponding to the steric size of carboxylate groups. These assembled sheets of **III-2** or **III-3** are alternately arranged in a zigzag jigsaw-like motif to complete the overall solid-state structure, as shown in Figure 10.

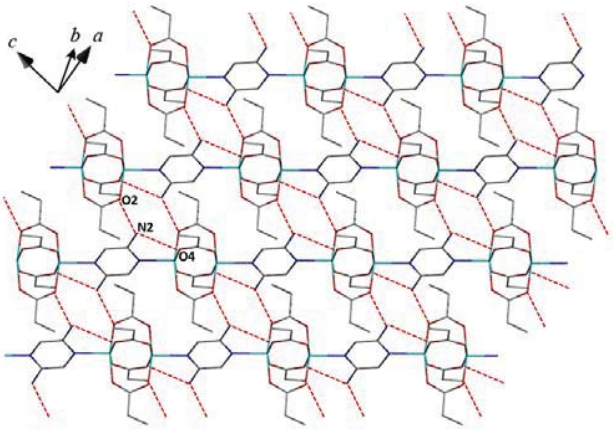

Figure 9 The 2D sheet formed by hydrogen bonding between the chains of **III-3**.

The copper paddle-wheel complexes have been investigated for a long time. The first 1D chain for the present system with a paddle-wheel SBU is $[Cu_2(pyz)(O_2C_2H_3)_4]_n$[46] and was reported in 2006.[47] The polymeric chain of **III-2** is almost the same as the previously reported structure (Figure 11). However, their crystal systems, space groups and packing motifs are dissimilar due to the amine groups appending on pyz moieties leading to the different arrangement in the solid-state structure. Contrary to **III-3**, the first mixed pyz and propionate in $[Cu_4(pro)_4(CH_3O)_4(pyz)]_n$ [48] gives rise to a 2D network as depicted in Figure 12. The distinctive structure is probably due to the higher steric effect of ampyz as compared to pyz. Therefore the paddle-wheel unit is possibly dominant leading to the 1D chain of **III-3**.

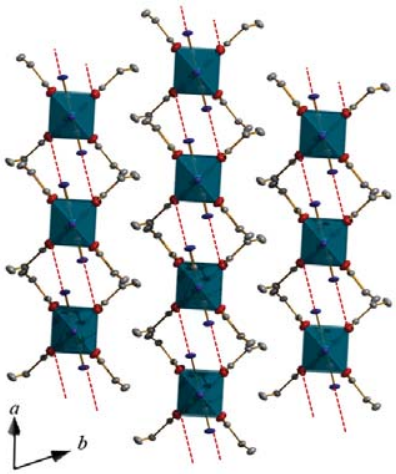

Figure 10 Packing diagram of the 2D sheets in **III-3** showing zigzag arrangement of layers in *ab* plane. The hydrogen bonding between H-donors and H-acceptors are shown in red broken lines, and the blue pyramids represent $CuNO_4$ chromophores. Both disordered positions of amino group are shown.

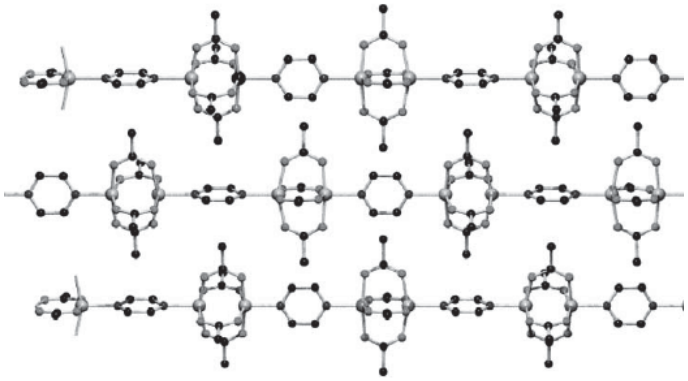

Figure 11 Packing diagram of reported $[Cu_2(pyz)(O_2C_2H_3)_4]_n$.[47]

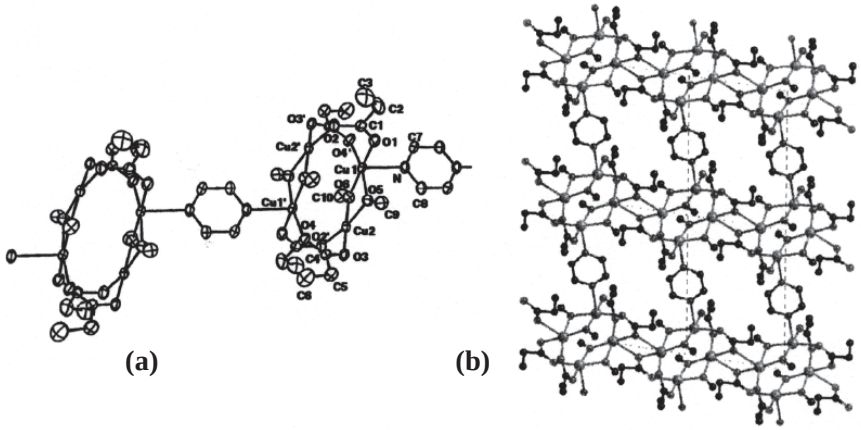

Figure 12 Crystal structure (a) and 2D layer of $[Cu_4(pro)_4(CH_3O)_4(pyz)]_n$ (b).[48]

$[Cu_2(ampyz)(O_4C_4H_4)_2]_n(H_2O)_n$ (III-4)

The structure of **III-4** with its atom labeling scheme is shown in Figure 13. Each Cu^{II} ion is five-coordinate showing distorted square pyramidal $CuNO_4$ chromophore with $\tau = 0.003$. The basal position of the square pyramid is occupied by four oxygen atoms from four different bridging succinate groups with average distance of 1.964(3) Å. The nitrogen of ampyz occupies the axial position of the square pyramid with a Cu–N distance of 2.206(3) Å. The basal plane is nonplanar with tetrahedral twist of 17.40°. The copper atom lies 0.212 Å above the mean basal plane toward the apical position. Four succinate anions are bridging between the Cu^{II} centers in a *syn*,*syn*–η^1:η^1:μ_2 coordinative mode of carboxylate forming a Cu^{II} paddle-wheel SBU. The Cu···Cu separation in each dinuclear unit is 2.6457(10) Å showing metal-metal bonding which is in good agreement with those reported for Cu^{II} paddle-wheel complexes of succinate.[49] The succinate anion is a dicarboxylate containing two aliphatic carbons in the backbone. For **III-4**, the succinate acts as a tetradentate ligand connecting four adjacent Cu centers of the paddle-wheel SBU to form a double-stranded chain of a paddle-wheel unit, which reveals the repeating 14-membered ring of $\{Cu_2(C_2O_4)_2\}$ with the cavity's dimension of ca. 6.594 × 5.880 Å. The closest Cu···Cu separation among the paddle wheel SBUs is 6.5942(9) Å. The conformation

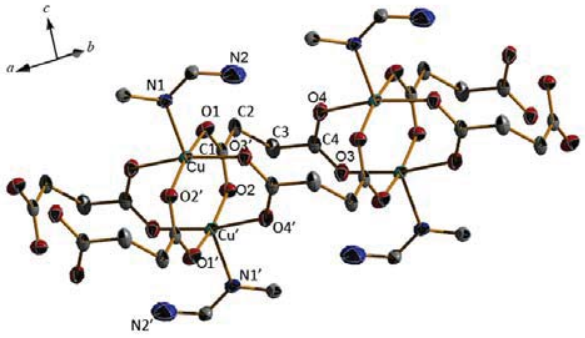

Figure 13 The double-stranded array of a paddle-wheel unit formed by four *syn-syn* succinate bridges of **III-4** with atom labels. The ellipsoids are shown at 35% probability level. The uncoordinated water molecule and the hydrogen atoms are omitted for clarity.

of the succinate group in **III-4** exhibits the *syn-anti* mode[32] with a torsion angle of 69.88°, and the orientation of carboxylate moiety with respect to the carbon aliphatic backbone line generates angles of ca. 67.50° and 62.25°. Furthermore, these double-stranded chains are connected by ampz spacers on an apical site of each paddle-wheel SBU with a Cu···Cu separation of 7.1951(6) Å *via* ampyz, giving rise to the 2D network together with uncoordinated water molecules filling on the upper and lower sites of the cavities (Figure 14(a)). The dimension of this cavity is about 6.594 × 7.195 Å.

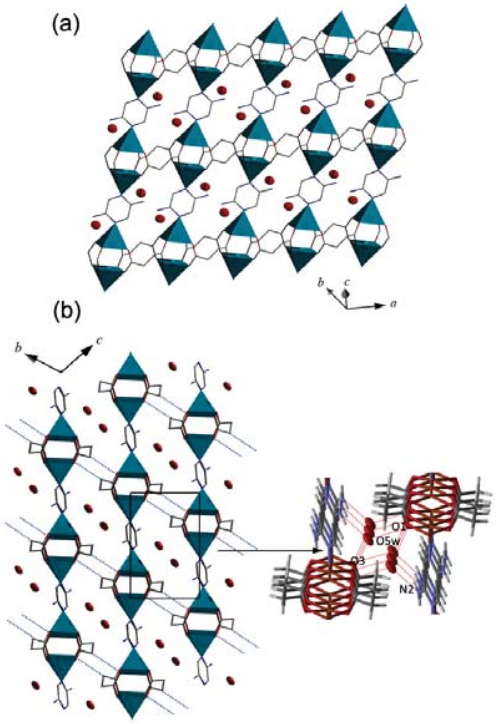

Figure 14 2D layer with uncoordinated water molecules filling up the windows of the sheet of **III-4**. (a) 3D packing structure of **III-4** formed by weak hydrogen bonding (blue dotted lines) between layers. The inset shows water molecules stabilizing the supramolecular network *via* hydrogen bonds. The blue pyramids are the $CuNO_4$ chromophores. Both disordered positions of amino group are shown (b).

In the molecular packing motif, each 2D layer of **III-4** is assembled *via* intermolecular weak hydrogen bonding between an aliphatic hydrogen of succinate and a bridging succinato oxygen of the adjacent layer [C3H···O3^{i} = 2.57 Å (147°), C3···O3^{i} = 3.431(6) Å, (i) = –*x*, –1–*y*, –*z*.] as shown in Figure 14(b). Moreover, the uncoordinated water molecules play an important role to stabilize the whole packing structure *via* hydrogen bonding between amine hydrogen of ampyz and water oxygen [N2H···O5w^{i} = 1.94 Å (150°), N2···O5w^{i} = 2.715(15) Å, (i) = 1+*x*, *y*, *z*] and supposing *via* hydrogen bonding between succinato oxygen and water hydrogen with the O1···O5w and O3···O5w distances of 2.854(9) Å and 2.974(12) Å, respectively. The neighboring O5w···O5w′ distances are 2.972(16) Å indicative of normal hydrogen bonds. The closest Cu···Cu interlayer distance is 7.9690(8) Å.

The comparison was made with known mixed bridging succinate-pyz complexes, like $[Cd_2(O_4C_4H_4)_2(pyz)(H_2O)]_n$ [32] which reveals a 2D infinite grid sheet containing a pentagonal bipyramidal chromophore. For the Cu^{II} system, the compound $[Cu_2(O_4C_4H_4)_2(H_2O)_2]_n(H_2O)_{2n}$ was obtained, being the

first example of double-stranded chain motif (Figure 15).[49] The pyz only acts as the molecular template which is uncoordinated with Cu centers. In contrast, ampyz can corporate in the network of **III-4** due to the maintenance of interlayer hydrogen bonding as well as the intralayer hydrogen bonding [N2H···O3^{i} = 2.00 Å (144°), N2···O3^{i} = 2.741(10) Å, (i) = 1–*x*, –*y*, –*z*] stabilizing the 2D network of **III-4**.

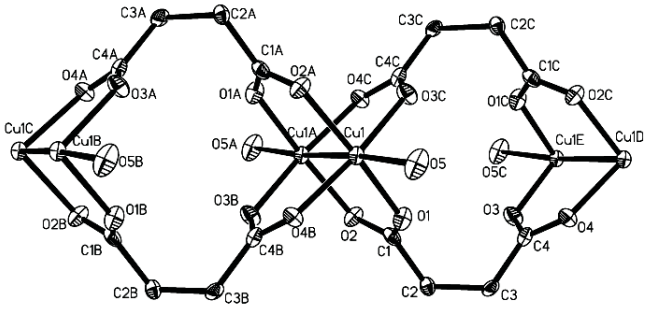

Figure 15 Infinite double-stranded chain structure of $[Cu_2(O_4C_4H_4)_2(H_2O)_2]_n(H_2O)_{2n}$.[49] Hydrogen atoms have been omitted for clarity.

$[Cu(ampyz)(O_4C_3H_2)]_n(H_2O)_{2n}$ (III-5)

The coordination environment of the Cu^{II} center is shown in Figure 16. Each Cu^{II} ion is five-coordinated, showing a distorted square pyramidal CuN_2O_3 chromophore with τ = 0.1058. Two oxygen (O2 and O3) atoms from two different malonate groups and two ampyz nitrogen atoms occupy the equatorial plane of the square pyramidal geometry with average Cu–O and Cu–N distances of 1.945(3) and 2.049(2) Å, respectively. The axial position is occupied by a malonate oxygen atom with Cu–O1 distance of 2.179(2) Å. The copper atom is shifted by 0.130 Å from the mean basal plane toward the apical position. Each malonate anion acts as tridentate ligand bridging two adjacent Cu^{II} centers by use of a bidentate chelating mode through O2 and O1 toward Cu, forming a six-membered ring with the subtended angle at the copper atom being 92.08°. The bidentate triatomic bridge through O1 and O3′ toward the adjacent Cu′ resulting in a 1D zigzag chain along crystallographic *a* axis in *syn-anti* coordinative mode of malonate yields a Cu···Cu separation of 4.9881(6) Å. The dihedral angle between the basal planes of two adjacent copper atoms is 24.32°. The values of the bond lengths and angles of malonate ligand are comparable to those previously reported for malonate bridged Cu^{II} complexes.[38]

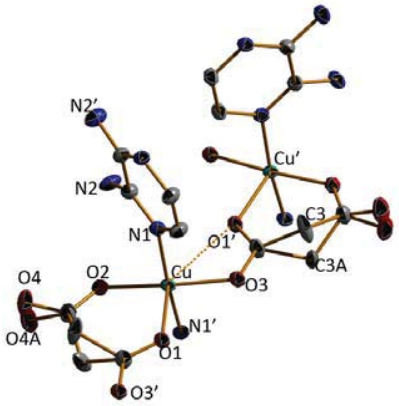

Figure 16 Asymmetric unit and the atom labeling scheme of **III-5** with 35% probability level. The two uncoordinated water molecules and the hydrogen atoms are omitted for clarity. Both disordered positions of N2 are shown. The dashed line represents weak interaction in the off-the-axis position.

Furthermore, these 1D zigzag chains are connected by ditopic ampyz spacer along the *b* axis leading to 2D layered structure with the unbound water molecules filling up the windows (Figure 17(a)). The Cu···Cu separation *via* ampyz is 6.8579(3) Å. Interestingly, the layers of **III-5** contain two sets of guest water molecules, as shown in Figure 17(b). The former set is filled in the cavities of the layer in zigzag fashion spreading along the *ab* plane where the hydrogen bonding stabilizes this water set *via* uncoordinated malonate oxygen of adjacent layer with O4′···O6w separations of 2.913(11) Å. The dimension of the grid cavity is about 6.858×4.988 Å. Another set of water molecules is filled among the layers which is stabilized by hydrogen bonding between the amine hydrogen of ampyz spacer and the water oxygen atom [$N2H_a$···O5w = 1.98 Å (137°), N2···O5w = 2.671(6) Å] and also by a hydrogen bond from the bridging malonate oxygen of the adjacent layer with O3′···O5w separations of 2.850(6) Å. The filling of the different positions of water

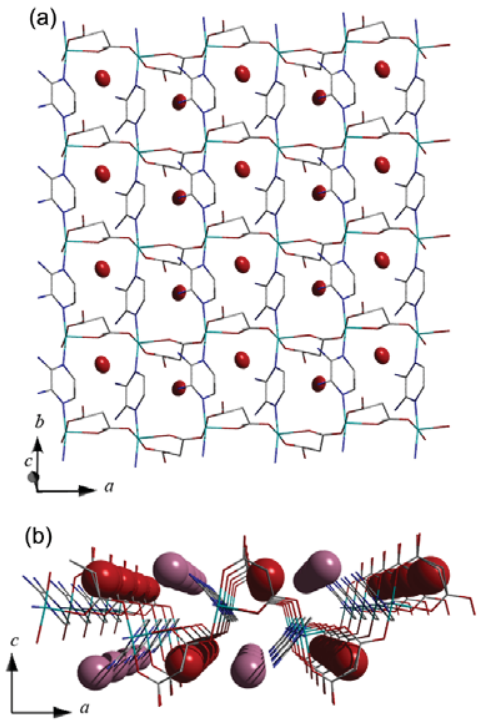

Figure 17 View of the 2D layer of **III-5** containing nearly perpendicular orientation of ampyz spacers and uncoordinated water molecules filling up the windows (a). Another view in the *ac* plane of a 2D stairlike layer showing the arrangement of two different groups of uncoordinated water molecules (b). The two sets of water molecules are represented in different colors in the space-filling model. Both disordered positions of amino group are shown.

molecules causes the arrangement of ampyz rings in the layers of **III-5** that are twisted nearly perpendicular one another with the dihedral angle between adjacent ampyz aromatic rings being 73.52° (Figure 17(a)). This structural feature contributes to the stairlike layered structure (Figure 18). In the packing motif, each 2D stairlike layer of **III-5** is assembled *via* hydrogen bonding between amine hydrogen and malonate oxygen atom [$N2H_b\cdots O2^i$ = 2.45 Å (160°), $N2\cdots O2^i$ = 3.274(5) Å, (i) = 1–*x*, –1/2+*y*, –*z* and $N2H_b\cdots O4^i$ = 2.11 Å (135°), $N2\cdots O4^i$ = 2.783(7) Å, (i) = –*x*, –*y*, 1–*z*] together with the uncoordinated water molecules stabilizing the layers which completely results to the overall 3D structure of **III-5** as shown in the inset of Figure 3.18.

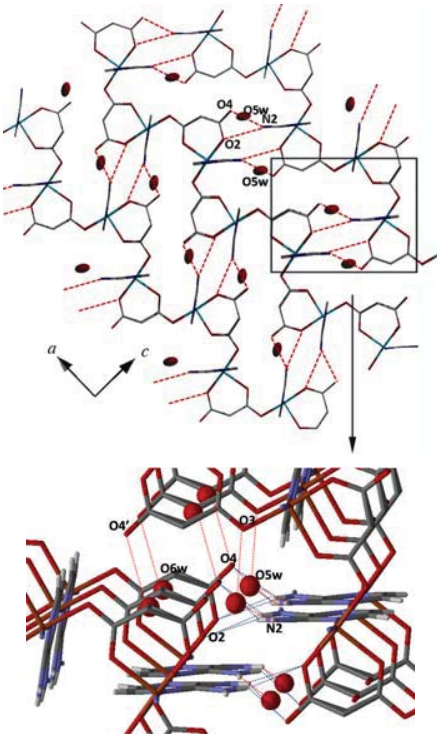

Figure 18 The 3D packing structure of **III-5** viewed along the *b* axis formed by the hydrogen bonding between stairlike layers. The inset presents the hydrogen bonds from uncoordinated water molecules stabilizing the supramolecular assembly.

A comparison was made with the mixed bridging malonate-pyz Cu^{II} complexes, like $[Cu_2(pyz)(O_4C_3H_2)_2]_n(H_2O)_{2n}$ [29] which was reported to exhibit a unique 3D network constructed from bridging tetradentate malonate groups and μ_2-pyz (Figure 19). Compound **III-5** reveals a 2D stairlike network that may be attributed from the higher steric effect of ampyz spacer which causes malonate only acting as a tridentate connector with a terminal oxygen atom.

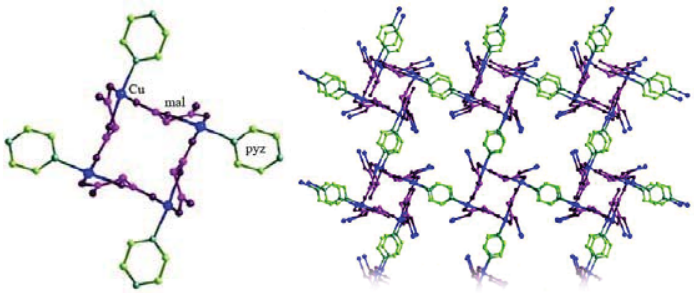

Figure 19 Asymmetric unit and 3D network of $[Cu_2(pyz)(O_4C_3H_2)_2]_n(H_2O)_{2n}$.[29]

3.1.3 EPR and magnetic measurements

EPR spectra

The X-band EPR was measured on polycrystalline samples at room temperature (RT) and 77 K for all five compounds. Compounds **III-2** and **III-4** showed in principle the same spectrum at 77 K, while at RT the intensities of particular features differed somewhat between them (Figure 20-22). In particular, at 77 K, where the triplet ($S = 1$) state is the only significantly populated excited state, two peaks are visible at around 250 and 4700 G, which are assigned to the turning points in the triplet powder pattern with $H_{//}$ and $H_{\perp}$, respectively. Other expected parallel turning points ($H_{//2}$) are either outside the available magnetic field range (>6000 G), or not observable in X-band because the value of D approaches that of the microwave quantum. The recorded spectra are indeed typical for a triplet state with a sizable zero-field splitting, such as that well-known for the classical paddle-wheel type dicopper tetracarboxylates.[50-54] In compound **III-3**, an additional feature is the hyperfine structure appearing on the parallel turning point of the spectrum at 77 K, due to hyperfine interaction of the unpaired electron with two equivalent Cu^{II} nuclei ($I = 3/2$) within the dinuclear unit. The occurrence of the several additional peaks in the 700-4000 G range in the RT-EPR spectra of compounds **III-2-4** are in all likelihood caused by higher excited states ($S = 2$) being populated at elevated temperatures.[55] The peak at around 3200 G is an $S = 1/2$ signal of a mononuclear Cu^{II} impurity and is ignored in the analysis. The EPR spectra of the classical paddle-wheel type dicopper tetracarboxylates may be described by the spin Hamiltonian:[55]

$$\hat{\boldsymbol{H}} = D\boldsymbol{S}^2_z + E(\boldsymbol{S}^2_x - \boldsymbol{S}^2_y)g_zH_z\boldsymbol{S}_z + g_xH_x\boldsymbol{S}_x + g_yH_y\boldsymbol{S}_y \qquad (1)$$

D and E values are the tetragonal and rhombic zero-field splitting parameters and $S = 1$. The x, y and z are the principal coordinate axes, where z-axis is taken parallel to the Cu–Cu direction inside the dimer. The other symbols have their usual meaning. The spin Hamiltonian parameters optimized to simulate the experimental triplet EPR spectra at 77 K are $S = 1$, $g_{//} = g_z = 2.00$, $g_{\perp} = (g_x+g_y)/2 = 2.05$, $E = 0$ $cm^{-1}$and $|D| = 0.336$ cm^{-1} for **III-2** and **III-4**. Compound **III-3** is characterized by an almost identical set of parameters, with the addition of two copper ($I = 3/2$) nuclei interacting with the $S = 1$ electron spin, with the $A_{//}$ component of the hyperfine tensor equal to 4×10^{-3} cm^{-1} (120 MHz), and $A_{\perp}$ unresolved. The appearance of triplet EPR spectra in compounds **III-2-4** is in accordance with the magnetic susceptibility observations and the fact that these three compounds all have very short Cu···Cu distances. Compounds **III-1** and **III-5**, which have different structures and both have a very long Cu···Cu distance, only show a broad isotropic $S = 1/2$ signal with $g = 2.12$ both at 77 K and RT (Figure 23), giving no information regarding the electronic ground state.

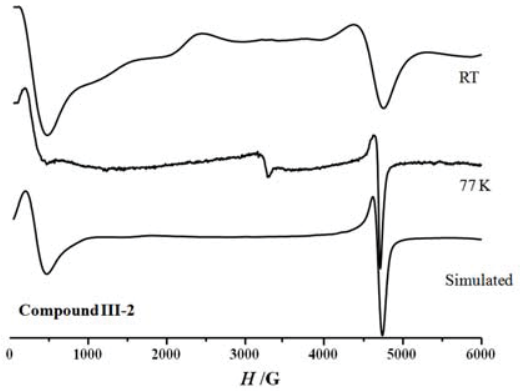

Figure 20 EPR spectra of **III-2** at RT and 77 K and the simulation for dinuclear Cu^{II} at 77 K.

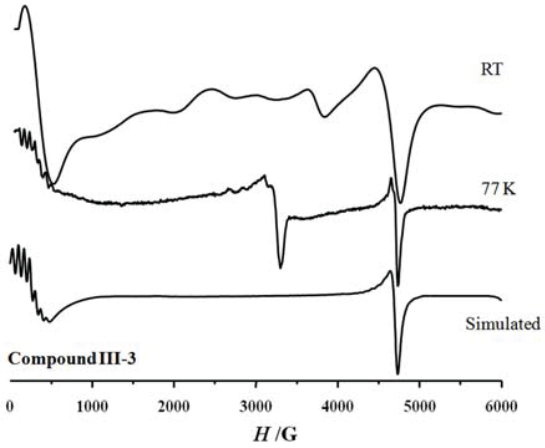

Figure 21 EPR spectra of **III-3** at RT and 77 K showing Cu hyperfine splitting at 77K around 200 G and the simulation for dinuclear Cu^{II} at 77 K.

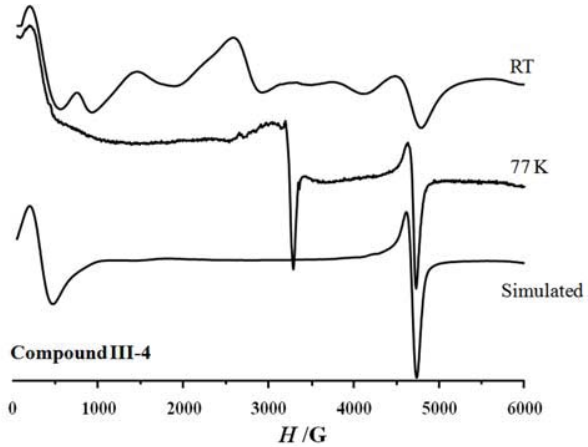

Figure 22 EPR spectra of **III-4** at RT and 77 K and the simulation for dinuclear Cu^{II} at 77 K.

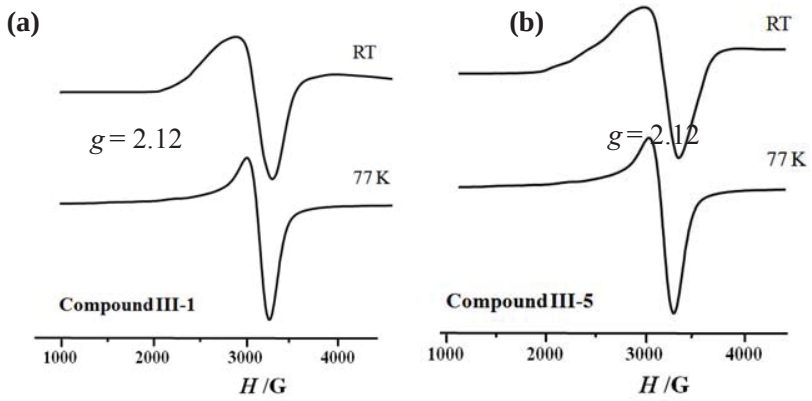

Figure 23 EPR spectra of **III-1** (a) and **III-5** (b) at RT and 77 K.

Magnetic measurements

The magnetic susceptibility of powdered sample of all five compounds was measured from 2-300 K under a constant magnetic field of 0.1 T. The magnetic properties of **III-1** and **III-5** are mutually the same because they are 2D layers that contain the similar μ_2-*syn-anti* carboxylato in axial-equatorial configuration and μ_2-ampyz spacer bridging between Cu^{II} centers. The magnetic susceptibilities of **III-1** and **III-5** are depicted in Figures 24 and 25. The $\chi_m T$ value of ca. 0.40 cm^3 K mol^{-1} at 300 K is slightly larger than value expected for uncorrelated Cu^{II} ion (0.375 cm^3 K mol^{-1} for g = 2), owing to the g-tensor anisotropy. Upon cooling from 300 K, $\chi_m T$ slowly increases, reaching a broad maximum around 50 K (0.45 cm^3 K mol^{-1} for **III-1** and 0.46 cm^3 K mol^{-1} for **III-5**), which indicates the dominance of ferromagnetic interactions *via* orthogonally μ_2-*syn-anti*-formato in **III-1** and μ_2-*syn-anti*-malonato in **III-5** bridging between Cu^{II} ions.[56-58] Below this, $\chi_m T$ decreases rapidly to 0.15 cm^3 K mol^{-1} for **III-1** and 0.17 cm^3 K mol^{-1} for **III-5**, due to the build-up of significant antiferromagnetic interactions *via* μ_2-ampyz spacer. There is no evidence for a transition to long-range ordering. The χ_m^{-1} values above 100 K were fitted with the Curie-Weiss law $\chi = C/(T-\theta)$ with a Curie constant C = 0.43 cm^3 K mol^{-1} for **III-1** and 0.45 cm^3 K mol^{-1} for **III-5**, yielding g = 2.14 for **III-1** and 2.19 for **III-5.** Weiss constants θ are +17.4 K for **III-1** and +19.1 K for **III-5** indicating dominant ferromagnetic coupling *via* μ_2-*syn-anti*-carboxylate bridges above 100 K. Both g and θ values agree very well to those values of $[Cu(HCO_2)(NO_3)(pyz)]_n$,[28] (g = 2.17 and θ = +17.4 K) which contains the same μ_2-*syn-anti* formato and μ_2-pyz spacer bridging between Cu^{II} centers (Figure 6).

As discussed previously, the adjacent Cu^{II} ions of **III-1** and **III-5** are linked by ferromagnetically μ_2-*syn-anti* carboxylato and antiferromagtically μ_2-ampyz which are the same as the reported rectangular 2D spin lattice of $[Cu(HCO_2)(NO_3)(pyz)]_n$. The analysis of the magnetic susceptibility for **III-1** and **III-5**, therefore 2D spin lattice is treated as chains, in which the intrachain spin exchange, J_{intra}, is negative and

the interchain spin exchange, J_{inter}, is positive. The effective susceptibility, χ_{eff} given by Hamiltonian $\hat{\boldsymbol{H}} = -\Sigma_{i,j} J \boldsymbol{S}_i \cdot \boldsymbol{S}_j$, is expressed in terms of the intrachain susceptibility, χ_{intra} and the interchain susceptibility, χ_{inter}, as[28]

$$\frac{1}{\chi_{eff}} = \frac{1}{\chi_{inter}} + \frac{1}{\chi_{intra}} \qquad (2)$$

The interchain susceptibility is given by

$$\chi_{inter} = -\frac{Ng^2\beta^2}{J_{inter}} \qquad (3)$$

The intrachain susceptibility is given by

$$\chi_{intra} = \frac{Ng^2\beta^2}{kT} \frac{0.25 + 0.14995x + 0.30094x^2}{1 + 1.9862x + 0.68854x^2 + 0.68854x^3} \qquad (4)$$

when

$$x = \frac{|J_{intra}|}{kT}$$

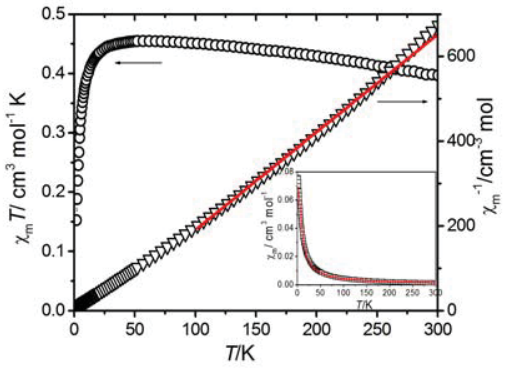

Figure 24 Temperature dependence of $\chi_m T$ and χ_m^{-1} of **III-1** from 2 to 300 K. Inset: plot of χ_m *vs.* T for **III-1**. The solid lines correspond to the best fit (see the text).

The least-square fitting analysis (inset of Figures 24 and 25) leads to the values of g = 2.17, J_{inter}/k = +6.9 K and J_{intra}/k = –2.3 K, $R = 2.2 \times 10^{-3}$ for **III-1** and g = 2.18, J_{inter}/k = +7.4 K and J_{intra}/k = –2.2 K, $R = 2.4 \times 10^{-3}$ for **III-5** (R is the agreement factor defined as $R = \Sigma[\chi_{m,\,calc} - \chi_{m,\,exp}]^2/(\chi_{m,\,exp})^2$. These g values practically close to the g values obtained from the Curie-Weiss law in the high temperature range and EPR spectra. The values of J_{inter} and J_{intra} show the same magnitude as those reported (J_{inter}/k = +8.2 K and J_{intra}/k = –5.4 K) for $[Cu(HCO_2)(NO_3)(pyz)]_n$[28]. However, it should be mentioned that both J_{intra} are lower than that found for $[Cu(HCO_2)(NO_3)(pyz)]_n$ which could be attributed to the less electron transfer in

the superexchange pathways for ampyz, due to an electron withdrawing amine group attached at the pyz ring.

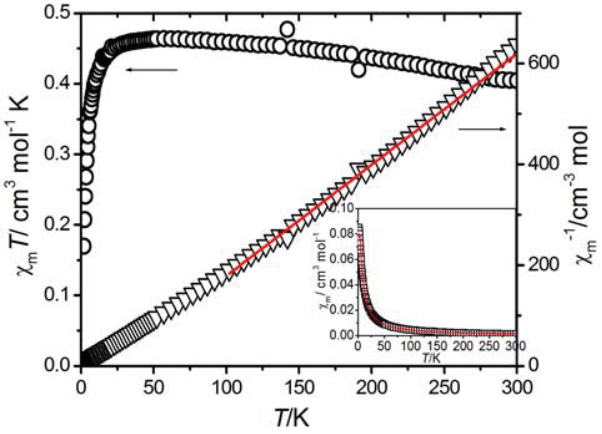

Figure 25 Temperature dependence of $\chi_m T$ and χ_m^{-1} of **III-5** from 2 to 300 K. Inset: plot of χ_m *vs. T* for **III-5**. The solid lines correspond to the best fit (see the text).

The magnetic properties of compounds **III-2-4** are in accordance with the earlier EPR observations. The $\chi_m T$ *vs. T* plots for one Cu^{II} ion of **III-2-4** are shown in Figures 26 and 27. For **III-2**, The $\chi_m T$ value per one Cu^{II} ion of ca. 0.18 cm^3 K mol^{-1} at 300 K is much smaller than value expected for uncorrelated Cu^{II} ion (0.375 cm^3 K mol^{-1} for g = 2), owing to the very strong antiferromagnetic coupling *via* four μ_2-*syn-syn* acetate bridging between Cu^{II} ions. Upon cooling from 300 K, $\chi_m T$ value smoothly decreases to 0.00 cm^3 K mol^{-1} at around 95 K, staying constant until 20 K. This magnetic behavior agrees with a very strong antiferromagnetic interaction which is well-known for the classical paddle-wheel type dicopper(II) tetracarboxylates (J ~ –300 to –400 cm^{-1}).[47, 49-54]

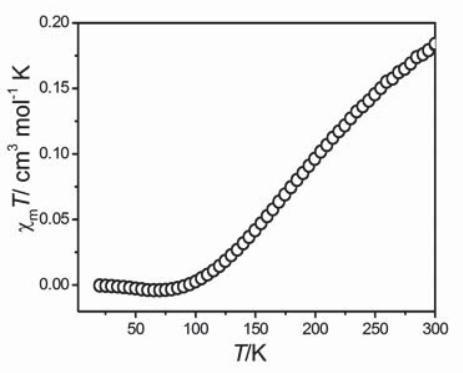

Figure 26 Temperature dependence of $\chi_m T$ of **III-2** from 20-300 K.

For **III-3** and **III-4**, At 300 K the $\chi_m T$ value per one Cu^{II} ion is almost diamagnetic and has a value at around 0.04 cm^3 K mol^{-1} for **III-3** and 0.02 cm^3 K mol^{-1} for **III-4**, which is much lower than the value expected for one uncorrelated Cu^{II} ion (0.375 cm^3 K mol^{-1}), owing to the very strong antiferromagnetic coupling. Upon cooling the $\chi_m T$ products gradually decrease and reach a plateau giving the minimum of –0.02 cm^3 K mol^{-1} for **III-3** and –0.03 cm^3 K mol^{-1} for **III-4** at around 100 K, then finally increase to 0.00 cm^3 K mol^{-1} at 2 K. This magnetic behavior agrees with a very strong antiferromagnetic interaction. It should be noted that the very much small $\chi_m T$ values of **III-3** and **III-4** should be attributed from an error in the SQUID system during the measurement which was not well working. The increase of $\chi_m T$ again at low temperature is due to the presence of a noncoupled Cu^{II} impurity which was clearly observed in EPR spectra at 77 K.[59]

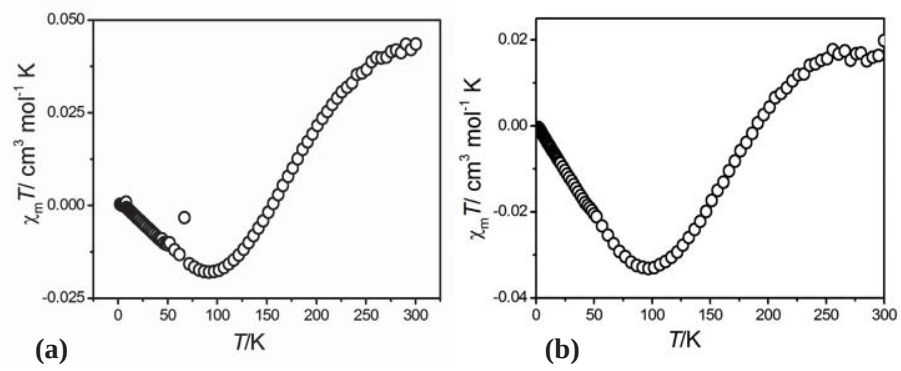

Figure 27 Temperature dependence of $\chi_m T$ of **III-3** (a) and **III-4** (b) from 2-300 K.

3.2 Reversible structural transformation with chromotropism in metal supramolecular frameworks containing aminopyrazine and sulfate anions

Flexible and dynamic molecular solids recently have received great attention because of their fascinating architectures with promising functional properties. Particularly, the guest removal and re-adsorption in metal-organic frameworks are of interest for many potential applications especially in the areas of gas storage and sensors.[60-68] The guest-induced crystalline-to-amorphous transformation and the guest-induced backward transformation are characteristic of the 3rd generation compounds (Figure 1.16) which are typically found in the flexible coordination frameworks supported by weak molecular interactions, such as hydrogen bonds, π–π stacking, van der Waals forces and others.[60, 61] Whereas, such reversible structural transformations in non-coordination supramolecular systems are not common[69-78] since the structural destruction accompanying with the guest removal is too severe to recover the crystallinity after re-adsorption process, contrastive to the cases of the flexible coordination polymers which contain the bridging spacers maintaining the skeleton of whole structures. Within the field of

inorganic-organic supramolecular chemistry, the utilization of transition metal ions and organic spacers can form a number of extended frameworks through either coordination or weak intermolecular interactions.[13, 14, 79-83] It is known that the metal sulfate is a good candidate for constructing the open-framework materials along with other organic spacers, especially *N,N′*-ditopic spacers, yielding various supramolecular architectures because sulfate anion (SO_4^{2-}) can behave as a versatile connector playing the role of monodentate ligand, bridging ligand, and good hydrogen acceptor.[84-90] For examples, $[Co_2(bipy)_3(SO_4)_2(H_2O)_2](bipy)(CH_3OH)$[85] and $[Co(SO_4)(H_2O)_3(bipy)]$ $(H_2O)_2$[86] (bipy = 4,4′-bipyridine) show distinctive structures supported by sulfate ions. Likewise, the structural diversity were also observed in Cu^{II} pyrazine complexes containing sulfato ligand.[87, 88]

3.2.1 General observations and spectroscopic characterizations

The layering diffusion reaction of metal(II) sulfate with ampyz in 1:2 molar ratio in a mixture of ethanolic and aqueous media yielded high purity single-crystals of **IV-1-4**. The IR spectra of four compounds (Figure 28) show strong bands in the region 3400-3100 cm^{-1} which can be assigned to the stretching ν(N–H) of the primary amine in the ampyz ligand overlapping with ν(O–H) of water molecule. The NH_2 scissoring mode[91] shows medium bands around 1660-1640 cm^{-1} and the strongest bands due to SO_4^{2-} stretching vibrations are observed around 1100 cm^{-1}.[92]

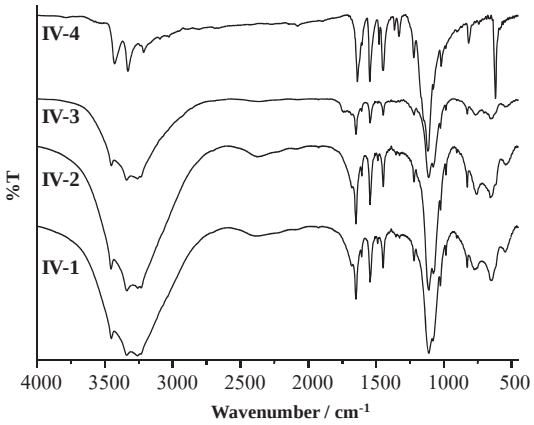

Figure 28 Infrared spectra for compounds **IV-1-4**.

The solid-state UV-vis diffuse reflectance spectra of **IV-1-4** are depicted in Figure 29. The spectrum of **IV-1** agrees with the typical *d-d* transition of high-spin Co^{II} in octahedral geometry with two observed bands at 22,000-19,500 and less than 9,000 cm^{-1}, which are assigned to the $^4T_{1g} \rightarrow {}^4T_{1g}(P)$ and $^4T_{1g} \rightarrow {}^4T_{2g}$ transitions, respectively. For compound **IV-2**, the broad band around 11,700 cm^{-1} is attributed to the $^5T_{2g} \rightarrow {}^5E_g$ transition for high-spin Fe^{II} in octahedral geometry.[93] The bands which appear at higher than 24,000 cm^{-1} due to charge transfer transition and internal transition within ampyz. Whereas compound **IV-3** is a

heterometallic complex, so the spectrum of **IV-3** shows the overlaying transitions between Co^{II} and Fe^{II} in octahedral geometries, resulting yellowish orange in the color which is between orange crystal of **IV-1** and yellow crystal of **IV-2**. Besides the crystallographic data, the positions of Co^{II} and Fe^{II} chromophores in **IV-3** were further verified by far-IR spectra (500–50 cm^{-1}) which yield the information of M–O and M–N vibrations in compounds **IV-1-3** as shown in Figure 30.

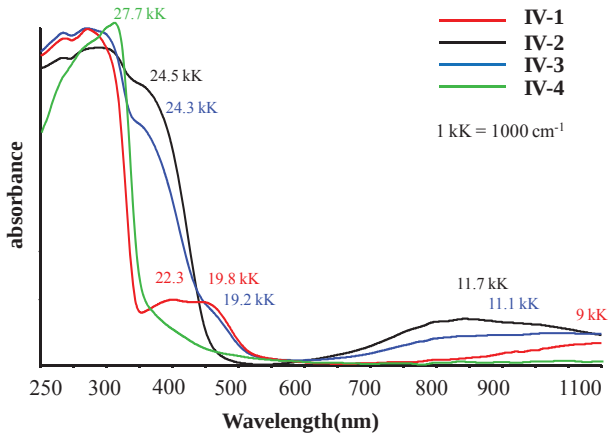

Figure 29 Solid-state UV-visible diffuse reflectance spectra for **IV-1-5**.

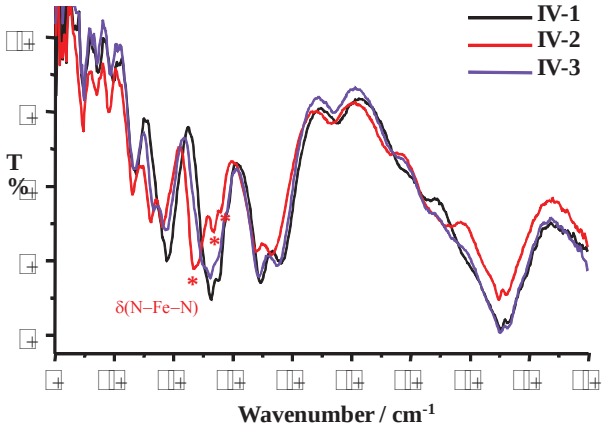

Figure 30 Far-IR spectra (500–50 cm^{-1}) of **IV-1-3**.

The far-IR spectrum of **IV-3** almost shows close resemblance to the spectrum of **IV-1**, especially in the range of 160–250 cm^{-1}, where the deformations of N–M–N and the asymmetric stretching vibrations of M–N . These low-frequency modes are sensitive to metal-ion mass and provide a clue to metal-site preference. This result strongly suggests that the Co^{II} ion in **IV-3** is accommodated in $[M(H_2O)_4(ampyz)_2]^{2+}$ unit rather than $[M(H_2O)_6]^{2+}$ unit, and supports the X-ray structure of $[Co(H_2O)_4(ampyz)_2][Fe(H_2O)_6](SO_4)_2(H_2O)_2$ for **IV-3**.

3.2.2 Description of crystal structures

$[Co(H_2O)_4(ampyz)_2][Co(H_2O)_6](SO_4)_2(H_2O)_2$ (IV-1)

$[Fe(H_2O)_4(ampyz)_2][Fe(H_2O)_6](SO_4)_2(H_2O)_2$ (IV-2)

and $[Co(H_2O)_4(ampyz)_2][Fe(H_2O)_6](SO_4)_2(H_2O)_2$ (IV-3)

Single-crystal X-ray diffraction analyses revealed that compounds **IV-1–3** are not only isostructural frameworks, but also form a beautiful isomorphous series and the structure of **IV-1** is only described in detail here. Crystal structure of **IV-1** is shown in Figure 31.

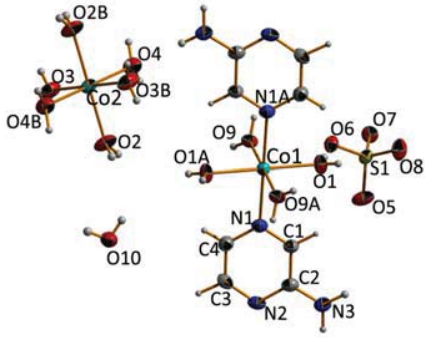

Figure 31 Crystal structure and atom labeling scheme of **IV-1**. The ellipsoids are shown at 50% probability level. Atoms labeled with the notation ''A'' and "B" are symmetry-generated equivalents, (A) *–x, 1–y, 1–z*; (B) *–x, 2–y, –z*.

Compound **IV-1** contains two crystallographically independent Co^{II} ions (Co1 and Co2) in $[Co(H_2O)_4(ampyz)_2]^{2+}$ and $[Co(H_2O)_6]^{2+}$ cationic units. Both Co^{II} ions are 6-coordinated and lie on independent inversion centers. Co1 shows elongated octahedral geometry comprised of four oxygen atoms from water molecules at equatorial positions with the average Co1–O distance of 2.0702(13) Å, and two nitrogen atoms from ampyz ligands at axial sites with Co1–N1 distance of 2.2071(16) Å. Co2 shows slightly compressed octahedron, surrounded by six water molecules with the average Co2–O bond length at equatorial plane of 2.1072(15) Å and the Co2–O3 distance at apical position of 2.0691(14) Å. The bond angles around octahedron are in the range of 87.33–180°, which are close to ideal octahedral geometry.

$[Co(H_2O)_4(ampyz)_2]^{2+}$ units are assembled by intermolecular hydrogen bonding between pyrazine nitrogen and hydrogen of coordination water along *b* axis [O9–H···$N2^i$ = 1.86 Å(173°), O9···$N2^i$ = 2.792(2) Å, (i) = *x, 1+y, z*.] and π-π stacking interaction among adjacent ampyz moieties along *a* axis with the separation of 3.417–3.557 Å, giving rise to 2D layer substructure in *ab* plane with the closest intermolecular Co···Co separation of 6.5697(4) Å (Figure 32). Moreover, these layers are supported by electrostatic forces and the intermolecular hydrogen bonds involving sulfate anions (O5–O8), amine

moieties on ampyz (N3), coordination waters in $[Co(H_2O)_6]^{2+}$ unit (O2–O4), and lattice water molecules (O10), to provide an entire 3D supramolecular structure of **IV-1** as shown in Figure 33.

The crystal structures of isostructures **IV-2-3** are depicted in Figure 34.

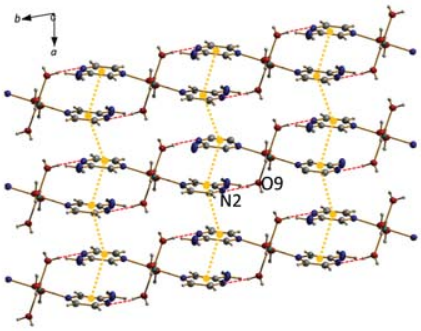

Figure 32 2D sheet structure of **IV-1** in the *ab* plane, assembled *via* the intermolecular π–π stacking and hydrogen bonding interaction which are represented in yellow and red broken lines, respectively.

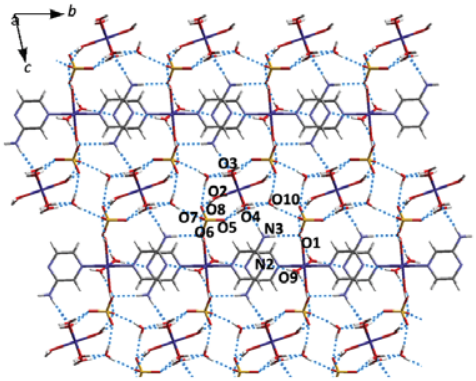

Figure 33 3D packing structure of **IV-1** in *bc* plane formed by intermolecular hydrogen bonding (blue dotted lines) among layers through ampyz, $[Co(H_2O)_6]^{2+}$ unit, SO_4^{2-}, lattice and coordination water molecules.

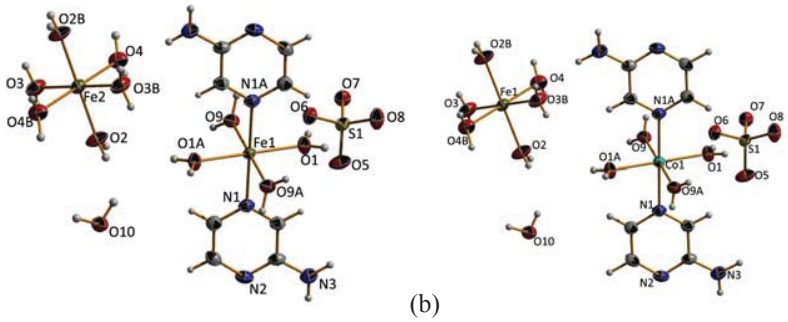

Figure 34 Crystal structure and atom labeling scheme of **IV-2** (a) and **IV-3** (b). The ellipsoids are shown at 50% probability level. Atoms labeled with the notation ‘‘A’’ and “B” are symmetry-generated equivalents, (A) *–x,* 1*–y,* 1*–z*; (B) *–x*, 2*–y*, *–z*.

$[Cd(ampyz)(H_2O)_2(SO_4)]_n(H_2O)_n$ (IV-4)

The coordination environment of the Cd^{II} center is shown in Figure 35. The Cd1 atom, sulfate atoms S1, O1, O2 and the water oxygen O4 all lie on a mirror plane in this structure. Each Cd^{II} ion is five-coordinated showing a distorted square-pyramidal CdN_2O_3 chromophore with $\tau = 0.04$.[44] The basal plane around the cadmium atom is comprised of one oxygen atom from coordination water (O4) and one oxygen atom from a μ_2-sulfato bridge (O2A) with the Cd–O distance of 2.303(6) and 2.297(5) Å, respectively and two ampyz-nitrogen atoms with the Cd–N distances of 2.315(4) Å. The apical position is occupied by a μ_2-sulfato oxygen (O2) with Cd–O2 length of 2.587(5) Å. The bond angles between axial shared with a neighbouring square pyramid and square corners are remarkably deviated from 90° and rather distorted from regular square pyramidal geometry of Cd^{II}.[94, 95] It is possibly attributed to three sulfato oxygen atoms excluded from μ_2–bridges, weakly interacting with adjacent Cd^{II} centers with Cd···O3 and Cd···O1 distances of 2.754(6) and 2.765(6) Å, respectively, forming the semi-eight coordination. The weak secondary bonds of Cd···O are also reported in other Cd^{II} complexes.[96-98]

The sulfato ligand acting as a monoatomic bridge connects Cd^{II} centers in *ac* plane, yielding the Cd^{II} dimer with the separation of 4.0359(5) Å. These Cd^{II} dimers are linked by the ditopic ampyz spacers along *b* axis leading to 1D ladder chain structure with Cd···Cd separation *via* ampyz of 7.3913(4) Å (see Figure 36). Moreover, when above-mentioned weak coordination bonds are considered, the inorganic double-stranded chain of metal sufate[84] is observed, which is comprised by CdN_2O_6 polyhedra and SO_4 tetrahedral units, as shown in Figure 36(a). The monoatomic sulfato bridge connects Cd^{II} ions, leading to edge-sharing CdN_2O_6 polyhedra that further share edges with tetradentate bridges of SO_4 tetrahedra to form a four-member ring ladder along *c*-axis. In addition this chain is linked by the ampyz spacers along *b* axis, giving rise to the 2D layer structure of **IV-4** as shown in Figure 36(b). The lattice water molecules (O5) are filled in between 2D sheets, which effectively provide the intermolecular hydrogen bonds with amine nitrogen of ampyz (N2), sulfato oxygen (O1, O3) and coordination water (O4), contributing to the stabilization of the overall 3D supramolecular structure as shown in Figure 37.

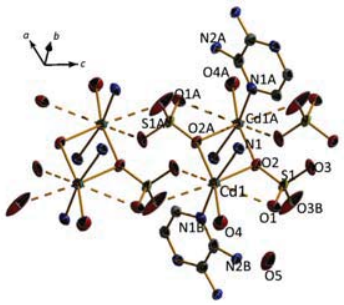

Figure 35 Expanded asymmetric unit and atom labeling scheme of **IV-4**.

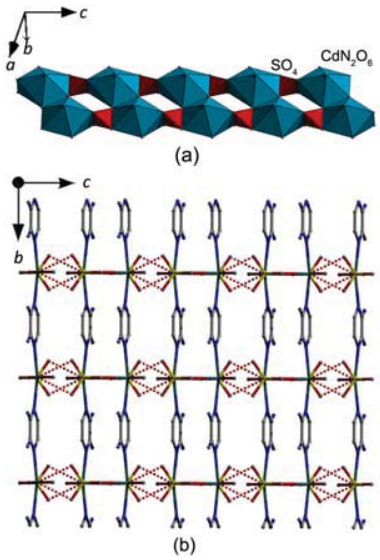

Figure 36 Double-stranded chain of $[Cd(ampyz)(H_2O)_2(SO_4)]_n$ (a).View of the 2D layer of **IV-4** in *bc* plane. The red broken lines represent the weak coordinative bonds between sulfate oxygen atoms and Cd(II) ions (b).

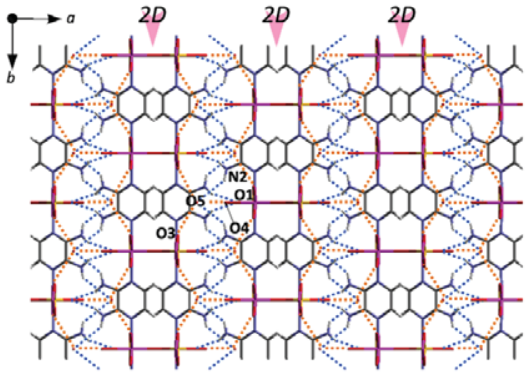

Figure 37 3D packing structure of **IV-4** in *ab* plane formed by intermolecular hydrogen bonding between layers and lattice water molecules. The blue and orange dotted lines represent the N2–H···O(1,5) and O5···O(4,3) intermolecular hydrogen bonds, respectively.

3.2.3 Reversible structural phase transformation with chromotropism

Thermogravimetric analyses

To examine the thermal stabilities of compounds **IV-1-4**, the TGA were performed in the temperature range 25–500°C, as shown in Figure 38.

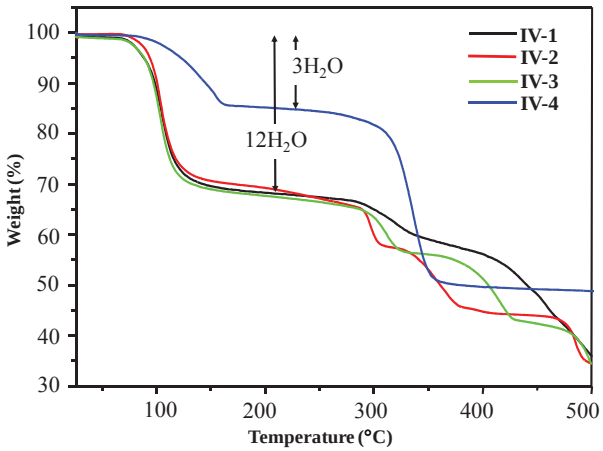

Figure 38 TGA curves of compounds **IV-1-4**.

The TGA profiles of **IV-1-3** indicate that the releases of all twelve water molecules including coordinated and lattice water molecules occur at the first step of weight loss in the temperature range 55–180°C (found, 31.46%; Anal. Calcd, 30.15% for **IV-1**; found, 29.44%; Anal. Calcd, 30.41% for **IV-2**; found, 31.48%; Anal. Calcd, 30.28% for **IV-3**), resulting to the dehydrated forms of $[M_2(ampyz)_2(SO_4)_2]$ (**IV-1A-3A**), which are stable up to ≈ 240°C and then the structures gradually decompose to the unidentified products. The TGA profile of **IV-4** shows two steps of weight loss. The first step (75–180°C) corresponds to the loss of all three water molecules (found, 15.20%; Anal. Calcd, 15.86%), resulting to the dehydrated forms of $[Cd(ampyz)(SO_4)]$ (**IV-4A**), which are stable up to ≈ 250°C. The second step (250-420°C) gives a mixture of the CdO and CdS as main products.

3.2.4 Water-induced reversible structural phase transformation with chromotropism

Aforementioned all compounds contain both lattice and coordination water molecules and weak intermolecular interactions stabilize entire 3D molecular frameworks. In addition the stable dehydrated forms of **IV-1A-4A** were clarified by TGA profiles. The dynamic structural behaviors of **IV-1-4** relating to their dehydration and rehydration processes are thus studied by elemental analyses, XRPD, and spectroscopic techniques.

When the single-crystals of **IV-1-4** were heated to 220°C in air for 30 minutes (Figure 39), these crystals suddenly lose the crystallinity and the colors changed from orange to purple for **IV-1**; yellow to orange for **IV-2**; yellowish orange to brown for **IV-3**; and no color changes was observed in colorless compound **IV-4**. Then these non-crystalline solids were exposed to the laboratory air for 8 hours and the colors of solids **IV-1A-3A** returned to their original crystalline ones. Consequently, the bulk samples of **IV-1-4** were used to study in the detail. The dehydrated forms of **IV-1A-4A** were obtained by heating the bulk

samples at 220°C in air for 4 hours and the rehydrated forms of **IV-1′-4′** were obtained by exposing the dehydrated samples to water vapor for 2 days at room temperature without condensation.

Figure 39 The colors of the single-crystals of **IV-1-4**, dehydrated forms of **IV-1A-4A** and rehydrated forms of **IV-1′-4′**.

The XRPD pattern of **IV-1** is shown in Figure 40. The TGA, elemental analysis of **IV-1A** (Anal. Calcd: C, 19.21; H, 2.02; N, 16.80%. Found: C,18.51; H, 2.10; N, 16.18%.) and XRPD results indicate that the dehydrated $[Co_2(ampyz)_2(SO_4)_2]$ (**IV-1A**) is in an amorphous phase which is formed by the collapse of supramolecular structure of **IV-1** accompanied with the destruction of hydrogen bonding networks when all water molecules are removed. The original crystalline phase $[Co(H_2O)_4(ampyz)_2][Co(H_2O)_6](SO_4)_2(H_2O)_2$ (**IV-1′**) can be restored from the amorphous phase of **IV-1A** after rehydration process which confirmed by the elemental analysis (Anal. Calcd: C, 13.41; H, 4.78; N, 11.73%. Found: C,13.39; H, 4.29; N, 11.72%.) and the XRPD pattern. These results suggest the crystalline-to-amorphous and amorphous-to-crystalline transformations in supramolecular network of **IV-1** triggered by the hydration control. Furthermore, this structural change of bulk sample is accompanied with a remarkable color change as confirmed by the solid-state UV-vis diffuse reflectance spectra in Figure 41 for **IV-1**. The UV-vis spectra clearly show that the bands observed in **IV-1** and **IV-1′** correspond very well to the identical transitions causing the same color of bulk products, and evidence that **IV-1** and **IV-1′** have the same Co^{II} environments.

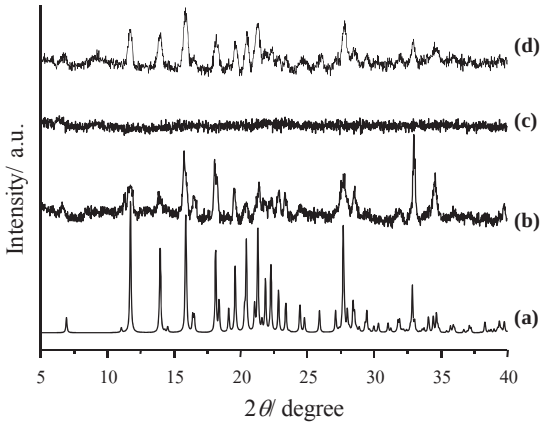

Figure 40 XRPD patterns: simulated from single-crystal X-ray data (a); as-synthesize **IV-1** (b); the dehydrated form **IV-1A** (c); the rehydrated form **IV-1′**(d).

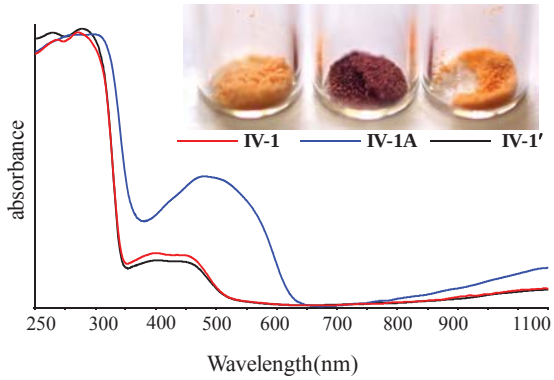

Figure 41 The UV-vis diffuse reflectance spectra of as-synthesize **IV-1** (red line), the dehydrated form **IV-1A** (blue line), and the rehydrated form **IV-1′** (black line), representing together with the chromatic changes in bulk samples.

Whereas the amorphous phase **IV-1A** shows the different *d-d* transition with a lower-energy broad band centered around 550 nm, giving the distinctive purple color. The chromotropic behaviors of **IV-1** are principally ascribed to the changes of the *d*-orbital energy level, induced by the drastic change in the coordination environments around metal center during dehydration and rehydration processes.[85, 99-101] In addition, these results agree with the reversible change of the sulfate vibrational band in IR spectra (Figure 42) where the different splitting peaks at ~1100 (ν_3) and ~630 cm^{-1} (ν_4) are observed for the amorphous phase, indicating that site symmetry at sulfate ions is lowered.[92] Reversely, these splits are removed in the IR spectra of the rehydrated form, which are identical to those of as-synthesized one. All of results confirm the water-induced reversible crystalline-to-amorphous phase transformation with chromotropism in supramolecular network of **IV-1**. This phenomenon is also observed in the isostructural **IV-2** and **IV-3**. The XRPD patterns, IR and UV-vis spectra of **IV-2-3** are given in Figure 43-48. The spectrum of **IV-3A** shows

the overlap bands between **IV-1A** and **IV-2A** indicating that **IV-3A** is also a hetero-metallic compound (Figure 47).

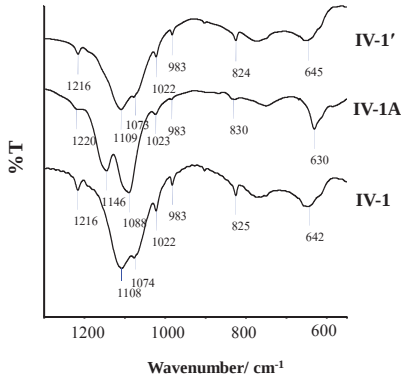

Figure 42 IR spectra (1300-550 cm^{-1}) for as-synthesize **IV-1**, the dehydrated form **IV-1A** and the rehydrated form **IV-1′**.

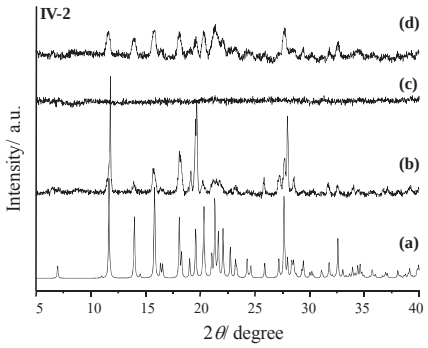

Figure 43 XRPD patterns: simulated from single-crystal X-ray data (a); as-synthesize **IV-2** (b); the dehydrated form **IV-2A** (c); the rehydrated form **IV-2′**(d).

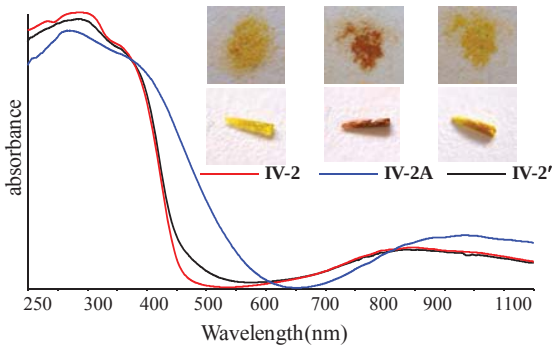

Figure 44 The UV-vis diffuse reflectance spectra of as-synthesize **IV-2** (red line), the dehydrated form **IV-2A** (blue line), and the rehydrated form **IV-2′** (black line), representing together with the chromatic changes in bulk samples.

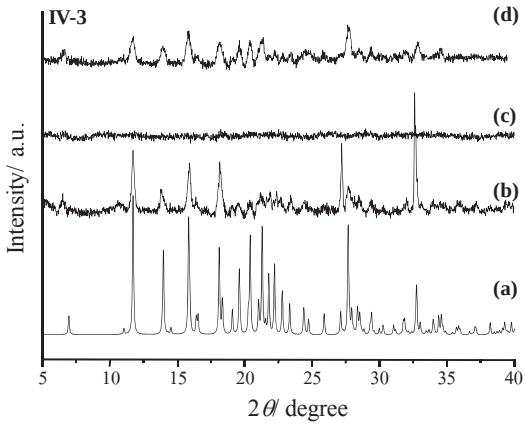

Figure 45 XRPD patterns: simulated from single-crystal X-ray data (a); as-synthesize **IV-3** (b); the dehydrated form **IV-3A** (c); the rehydrated form **IV-3′**(d).

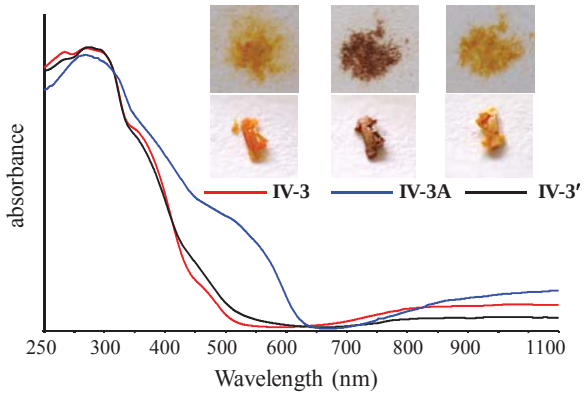

Figure 46 The UV-vis diffuse reflectance spectra of as-synthesize **IV-3** (red line), the dehydrated form **IV-3A** (blue line), and the rehydrated form **IV-3′** (black line), representing together with the chromatic changes in bulk samples.

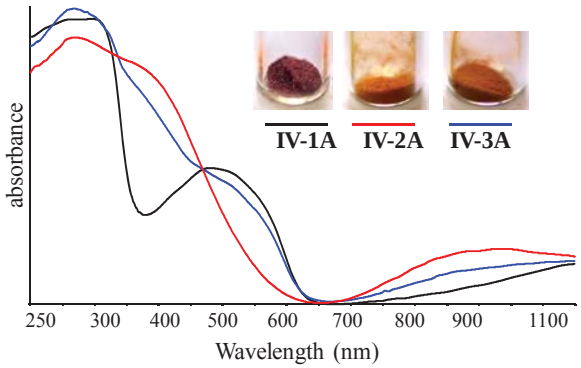

Figure 47 UV-vis diffuse reflectance spectra of the dehydrated compounds **IV-1A**–**3A**, represented together with the colors of their dehydrated samples. The spectrum of **IV-3A** shows the overlap bands between **IV-1A** and **IV-2A** indicating that **IV-3A** is also a hetero-metallic compound.

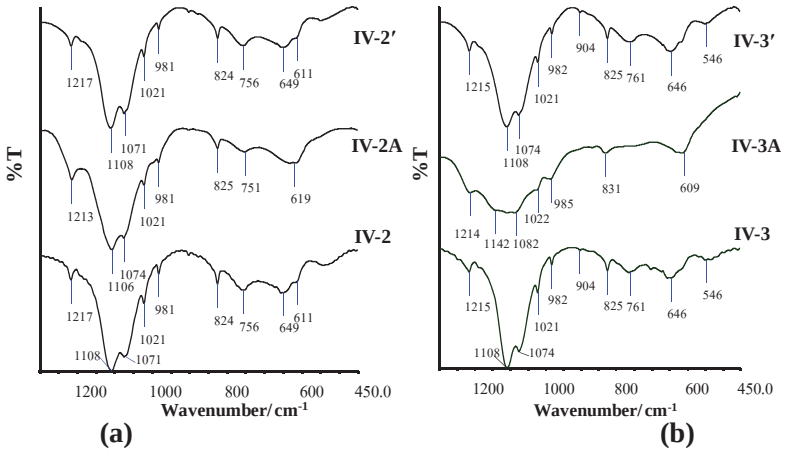

Figure 48 IR spectra (1300-450 cm^{-1}) for as-synthesize **IV-2**(a), **IV-3**(b), the dehydrated form **IV-2A** (a), **IV-3A** (b) and the rehydrated form **IV-2′** (a), **IV-3′**(b).

On the other hand, the coordination network **IV-4** exhibits the structural phase change in the dehydrated phase, [Cd(ampyz)(SO_4)] (**IV-4A**) which reveals the different XRPD pattern comparing with as-synthesized **IV-4** (Figure 49). Interestingly, this crystalline phase is converted to the same structure of original one (**IV-4′**) by rehydration process, which can be confirmed by the XRPD, IR-spectra (Figure 50), and elemental analysis. These results confirm the water-induced structural phase transformation in coordination network **IV-4**.

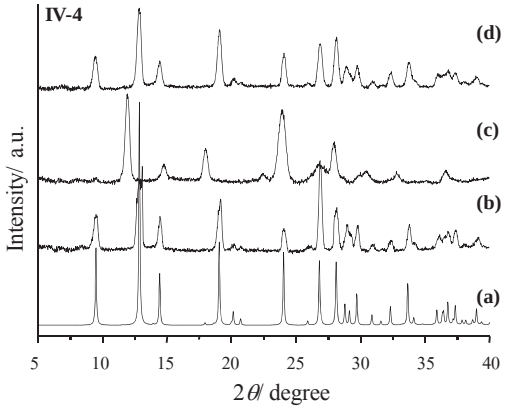

Figure 49 XRPD patterns: simulated from single-crystal X-ray data (a); as-synthesize **IV-4** (b); the dehydrated form **IV-4A** (c); the rehydrated form **IV-4′**(d).

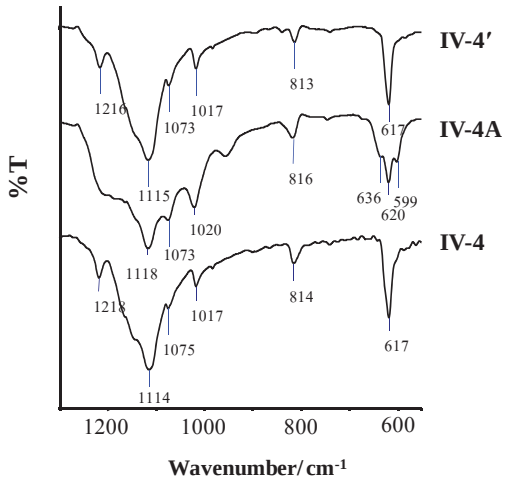

Figure 50 IR spectra (1300-550 cm^{-1}) for as-synthesize **IV-4**, the dehydrated form **IV-4A** and the rehydrated form **IV-4′**.

When the lattice and coordination water molecules are removed, the supramolecular networks **IV-1-3** collapse due to the destruction of the hydrogen bonding networks while the coordination polymer **IV-4** does not collapse but exhibits another crystalline phase. This result indicates that the coordination bridges *via* ampyz spacer and sulfato ligand play an important role for supporting the structural skeleton in **IV-4**. Remarkably, all compounds recover original crystalline phases after the exposure to water vapor, indicating that the significant role of hydrogen bonding through water molecules can trigger the reformation of other weak intermolecular interactions such as π–π stacking among ampyz moieties in **IV-1-3** and other hydrogen bonds through sulfate ions in **IV-1-4**.

3.2.5 Selective guest accommodation with chromotropism

One of the interesting aspects of cobalt in contrast to nickel, iron and manganese is the range of stable geometries, such as octahedral, tetrahedral, square pyramidal, trigonal bipyramid and square-planar together with a wide range of colors.[102] Consequently, in order to investigation of the guest-induced structural transformation phenomena, the dehydrated $[Co_2(ampyz)_2(SO_4)_2]$ (**IV-1A**) was used to study with various solvents, *i.e.* methanol, ethanol, propanol, butanol, acetone, acetonitrile, tetrahydrofuran and dichloromethane. The dehydrated **IV-1A** was exposed to solvent vapor for 2 days at room temperature in a closed vial. Remarkably the chromotropism is observed only in **IV-1A** which was exposed to methanol vapor (**IV-1A·MeOH**) and the colors change from purple (**IV-1A**) to red (**IV-1A·MeOH**). For other ones, the purple solids (**IV-1A**) still remain. IR spectra of all compounds including **IV-1A·MeOH** show the vibrational bands as same as those of dehydrated **IV-1A** (Figure 51) indicating the similar environments of

functional groups that are observed in amorphous phase **IV-1A**. The dynamic structural behaviors of **IV-1A** relating to the accommodation of methanol are studied in details by TGA, XRPD and spectroscopic techniques. The red solid **IV-1A·MeOH** which was obtained by exposing the purple dehydrated **IV-1A** to methanol vapor shows the amorphous phase as confirmed by XRPD patterns (Figure 52). However, the **IV-1A·MeOH** easily loses methanol molecules after exposing in laboratory air within 2 hrs and the colors change from red (**IV-1A·MeOH**) to the original orange crystalline sample (**IV-1″**), as depicted in Figure 53. Furthermore after heating **IV-1A·MeOH** at ≈200°C for 10 min the color changes from red (**IV-1A·MeOH**) to the previous purple sample (**IV-1A**) which denotes the reversible process of methanol accommodation in **IV-1A** with chromotropism. These results agree with the thermal analysis of **IV-1A·MeOH** in the temperature range 25–500°C as depited in Figure 54. The TGA profile indicates that the release of four methanol molecules from $[Co_2(ampyz)_2(SO_4)_2](MeOH)_4$ (**IV-1A·MeOH**) occurs at room temperature to ≈220°C (found, 80.85%; Anal. Calcd, 80.15%) resulting to the dehydrated forms of $[Co_2(ampyz)_2(SO_4)_2]$ (**IV-1A**), which are stable up to ≈240°C and then the structures gradually decompose to the unidentified products. The XRPD and IR spectrum of **IV-1″** which was obtained by the evaporation of methanol from **IV-1A·MeOH** in laboratory air, reveal the identical XRPD positions and IR bands to the original crystalline **IV-1** (Figures 51 and 52). These results are indication of high selective recognition of **IV-1A** to water molecules. The selective methanol accommodation with chromotropism in dehydrated **IV-1A** when comparing with many solvents excluding water could be attributed to proper size of methanol molecule and weak host-guest interactions. The remarkable color change was also confirmed by the solid-state UV-vis diffuse reflectance spectrum in Figure 55. The spectrum of **IV-1A·MeOH** agrees with the typical *d-d* transition of high-spin Co^{II} in octahedral geometry with two observed bands at 21,200–19,300 and less than 9,000 cm^{-1}, which are assigned to the $^4T_{1g} \rightarrow {}^4T_{1g}(P)$ and $^4T_{1g} \rightarrow {}^4T_{2g}$ transitions, respectively. These bands are slightly shifted to a lower energy when evaluating with the bands of **IV-1**, resulting the distinctive red color. As found in nature, cobalt-containing MOFs can have a wide range of colors which makes it easy, in many cases, to identify different phases. The most common colors are a very light pink for octahedral coordinated ones and an intense blue for tetrahedral coordination. For distorted octahedra, the pink color can intensify to orange, dark red, purple and violet depending on the ligand and the type of distortions.[102] The selective guest accommodation with chromotropism of **IV-1** is summarized in Figure 56.

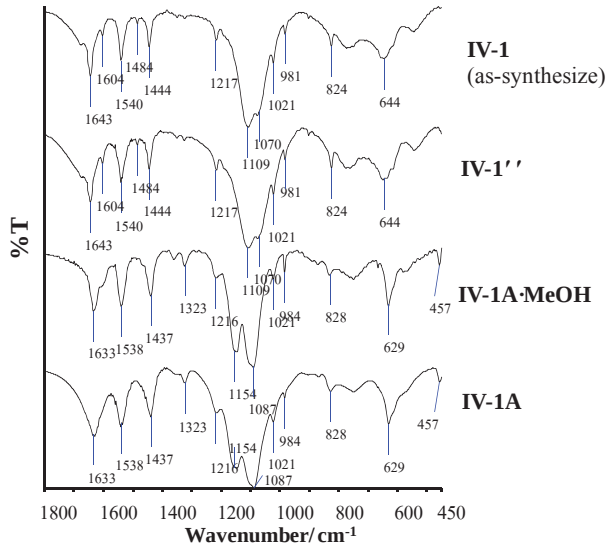

Figure 51 IR spectra for the dehydrated form **IV-1A**, the methanolic form **IV-1A·MeOH**, the rehydrated form **IV-1′′** and as-synthesize **IV-1**.

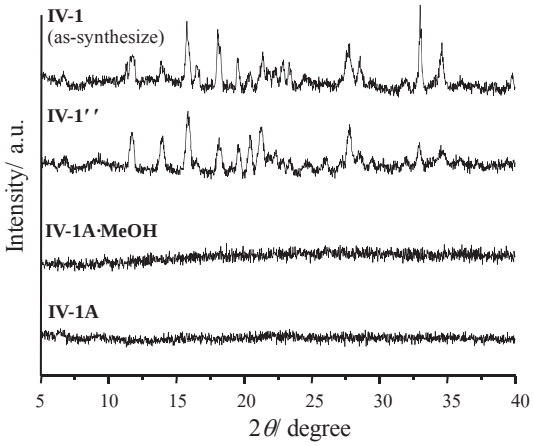

Figure 52 XRPD patterns for the dehydrated form **IV-1A**, the methanolic form **IV-1A·MeOH**, the rehydrated form **IV-1′′** and as-synthesize **IV-1**.

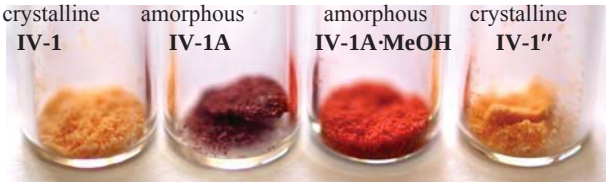

Figure 53 The chromatic changes in bulk samples**.**

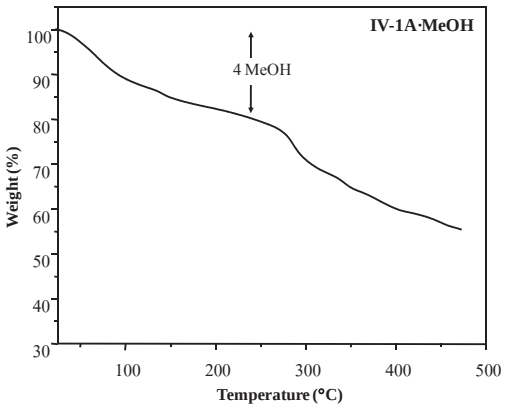

Figure 54 TGA curve of **IV-1A·MeOH**.

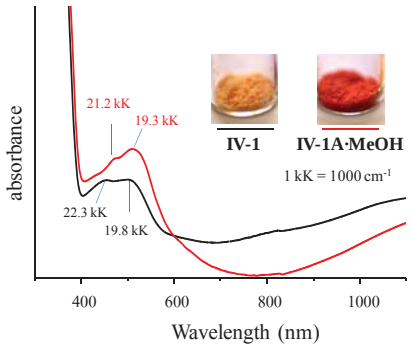

Figure 55 UV-vis diffuse reflectance spectra of as-synthesize **IV-1** (black line) and **IV-1A·MeOH** (red line).

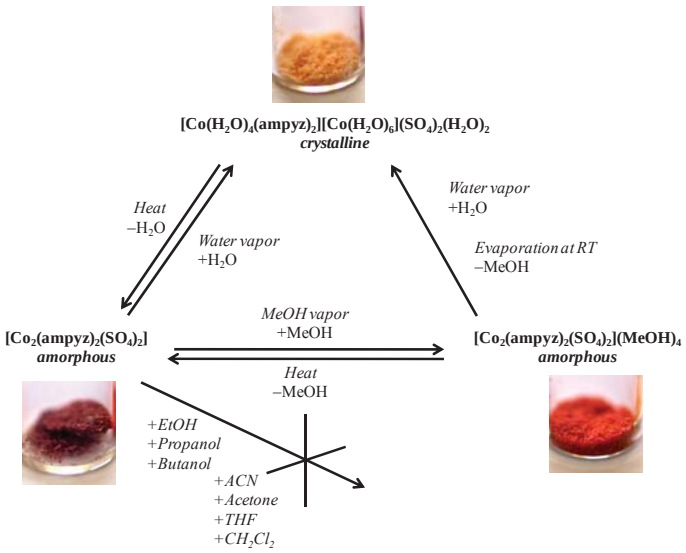

Figure 56 Selective guest accommodation with chromotropism of **IV-1**.

3.3 2D-1D Structural Phase Transformation of Co(II) 3,5-Pyridinedicarboxylate Frameworks with Chromotropism

3.3.1 Syntheses

Compound $[Co(pydc)(H_2O)_2]_n$ (**IV-5**) as well-shaped, high purity, and high quality single crystals suitable for X-ray diffraction was obtained by the direct reaction of the cobalt(II) nitrate hexahydrate with 3,5-pyridinedicaboxylic acid (H_2pydc) and potassium hydroxide in mixture of methanol, *N,N′*-dimethylformamide and aqueous media. Whereas the layering diffusion of aqueous solution of cobalt(II) nitrate hexahydrate into a *N,N′*-dimethylformamide solution of 3,5-pyridinedicaboxylic acid resulted in the single crystal formation of compound $[Co(pydc)(H_2O)_4]_n(H_2O)_n$ (**IV-6**). These crystalline solids are stable in air and insoluble in water or common organic solvents such as methanol and ethanol. The 2D and 1D cobalt(II) coordination polymers containing two different coordination modes of 3,5-pyridinedicaboxylate bridges were obtained. The structures of **IV-5** and **IV-6** are described in the details here.

3.3.2 Description of crystal structures

$[Co(pydc)(H_2O)_2]_n$ (IV-5)

The coordination environment of the Co(II) center is shown in Figure 57a. The Co^{2+} ions, with a $CoNO_4$ chromophore, have an intermediate geometry with a τ value of 0.57. The Co^{2+} ions is five-coordinated with a basal plane consisting of two oxygen atoms from coordination water molecule (O3 and O3A) with the Co–O distance of 2.075(1) Å and two oxygen atom from pydc bridges (O2 and O2A) with the Co–O distance of 2.149(1) Å. The apical position is occupied by nitrogen atom from pydc bridge (N1B) with the Co–O length of 2.188(2) Å. In addition, weak interactions are formed by two pydc-oxygen atoms (O1 and O1A) with the Co···O distance of 2.431(2) Å, forming seven-coordination. These secondary Co···O bonds are also reported in other Co complexes, for example, $[Co(4,4'\text{-bipy})_{1.5}(NO_3)_2]$, $[Co(1,2\text{-bis}(4\text{-pyridyl})\text{ethane})_{1.5}(NO_3)_2]_n$, $[Co(1,2\text{-bis}(4\text{-pyridyl})\text{ ethyne})_{1.5}(NO_3)_2](MeOH)$ and $[Co(1,4\text{-bis}(3\text{-pyridyl})\text{-}2,3\text{-diaza-}1,3\text{-butadiene})_{1.5}(NO_3)_2(H_2O)]_n$.[22] However, the Co···O bond distances that found in compound **IV-5** are significantly longer than those in the reported compounds; therefore, it can be considered as semi-coordination.

The $pydc^{2-}$ anion is not planar since the dihedral angles between the carboxylate group and the pyridyl ring is 13.62°. Each pydc act as tridentate ligand bridging three adjacent Co(II) centers. Two carboxylate groups are all deprotonate and coordinate to two cobalt atoms in a monodentate fashion, and pydc-nitrogen atom coordinates to the third cobalt atom, forming an infinite 2D layer structure in *ab* plane as shown in Figure 57b.The three metal centers are in an isosceles triangle with the edge lengths (Co···Co separations) of 9.887(1) and 7.759(1) Å. Such unit repeats along the *ab* plane to generate an infinite 2D honeycomb network, which contains edge-sharing hexagons, with the metal ion and the

geometrical center of the pyridyl ring of pydc ligand being the vertex alternately and each arm of pydc ligand being the edge (Figure 58a). The layers are stacked together in an ABAB-sequence with the distance between layers of 3.566 Å, resulting in novel layer structures, eschewing interpenetration.

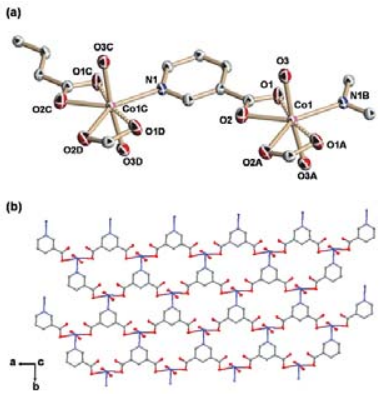

Figure 57 (a) Expanded asymmetric unit and atom labeling scheme of **IV-5**. The ellipsoids are shown at 50% probability level. Atoms labeled with the notation A, B, C and D are symmetry-generated equivalents, (A) -x,y,1/2-z; (B) -1/2+x,1/2+y,z; (C) 1/2+x,-1/2+y,z; (D) 1/2-x,-1/2+y,1/2-z. The dash lines present the weak coordinative bonds between pydc oxygen atoms and Co(II) ions and hydrogen atoms are omitted for the clarity. (b) 2D layer structure of **IV-5** in the ab plane.

These adjacent 2D sheets are mutually interlinked via the π-π interactions between the pyridyl rings of pydc in adjacent layers with a distance of 3.813 Å. (Figure 58a) an the 3D supramolecular architecture is further reinforced by strong interlayer hydrogen bonding among the carboxylate groups of $pydc^{2-}$ ligands and coordinated water molecules (O(3)-H(1)···O(2) and O(3)-H(2)···O(1)) with O···O distances of 2.795(1) and 2.771(1) Å as shown in Figure 59.

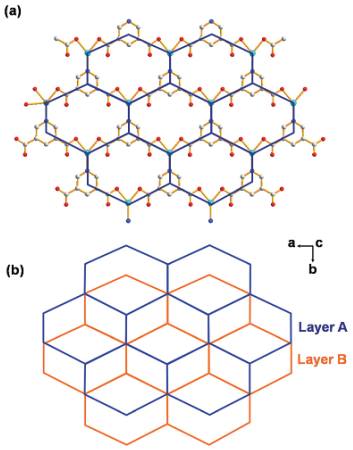

Figure 58 (a) Perspective view of the 2D layer with the honeycomb structure (blue line). (b) Schematic view of the two layers showing the honeycomb structure stacking viewed along *c*-axis.

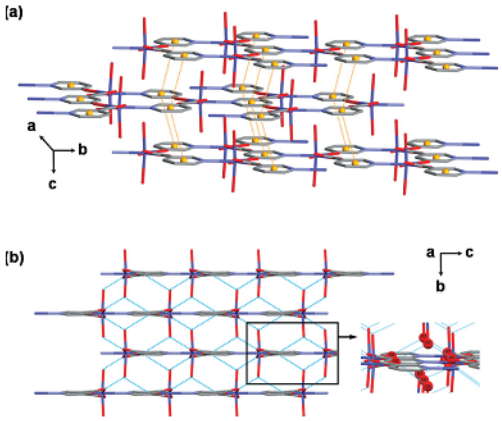

Figure 59 (a) The 3D framework formed by the intermolecular π-π interactions between the layers of **IV-5**. (b) Packing diagram of 3D network showing zig-zag arrangement of layers viewed along *a*-axis. The hydrogen bonding between the layers are shown in blue broken lines. The inset presents the hydrogen bonds from coordinated water molecules and carboxylate oxygen of pydc ligands.

$[Co(pydc)(H_2O)_4]_n(H_2O)_n$ (IV-6)

Asymmetric unit of compound **IV-6** consists of two crystallographically independent Co^{2+} ions which are sited at the crystallographic symmetry center with half site occupancy, one $pydc^{2-}$ anion, four coordinated and one uncoordinated water molecules as shown in Figure 60. Co1 shows elongated octahedral geometry comprised of four oxygen atoms from water molecules at equatorial positions with the average Co1–O distance of 2.0850(10) Å, and two nitrogen atoms from pydc ligands at axial sites with Co1–N1 distance of 2.1698(12) Å. Co2 also shows an elongated octahedral geometry, surrounded by four water molecules at equatorial plane with the average Co2–O bond length of 2.0840(11) Å and two pydc-oxygen atoms at apical positions with the Co2–O6 distance of 2.0980(9) Å. The O/N−M−O/N bond angles are in the range of 84.63(5)−180.00(7)°, which are close to the ideal octahedral geometry.

The pydc acts as a didentate ligand connecting two Co, leading to a 1D zig-zag chain running along *c* axis with the Co···Co separation of 7.372(1) Å as shown in Figure 61a. These adjacent 1D chains are mutually interlinked via the hydrogen bonds between the carboxylate groups of $pydc^{2-}$ ligands, uncoordinated and coordinated water molecules, forming a 2D hydrogen-bonded layer as shown in Figure 61b. Additionally, these 2D layers are arrayed orderly in a staggered ABAB... packing pattern viewing along the crystallographic *b*-axis with a distance of 3.675 Å between the pyridyl rings of the adjacent layers and then extended to a 3D network, via the π−π interactions between the pyridyl rings of $pydc^{2-}$ ligands as shown in Figure 62a, forming 1D channels along the crystallographic *b* axis with guest water molecules inside as shown in Figure 62b. The 3D supramolecular architecture is further reinforced by the O−H···O

hydrogen bonding among the coordinated water molecules and $pydc^{2-}$ ligands with the O···O distances in the range of 2.651(1)-2.831(1) Å.

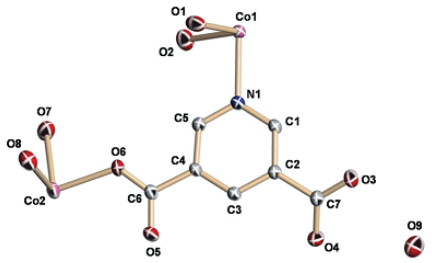

Figure 60 Asymmetric unit and atom labeling scheme of **IV-6**. The ellipsoids are shown at 50% probability level. All hydrogen atoms are omitted for the clarity.

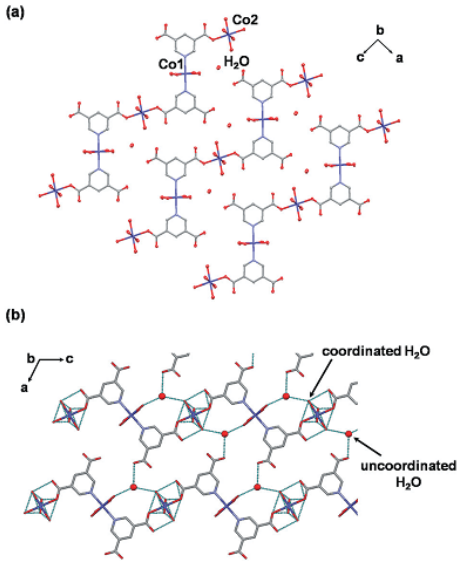

Figure 61 (a) 1D zig-zag chain of **IV-6** in the *ac* plane formed by the Co(II) and $pydc^{2-}$ ligand. Water molecule filled in the cavity between chains. (b) The 2D hydrogen-bonded layered network via hydrogen bonds between $pydc^{2-}$ ligands, coordinated- and uncoordinated water molecules among the 1D zig-zag chains (blue dash lines). All hydrogen atoms are omitted for the clarity.

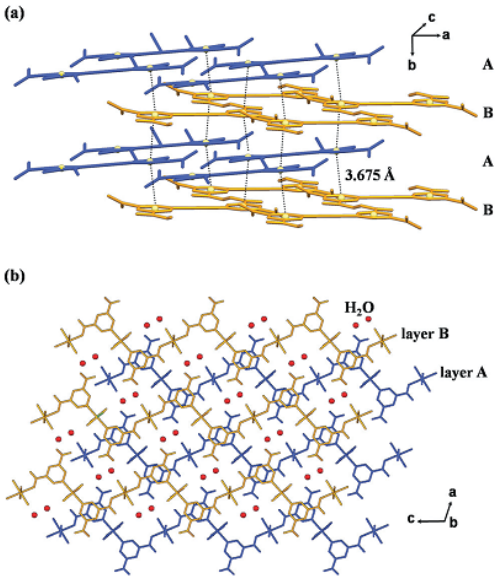

Figure 62 (a) Formation of the 3D framework in **IV-6** by face-to-face π···π interactions between staggered ABAB sheets (black dash lines). Uncoordinated H_2O are omitted for the clarity. (b) Packing diagram of **2** viewed along *b*-axis, showing 1D channels with guest water molecule inside.

3.3.3 Thermogravimetric Analysis

To assess the thermal stability, the thermal gravimetric (TGA) was recorded for the single-phase polycrystalline samples in the temperature range 30–800 ˚C. During the heating process, the TGA profile of **IV-5** (indicates that the releases of two coordinated water molecules occur at the first step of weight loss in the temperature range 80-190 ˚C (found, 13.71%; Anal. Calcd, 13.84%), resulting to the dehydrated form of [Co(pydc)] (**IV-5A**), which are stable up to ≈340 ˚C and then the structure rapidly decomposes at higher temperatures. For compound **IV-6**, TGA curve revealed that compound **IV-6** underwent a two-step weight loss. One solvated and four coordinated water molecules were loss below 190 ˚C with the weight loss of 26.19% (calcd. 28.68%), resulting to the dehydrated form of [Co(pydc)] (**IV-6A**). This dehydrated form **IV-6A** is stable up to ≈340 ˚C and then rapidly decomposes to the unidentified products.

3.3.4 Structural Phase Transformation by Thermal De/Rehydration Processes.

To verify the dynamic structural behavior of compounds **IV-5** and **IV-6**, the ad/desorption of coordinated and uncoordinated water molecules in both compounds have been studied relating to their dehydration and rehydration processes by elemental analyses, TGA, XRPD and spectroscopic techniques. Interestingly, the water molecules can be adsorbed fully by exposing the

evacuated samples to water vapor at room temperature. The heating and exposing procedures were repeated for four times to demonstrate the reversibility of the de- and rehydration processes.

The most promising feature of the crystals of **IV-5** is that it undergoes the water induced irreversible crystal-to-amorphous transformation with chromotropism driven by thermal dehydration and rehydration. When the single crystals of **IV-5** was heated to 200 ˚C in air for 30 min, these crystals suddenly lose the crystallinity and the colors changed from deep pink (**IV-5**) to purple (**IV-5A**). Then this non-crystalline solid was exposed to the water vapor for 12 h and the color of solid **IV-5A** was not return to that of the original crystalline one but change to pale orange (**IV-5B**). Therefore, the bulk sample of **1** was used to study in detail. The dehydrated form **IV-5A** was obtained by heating the bulk samples at 200 ˚C in air for 2 h and the rehydrated form **IV-5B** was obtained by exposing the dehydrated sample to water vapor for 24 h at room temperature without condensation. The XRPD pattern and TGA curve of **IV-5** are shown in Figures 63 and 64. The elemental analysis of **IV-5A** for [Co(pydc)] (Anal. Calcd: C, 37.53; H, 1.35; N, 6.25%. Found: C, 37.37; H, 1.41; N, 6.28%), and XRPD results indicate that the dehydrated form **IV-5A** is in an amorphous phase which is formed by the collapse of framework structure of **IV-5** accompanied with the destruction of hydrogen bonding networks when all water molecules are removed. The original crystalline phase **IV-5** cannot be restored from the amorphous phase of **IV-5A** after rehydration process but it is readily converted into the second crystalline phase **IV-5B** with the chemical composition of $[Co(pydc)(H_2O)_4](H_2O)$ (Anal. Calcd: C, 26.77; H, 4.17; N, 4.46%. Found: C, 26.73; H, 3.76; N, 4.54%) and the XRPD pattern as shown in Figure 63 and the de/rehydrated processes between **IV-5A** and **IV-5B** take place reversibly. These results suggest the crystalline-to-amorphous and reversible amorphous-to-crystalline transformations in the framework of **IV-5** induced by the hydration control. However, XRPD pattern of **IV-5B** shows broad and low intensities diffraction peaks indicating that the crystallinity was incompletely recovered after rehydration processes.

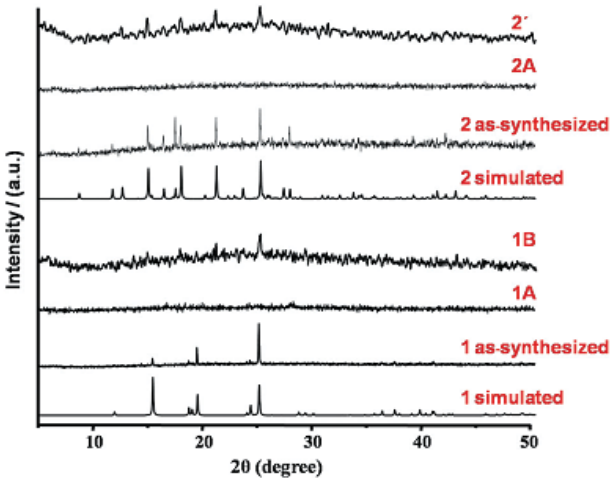

Figure 63 XRPD patterns of compounds **IV-5** (**1**) and **IV-6** (**2**).

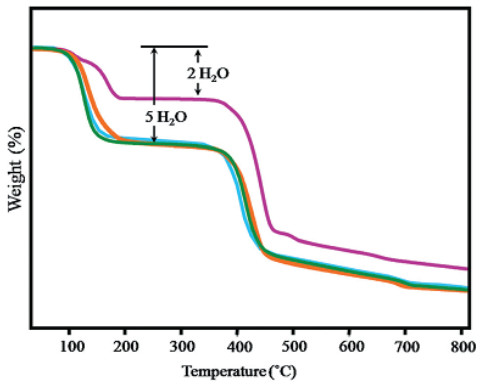

Figure 64 TGA curves of as-synthesized **IV-5** (pink line), the rehydrated form **IV-5B** (orange line), as-synthesized **IV-6** (green line) and the rehydrated form **IV-6´** (blue line).

For compound **IV-6**, after the as-synthesized compound **IV-6** was heated with the same condition to that of **IV-5**, a purple powder (**IV-6A**) was obtained. The elemental analysis and XRPD pattern results indicate that the chemical composition of the powder is [Co(pydc)] (**IV-6A**) in an amorphous phase (Anal. Calcd: C, 37.53; H, 1.35; N, 6.25%. Found: C, 37.25; H, 1.42; N, 6.31%). Interestingly, this amorphous phase **IV-6 A** can be restored to the original crystalline phase of **IV-6´** in which the color returns to that of the original one after being soaked in water vapor for 24 h, as indicated by the elemental analysis with the chemical composition of $[Co(pydc)(H_2O)_4](H_2O)$ (Anal. Calcd: C, 26.77; H, 4.17; N, 4.46%. Found: C, 26.77; H, 3.98; N, 4.65) and the XRPD measurement results. The restored solid has the same XRPD pattern as the simulated one from single-crystal X-ray diffraction data of **IV-6** as shown in Figure 4.37, indicating that **IV-6´** and **IV-6** are the same compound. Therefore, **IV-6** could be a new absorbing agent for water molecules. In fact, **IV-6** has a dynamic structure resulting from the water adsorption behavior of its evacuated solid which is typical for a first-generation porous solid following the Kitagawa classification with the "guest-induced crystal-to-amorphous transformation (CAT)" framework. When the water molecules (guest and coordinated) are removed, the framework collapses due to the destruction of the hydrogen bond system. The framework of **IV-6** is restored with the reintroduction of water molecules between chains and the reformation of the hydrogen-binding system. The analogous situation was reported on the 1D linear chains of $[\{Cu(BF_4)_2(4,4'\text{-bipy})(H_2O)_2\}4,4'\text{-bipy}]_n$, which are linked by hydrogen bonds between metal-free 4,4′-bipy molecules and coordinated H_2O molecules to form 2D non-interpenetrated sheets.

Furthermore, the IR spectra were present to confirmthe structural phase transformation behavior in **IV-5** and **IV-6** where the decreasing intensity peak at ~1560 (ν_s COO^-) and the different splitting peaks at ~1440 cm^{-1} (ν_s COO^-) are observed for the amorphous phase (Figure 65). These indicate that the

coordination mode of carboxylate bridging ligand was lost of symmetry. In contrast, these features are removed in the IR spectra of the rehydrated form, which are unidentical to those of the as-synthesized one for **IV-5** but being identical to those of the fresh one for **IV-6**. All of these results confirm the water-induced crystalline-to-amorphous phase transformation with chromotropism in the supramolecular network of **IV-5** and **IV-6** with irreversible and reversible processes, respectively. In addition, the reversibility of the water adsorption and the change in the coordination environment can be visualized by the change in color of the compounds. This change of color can be attributed to the change of the crystal field splitting of the central Co^{2+} ions during the adsorption and removal of molecules. The change of the color of the Co compounds prompted us to study the changes in the electronic transitions in the samples. For this, the solid-state UV-vis diffuse reflectance spectra as shown in Figure 66 clearly show that the bands observed in **IV-6** and **IV-6**′ correspond very well to the identical transitions causing the same color of bulk products, and evidence that **IV-6** and **IV-6**′ have the same Co^{2+} environments. While **IV-5** and **IV-5B** exhibit the different spectra indicating that the geometry of Co^{2+} center rearranged when the water molecules are adsorbed. In addition, the spectrum of **IV-5B** is found to be identical to that of **IV-6** and **IV-6**′, indicating the same Co^{2+} environments and the same orange color. Whereas the amorphous phases **IV-5A** and **IV-6A** show the identical spectra with a lower-energy broad band centered around 550 nm, but different from those of other samples, giving the distinctive purple color. The chromotropic behaviors of both compounds are principally ascribed to the changes of the d-orbital energy level, induced by the drastic change in the co-ordination environments around metal center during dehydration and rehydration processes. All of these results confirm the water-induced structural phase transformation in coordination networks **IV-5** and **IV-6**.

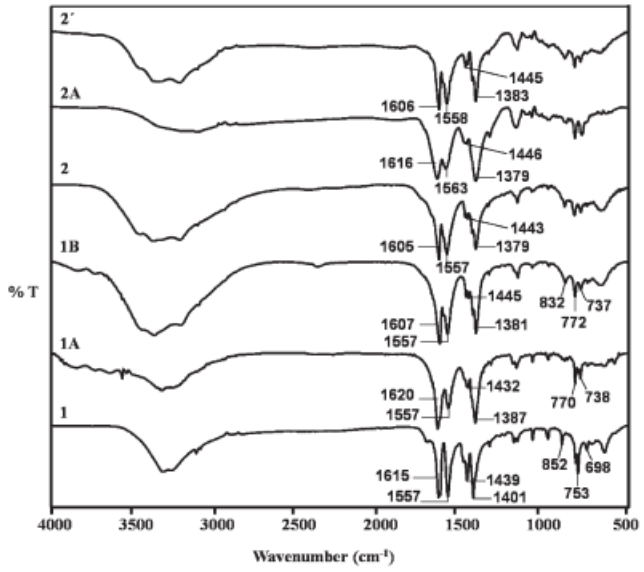

Figure 65 IR spectra of compounds **IV-5** and **IV-6**.

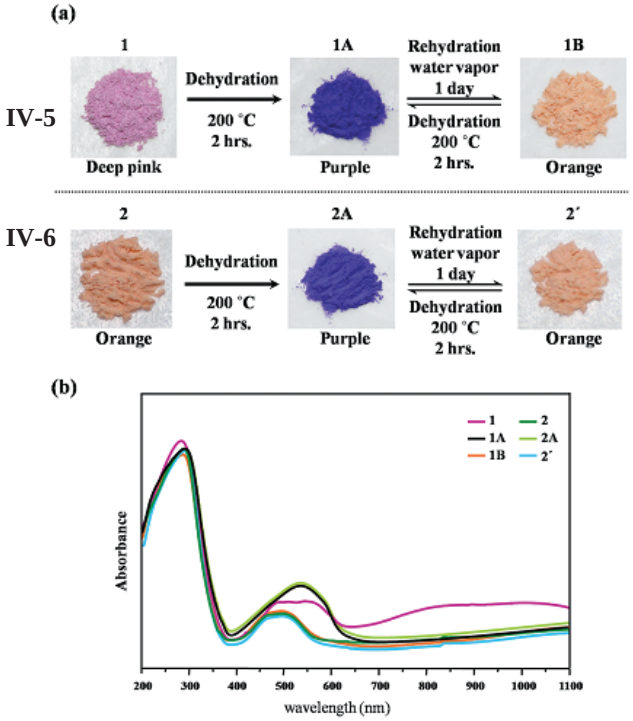

Figure 66 (a) Change in color during de- and rehydration in bulk samples of **IV-5** and **IV-6**. (b) The UV-vis diffuse reflectance spectra of as-synthesized **IV-5** (pink line), the dehydrated form **IV-5A (**black line**)**, the rehydrated form **IV-5B** (orange line), as-synthesized **IV-6** (deep green line), the dehydrated form **IV-6A** (pale green line) and the rehydrated form **IV-6´** (blue line).

However, the rehydrated form **IV-5B** and **IV-6´** were heated and cooled for four times to repeat the reversibility of the de- and rehydration processes. The results exhibit the color shuttle change between pale orange (**IV-5B** and **IV-6´**) and purple (**IV-5A** and **IV-6A**), suggesting the water induced reversible crystal-to-amorphous transformation phenomenon. The IR spectra, UV-vis diffuse reflectance spectra, XRPD spectra, elemental analysis and TGA curve of **IV-5B** and **IV-6´** correspond very well to the identical results, these indicate that the structure of **IV-5** completely transforms to the structure of **IV-6** through the dehydration and rehydration processes as the schematic representation of this structural phase transformation shown in Figure 67.

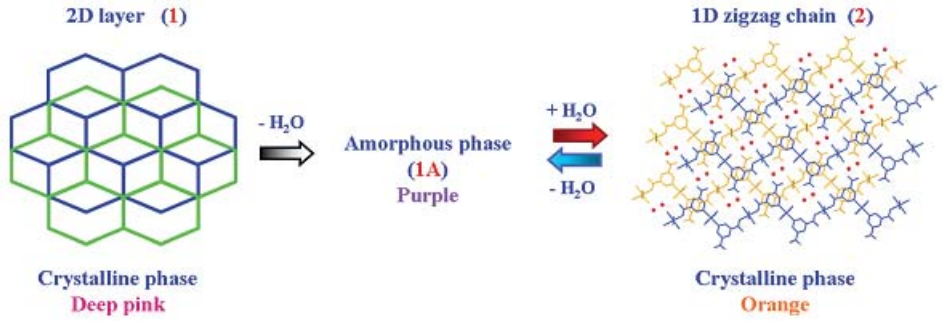

Figure 67 Schematic diagram illustrates the structural conversion of 2D layer to 1D chain structures by thermal dehydration and rehydration processes.

In order to elucidate the important role of the crystal structure (via the intermolecular interactions) on the dynamic behavior of the frameworks we have compiled our previously published data of the mononuclear compounds $[M(H_2O)_4(ampyz)_2][M(H_2O)_6]$ $(SO_4)_2(H_2O)_2$ and the present data of 2D and 1D frameworks. Both compound systems exhibit crystal-to-amorphous phase transformation with chromotropism but with different dynamic behaviors. The previous compounds contain numerous hydrogen donors and hydrogen acceptors from coordinated and uncoordinated water molecules, amino and sulfate groups to generate the intermolecular hydrogen bond interactions as well as π-π stacking. Thus, they have more accessible intermolecular hydrogen bonding that able to trigger the reversible crystal-to-amorphous phase transformation after de/readsoption processes. While in the present compound **IV-5** after the water readsoption process, the 2D framework of **IV-5** was not recovered but change to another crystalline phase of 1D framework (compound **2**). This new phase is more stable and responsible for the reversible crystal-to-amorphous phase transformation with chromotophism. This may be due to the less intermolecular interactions which are not enough to trigger the phase transformation to the original 2D framework as compared to that of **IV-6**.

3.4 Structural diversity and magnetic studies in 1D, 2D and 3D azido-bridged cobalt(II) hybrid frameworks

3.4.1 Structural diversity and magnetic properties in 1D and 2D azido-bridged cobalt(II) complexes with 1,2-bis(2-pyridyl)ethylene

Molecule-based magnetic materials involving azido bridges have incessantly attracted much attention because of their diverse architectures with interesting physical properties, such as single molecule magnet, single chain magnet and long-range magnetic ordering behaviours.[2, 102-105] The crystal engineering of molecular magnetism aims to control the spins in molecules and molecular assemblies.[59, 106] As an excellent ligand, containing several pairs of electrons, azido can readily bridge two or more spin

carriers (Figure 5.1) and effectively mediate either ferromagnetic or antiferromagnetic coupling, normally through EO and EE modes, respectively.[2, 102-105] It is known that one of the interesting structural aspects of working with the cobalt ion is the wide range of stable geometries.[102] Consequently, when the azide ion and coligands are coupled with cobalt(II) ions, which accommodate four-, five- and six-coordination depending on the situation, various low-dimensional structures are expected along with interesting magnetism.[107-112] The versatile *N*,*N*′-ditopic bridging spacer 1,2-bis(4-pyridyl)ethylene and its derivatives have been used as coligands widely in organic-inorganic hybrid materials including azido complexes and they usually give unexpected structures with interesting magnetic orders.[113-116] However, the *trans*-1,2-bis(2-pyridyl)ethylene (2,2′-bpe) (Figure 68) has not yet been reported in any azido complexes. Herein this chapter shows that 2,2′-bpe can act as both terminal (*endo*) and bridging (*exo*) co-ligands in a Co^{II} azido system, which effectively support either blocking the metal's coordination sites or extending the structural dimensions.

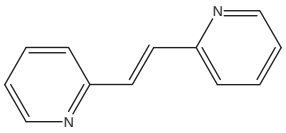

Figure 68 *trans*-1,2-bis(2-pyridyl)ethylene (2,2′-bpe)

3.4.1.1 General observations and spectroscopic characterizations

The layered diffusion reaction of $CoCl_2 \cdot 6H_2O$, 2,2′-bpe and NaN_3 in a 1:1:2 molar ratio in water and ethanol media yielded the mixture of blue rod-shaped crystals of **V-1** and pink square-shaped crystals of **V-2**. The crystals were manually separated because of their visible differences in colors and shapes of the crystals. Then the physical purities of crystalline phase of bulk products were confirmed by XRPD technique comparing with their simulated XRD patterns from the single-crystal data (Figure A6, Appendix A). An attempt has been made to find the optimal condition for preparing a single phase of **V-1** or **V-2,** based on molar ratios and solvents without success. The IR spectrum (Figure 69) of **V-1** with end-on mode of azide shows a very strong band at 2089 cm^{-1} $\nu_{as}(N_3^-)$ with a shoulder peak and medium band at 1296 cm^{-1} $\nu_s(N_3^-)$. Compound **V-2** containing both μ_2-1,1and μ_2-1,3 bridging azides shows two very strong bands due to $\nu_{as}(N_3^-)$ mode at 2097 and 2072 cm^{-1} and medium band at 1296 cm^{-1} $\nu_s(N_3^-)$. The electronic spectra show the overlapped bands of the *d-d* transitions arising from penta-coordination and octahedral geometries of high-spin Co^{II} ions for **V-1** and exhibit the typical *d-d* transitions of octahedral geometry for V-**2** (Figure 70).

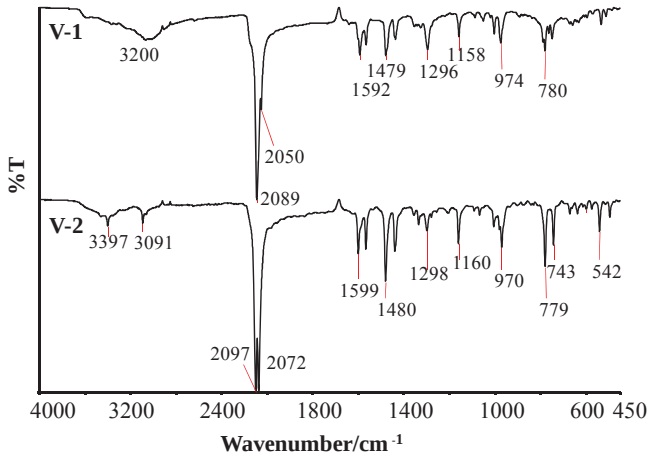

Figure 69 Infrared spectra of **V-1** and **V-2**.

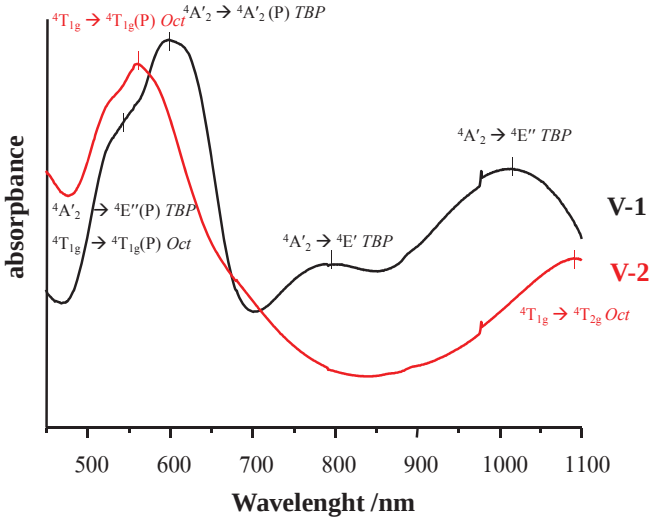

Figure 70 UV-Vis diffuse reflectance spectra of **V-1** and **V-2** with the *d-d* transitions labeled.[93]

3.4.1.2 Description of crystal structures

$[Co_3(N_3)_6(OH_2)_2(2,2'\text{-bpe})_2]_n(2,2'\text{-bpe})_n$ (V-1)

X-ray analysis revealed that compound **V-1** contains two crystallographic independent Co1 and Co2 ions bridged by three independent EO azido ligands as shown in Figure 71(a). Co1 is placed in an intermediate 5-coordination geometry, slightly distorted toward trigonal bipyramid with a τ value[44] of 0.55, where the metal atom is coordinated by four N atoms from four EO azide anions and a N atom from a monodentate 2,2′-bpe. Co2 has a CoN_4O_2 compressed octahedral geometry, which is located on the crystallographic inversion centre and it is coordinated by four N atoms from EO azido ligands in the equatorial positions and two water molecules in the axial sites.

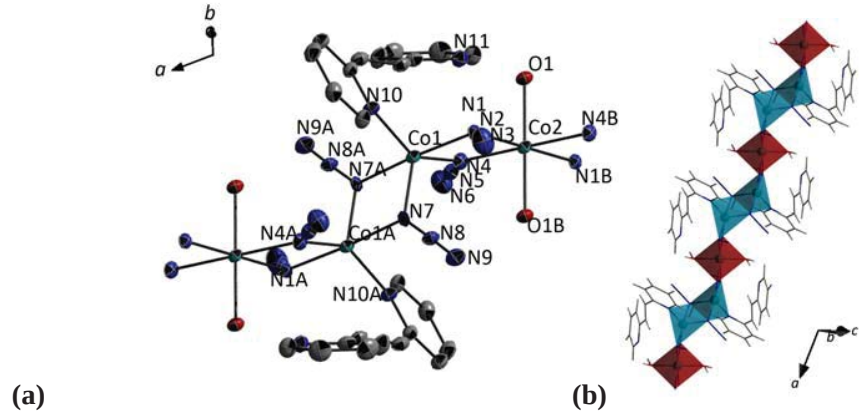

Figure 71 Crystal structure and atom labeling scheme of **V-1**. The ellipsoids are shown at 50% probability level (a). Atoms labeled with the notation ‘‘A’’ and “B” are symmetry-generated equivalents, (A) 1–*x*, –*y*, 1–*z*; (B) –*x*, –*y*, 1–*z*. The 1D chain of **V-1** is running along *a* axis with octahedra and hexahedra of Co^{II} ions (b). The free 2,2′-bpe and H atoms are omitted for clarity.

The adjacent Co^{II} centres are connected by an azide in the double-EO mode along the *a* axis associated with the inversion centre, to build a 1D zigzag chain with the rare $[–5–5–6–]_n$ sequence of cobalt(II) coordination numbers (Figure 71(b)). The bond angles of Co–N–Co are in the range between 97.09(12)° and 100.37(12)° and the intrachain Co···Co separations through double EO azido bridges are 3.174(1) Å for Co1···$Co1^i$ (*i* = 1–*x*, –*y*, 1–*z*), and 3.207(1) Å for Co1···Co2, as usually observed for this kind of bridging in cobalt(II) azido compounds.[107] The coordination 2,2′-bpe acts as terminal coligand because the intrachain hydrogen bonding between N atom on terminal pyridine of coordination 2,2′-bpe and H atom of coordination water [O1H···N11 = 1.89 Å (172°), O1···N11 = 2.811(4) Å] causes the arrangement of 2,2′-bpe in *cis* position with the dihedral angle between two pyridine rings of 55.65(1)°. In addition, the chains are assembled *via* C–H···π interactions and the intermolecular hydrogen bonds between uncoordinated 2,2′-bpe and coordination water along *b* axis [O1H···N12 = 1.80 Å (172°), O1···$N12^i$ = 2.750(4) Å], yielding 2D structure of **V-1** as shown in Figure 72. The interchain C–H···π interactions involve C4–H interacting to the centroid of terminal pyridine ring of adjacent coordination 2,2′-bpe with the distance of 2.876(4) Å and a C4–H···π angle of 133°.

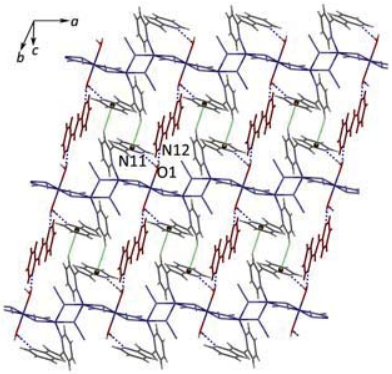

Figure 72 Formation of 2D sheet of **V-1** in *ab* plane formed by C–H···π interactions and hydrogen bonds between the neighbouring chains. The dotted lines represent the intramolecular O1–H···N11 hydrogen bond and the intermolecular O1–H···N12 hydrogen bond and C–H···π interaction.

$[Co(N_3)_2(2,2'\text{-bpe})]_n$ (V-2)

The crystal structure of **V-2** is depicted in Figure 73. Compound **V-2** has a 2D wavy layer structure which consists of an azido-Co^{II} neutral chain with alternating double EE and double EO azido bridges along *a* axis and ditopic 2,2′-bpe bridging Co^{II} ions along *b* axis. There is only one crystallographically independent Co^{II} ion, which has elongated octahedron comprised of two N atoms from bridging 2,2′-bpe in the axial sites and four N atoms from two EE and two EO azide ions located in the equatorial positions. The adjacent Co^{II} ions in a chain are related by inversion centers and linked alternately by double EE and double EO azido bridges with the Co···Co distances of 5.052(2) Å and 3.314(1) Å, respectively. These bridging modes of azide are widely found in the polymeric chain complexes containing additional chelating ligands.[115, 117-123]

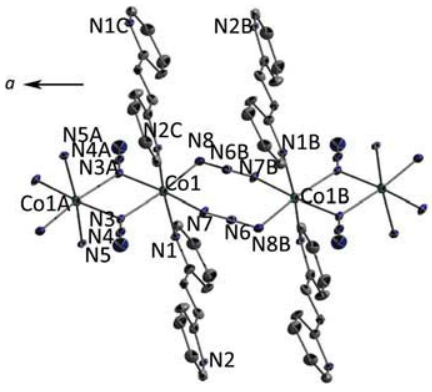

Figure 73 Expanded asymmetric unit and atom labeling scheme of **V-2**. The ellipsoids are shown at 50% probability level. Atoms labeled with the notation ‘‘A’’, “B” and “C” are symmetry-generated equivalents, (A) 1–*x,* 1–*y,* 1–*z*; (B) –*x,* 1–*y,* 1–*z.*; (C) *x*, 1+*y*, *z*.

In double EO bridged $Co(N_3)_2Co$ moiety, the Co1–N3–Co1A–N3A ring is strictly planar due to the existence of the inversion center with the Co1–N3–Co1A angle of 102.25(14)°. For double EE mode, the EE bridges adopt a chair conformation for the Co–$(N_3)_2$–Co unit with the dihedral angle between N7N6N8BN8N6BN7B plane and CoN8N7 plane of 33.8(1)°. The 2,2′-bpe acts as ditopic connector in *trans* position bridging the cobalt(II) azido neutral chains along *b* axis, building 2D wavy sheet of **V-2** (Figure 74). The Co···Co separation *via* 2,2′-bpe spacer is 8.322(2) Å.

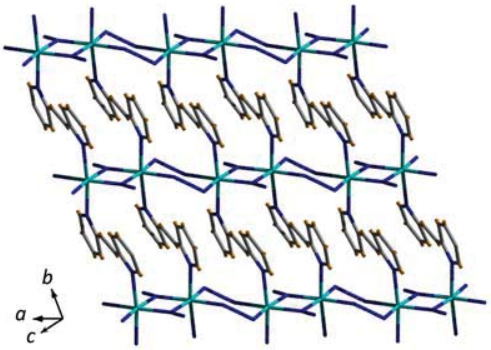

Figure 74 2D wavy coordination network of **V-2**.

3.4.1.3 Long-range magnetic ordering behaviors

The magnetic susceptibility of a polycrystalline sample of **V-1** at 2-310 K is shown in Figure 75. At 310 K, the $\chi_m T$ value is 11.16 cm^3 K mol^{-1} per Co_3 unit, which is significantly higher than the spin-only value of 5.62 cm^3K mol^{-1} expected for uncoupled three S = 3/2 ions, owing to ferromagnetic interactions and the significant orbital contribution of high-spin Co^{II} in an octahedral surrounding. $\chi_m T$ value increases gradually upon cooling to *ca.* 50 K. Below this temperature, $\chi_m T$ increases abruptly to a maximum value of 48.75 cm^3 K mol^{-1} at 15 K because of rapidly increasing ferromagnetic coupling between adjacent spin carriers. Upon cooling to 2 K, $\chi_m T$ decreases quickly to 8.32 cm^3 K mol^{-1} because of magnetization saturation and possible interchain antiferromagnetic interactions. The similar behavior has been observed in other related complexes containing 1D double EO azido bridge such as $[Co(2,2'\text{-bithiazoline})(N_3)_2]_n$ [107], $[Mn(N_3)_2(pyz)]_n$ [124] (pyz = pyrazine) and $[Ni(en)(N_3)_2]_n$ [125] (en = ethylenediamine). The χ_m^{-1} values above 100 K were fitted with the Curie-Weiss law $\chi = C/(T-\theta)$ with a Curie constant C = 9.59(3) cm^3 K mol^{-1} and a Weiss constant θ = +43.7(5) K indicating dominant ferromagnetic coupling between Co^{II} ions *via* double EO azido bridges. Owing to lack of theoretical model for the complicated chain composed by octahedral Co^{II} and non-octahedral Co^{II} ions, the exchange parameters could not be estimated.

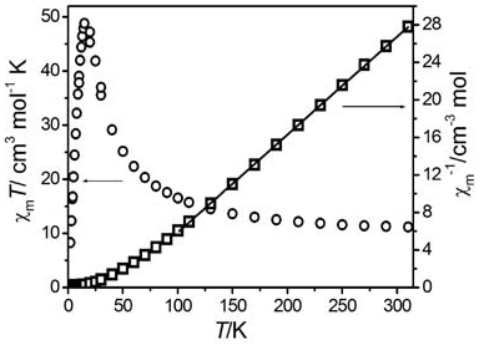

Figure 75 Temperature dependence of $\chi_m T$ and χ_m^{-1} of **V-1** at H = 10 kOe from 2 to 310 K. The solid line represents the best fit to the Curie-Weiss law.

In addition, the dominant ferromagnetic coupling was confirmed by magnetization measurements performed at 1.8 K in an external field 0–5 T, as shown in Figure 76. The molar magnetization curve exhibits a rapid increase, reaching about 80% of M_s at 1 kOe which appears to be a soft ferromagnet because coercivity was not observed. At higher field, the saturation magnetization, M_s = 8.81 $N\beta$ agrees with three ferromagnetically coupled Co^{II} ions with an expectation value of M_s = 6–9 $N\beta$.[126, 127] A comparison with the Brillouin function for three isolated S = 3/2 spins stresses the remarkable cooperativity in this system, consistent with the ferromagnetic interaction.

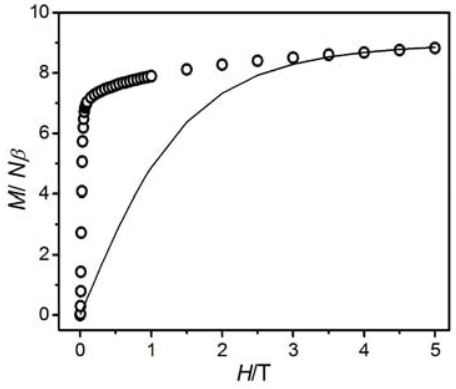

Figure 76 Field dependence of magnetization of **V-1** at 1.8 K. The continuous line corresponds to the Brillouin function for three Co^{II} ions S = 3/2 with g = 2.0.

All evidence points to the long-range magnetic ordering, likely due to interchain coupling through the extensive hydrogen bonds and C–H···π contacts. The field-cooled (FC) and zero-field-cooled (ZFC) magnetization plot under a field of 50 Oe (Figure 77, inset) showed a disagreement below 6 K and presented a swell at around 6 K, suggesting the onset of long-range antiferromagnetic ordering

among the ferromagnetic chains. However, the ZFC-FC plot under a field of 1000 Oe shows no maximum and trends to saturate at lower temperature and does not show the irreversibility, thus indicating that the weak interchain antiferromagnetic interaction is overcome by the external field. These features are indicative of a metamagnet built of ferromagnetic chains. The temperature dependence of *ac* susceptibility was also measured at zero *dc* field (Figure 78). The χ' signal shows a peak at 6 K confirming the occurrence of phase transition, and the nonzero χ'' signal below 6 K is consistent with the ferromagnetic order. No frequency dependence of the *ac* signals was observed among 25-997 Hz. The metamagnetic behavior was further confirmed by the hysteresis loop measurements, as given in Figure 77, which revealed that **V-1** is a metamagnet with a typical crossover magnetic hysteresis in the slightly sigmoid shape of the $M(H)$ curve.[128-130] The critical field H_c is ≈ 70 Oe, estimated as the field at which a maximum $\delta M/\delta H$ value is reached.

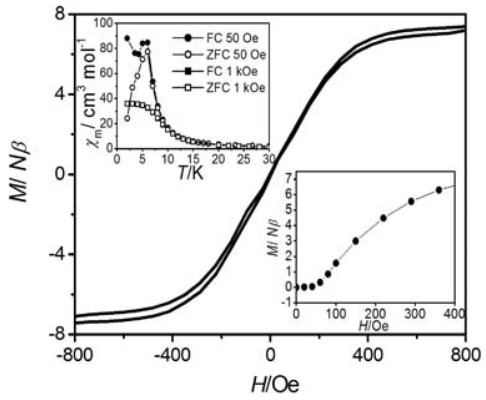

Figure 77 Hysteresis curve for **V-1** at 1.8 K. The insets show the initial plot in a low field (right) and the ZFC-FC plots of **V-1** at 50 Oe and 1 kOe (left).

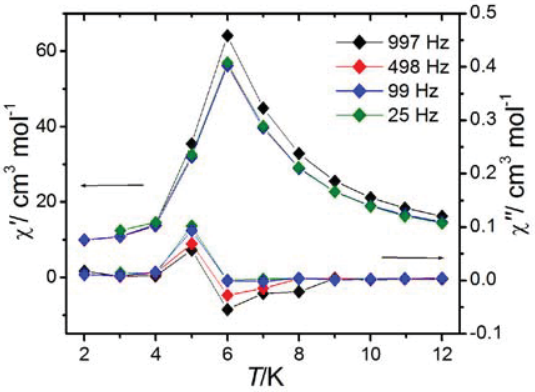

Figure 78 Temperature dependence of the *ac* susceptibility for **V-1** at H_{dc} = 0 Oe, H_{ac} = 3 Oe, with frequencies of 25 – 997 Hz.

This metamagnetic-like transition results from the presence of weak interchain antiferromagnetic interactions among the strong ferromagnetic chains. At low temperature, the antiferromagnetic coupling of the ferromagnetic chains leads to an antiferromagnetic ground state. With an increase in the external magnetic field (H_c > 70 Oe), the ferromagnetic chains tend to parallel align, resulting in ferromagnetic ordering. This behavior is characteristic of a metamagnet built of ferromagnetic chains.[26, 125, 128-135] However, because of the strong spin-orbit coupling of Co^{II} ions, the magnetic interaction might be more complicated.[102, 129] This similar metamagnetic-like transition was also observed in other polymeric chain systems containing ferromagnetically 1D double EO azido bridge with weak interchain antiferromagnetic interactions.[26, 125, 128, 130] For instance, the previous related compound $[Mn(tptz)(N_3)_2]_n$[130] (tptz=2,4,6-tris(2-pyridyl)-1,3,5-triazine) (Figure 79) which contains similar double EO azide-bridged 1D chains assembling by face-to-face π-π and C–H···π interactions, revealed overall metamagnetic behavior below 2.7 K with very small H_c of approximately 80 Oe. This reported value of H_c is very close to that of this work.

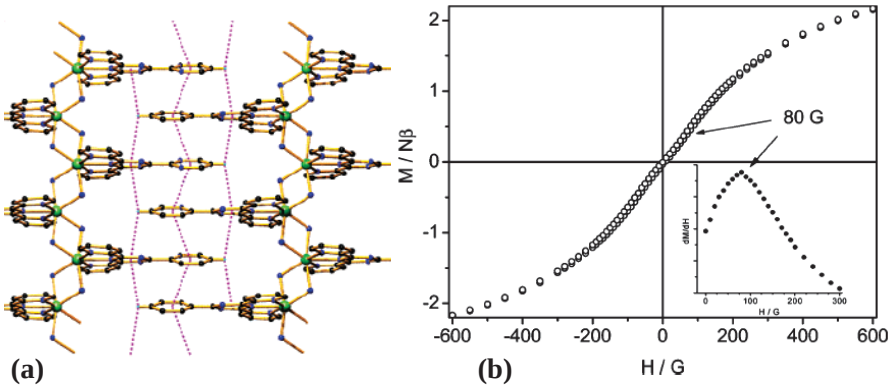

Figure 79 Formation of a 2D sheet of $[Mn(tptz)(N_3)_2]_n$ (a) and the hysteresis curve with inset of $\delta M/\delta H$ at low field (b).[130]

The magnetic susceptibility of **V-2** is depicted in Figure 80. The $\chi_m T$ value of ca. 3.01 cm^3 K mol^{-1} at 310 K is much higher than the spin-only value of high-spin d^7 ion (1.87 cm^3Kmol^{-1}), owing to ferromagnetic interactions *via* μ_2-1,1 N_3^- bridges and the significant orbital contributions of the octahedral Co^{II} ions. Upon cooling, the $\chi_m T$ decreases gradually down to 0.04 cm^3 K mol^{-1} at 2 K, indicating dominant antiferromagnetic coupling *via* μ_2-1,3 N_3^- bridges. The plot of χ_m versus T (Figure 5.16, inset) exhibits an abrupt increase below about 17 K to a maximum value of 0.02 cm^3 mol^{-1} at 2 K, which is probably attributed to paramagnetic impurity or possible spin canting. The data above 150 K obey the Curie-Weiss law with a Curie constant C = 3.58(3) cm^3 K mol^{-1} and a Weiss constant θ = –58(2) K. The

negative θ suggests the antiferromagnetic coupling between Co^{II} ions and spin-orbital coupling of Co^{II} ions in an octahedral field.

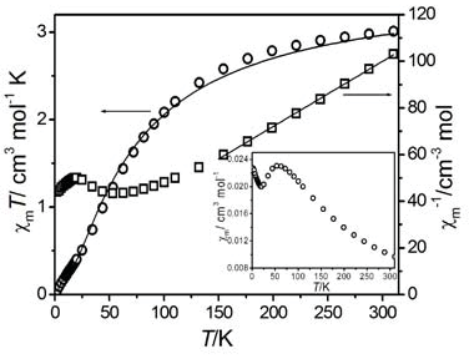

Figure 80 Temperature dependence of $\chi_m T$ and χ_m^{-1} of **V-2** from 2 to 310 K. The solid lines correspond to the best fit (see the text). Inset: plot of χ_m *vs. T* for **V-2**.

Because of the spin-orbit coupling contribution of Co^{II} ions, it is difficult to find an accurate analytical expression to describe the temperature dependence of the magnetic susceptibility for the polymeric chains of the Co^{II} ions. However, Rueff et al.,[136-138] have proposed a very successful phenomenological approach for a low-dimensional antiferromagnetic Co^{II} system that allows an estimation of the strength of the antiferromagnetic exchange interactions and also the effects of spin-orbit coupling. They postulate the phenomenological equation:

$$\chi_m T = A \exp(-E_1/kT) + B \exp(-E_2/kT) \qquad (5)$$

$A + B$ equals the Curie constant (≈ 2.8-3.4 cm^3 K mol^{-1} for octahedral Co^{II}) and E_1 and E_2 represent the activation energies corresponding to the spin-orbit coupling parameter and the antiferromagnetic exchange interaction, respectively where E_2 is related to the magnetic coupling constant J according to the Ising chain approximation, $\chi_m T \propto \exp(+J/2kT)$. This equation adequately describes the spin-orbit coupling, which results in a splitting between discrete levels and the exponential low-temperature divergence of the susceptibility. The reasonable values for magnetic coupling and spin-orbit interaction have been reported in several studies of 1D and 2D Co^{II} networks. [136-141] The fitted parameters are $A + B = 3.58$ cm^3 K mol^{-1}, equivalent to the Curie constant obtained from the Curie-Weiss law in the high temperature range; E_1/k = +61(2) K which is consistent with those reported for 1D and 2D cobalt(II) systems.[126, 136, 137, 140] For the value found for the antiferromagnetic exchange interaction, E_2/k equals to +4.1(2) K, corresponding to J = –8.2 K, according to the Ising chain approximation, $\chi_m T \propto \exp(+J/2kT)$.

It can be seen from the abrupt increase of the plot of χ_m *vs. T* below about 17 K and from the other reported complexes containing chains of alternating double *EO* and double *EE* bridging modes of azides that these complexes frequently exhibit weak ferromagnetism due to spin canting,[117, 119-

[122] thus the magnetic behaviors of **V-2** were further clarified. The temperature dependencies of the ZFC and the FC magnetization were measured at a low field of 20 Oe, as shown in Figure 81(inset). The obvious divergence of the ZFC and FC plots below 12 K indicates hysteretic long-range magnetic order, which is compatible with the maxima in χ' and the nonzero χ'' signal around 12 K in *ac* susceptibility at 997 Hz (Figure 82). The isothermal magnetization with a field up to 5 T at 1.8 K is depicted in Figure 81. The initial increase of magnetization shows a slight positive curvature and is not linear with the field up to 7 kOe, and then it becomes almost linear up to to 0.146 $N\beta$ at 5 T, far from the theoretical saturation magnetization of Co^{II} ion, suggesting the overall antiferromagnetic coupling between Co^{II} ions. A hysteresis loop of **V-2** is clearly observed when the field is less than 10 kOe, giving a coercive field of ≈ 300 Oe and remanent magnetization (M_r) of ≈ 0.002 $N\beta$. These results indicate that the spin-canting effect between overall antiferromagnetically coupled Co^{II} ions leads to residual spins. The canting angle (α) is estimated to be about 0.05° based on the equation 1.17, $\alpha = \sin^{-1}M_r/M_s$ (theoretical saturation magnetization (M_s) = $g'S'N\beta$ = 2.16 $N\beta$, S' = 1/2, g' = 4.33 for octahedral Co^{II} at 1.8 K).[59, 106]

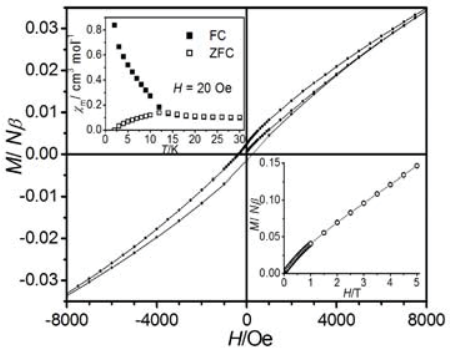

Figure 81 The hysteresis loop of **V-2** at 1.8 K. The insets show the ZFC and FC magnetization at H = 20 Oe from 2 to 30 K. (left) and the field dependence of magnetization at 1.8 K (right).

Compound **V-2** exhibits hard ferromagnetism whereas **V-1** is soft ferromagnetism, which may be attributed to the difference between parallel anisotropy axes in **V-2** and almost orthogonal trigonal bipyramidal and octahedral axes in **V-1**. It is well known that two mechanisms lead to spin canting (equation 1.16): (i) magnetic anisotropy and (ii) antisymmetric exchange.[59, 106] However, the spin canted structure is not compatible with the crystal structure of **V-2** because of the presence of an inversion center between the bridged Co^{II} sites, which forbids the occurrence of antisymmetric interactions. The observation of the spin canting in **V-2** should be attributed to the great single-ion anisotropy of octahedral cobalt(II) ions or a possible structure phase transition at low temperature.[117, 119-122] The weak ferromagnetism due to spin canting in the presence of an inversion center between metal sites were also observed in other complexes containing the same bridging mode of azide,

such as $[Co(dpa)(N_3)_2]_n$[121] (dpa = 2,2′-dipyridylamime), $[Mn(dpq)(N_3)_2]_n$[120] (dpq = dipyrido-(3,2-*d*:2′,3′-*f*)quinoxaline) and $[Mn(TaiEt)(N_3)_2]_n$[117] (TaiEt = 1-ethy-2-(*p*-tolyazo) imidazole). The spin canting of **V-2** will be discussed and compared with compounds **V-3**, **V-4** and the related azido complex systems next topic.

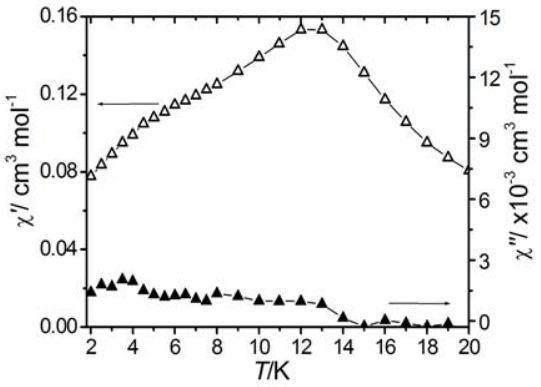

Figure 82 Temperature dependence of the *ac* susceptibility for **V-2** at H_{dc} = 0 Oe, H_{ac} = 3 Oe, with frequency of 997 Hz.

3.4.2 Spin canting and metamagnetism in 2D and 3D cobalt(II) coordination networks with alternating double end-on and double end-to-end azido bridges

The crystal engineering and magnetism of molecule-based coordination frameworks with low- or high dimensional structures have been of great interest in recent years with the intention of understanding the fundamental magneto-structural correlations within the structure and controlling the spins in molecules and molecular assemblies for conceiving practical functional molecule-based materials.[59, 102, 142-144] To rational design of magnetic molecular assemblies, it is important to select the appropriate bridging ligands that effectively transmit the exchange interactions between the spin carriers together with the aspects of diverse topologies. An excellent azido ligand is the one of the extensively used bridging ligands in the construction of magnetic molecular materials because it can provide a short bridge with the extremely versatile coordination modes and effectively mediates either ferromagnetic or antiferromagnetic coupling generally through μ_2-1,1 (end-on, EO) and μ_2-1,3 (end-to-end, EE) modes, respectively. In addition the different combinations of EO and EE azido bridging modes may exist in the same structure, leading to several topologies as well as competing magnetic interactions in sign according to a certain EO and EE azido bridging sequence.[103, 118, 122, 145-148] Consequently, the fascinating magnetic phenomena have been recognized in many azido-bridged coordination polymers which have been an active research area so far.[2, 103, 105, 149] Likewise, the organic coligands are very significant to the formation of some particular architecture and to the structural modification. It is well-known that the *N,N*′-ditopic diimine spacer, pyrazine (pyz) is a long bridge for magnetic systems and effectively transfers electron in

the antiferromagnetic superexchange pathways between metal centers. With pyz and derivative of pyz ligands, the azido complexes usually exhibit various structural topologies together with interesting magnetic properties.[26, 124, 150-152] For instances, 2D layer of $[Fe(N_3)_2(pyz)]_n$ (Figure 83) showed metamagnetism arising from the competition of ferromagnetically coupled EO azido chain and 2D antiferromagnetically coupling *via* pyz.[26] In contrast with the lack of local anisotropic ions, this metamagnetic feature for the Mn^{II} and Cu^{II} analogues was not observed.[124, 152]

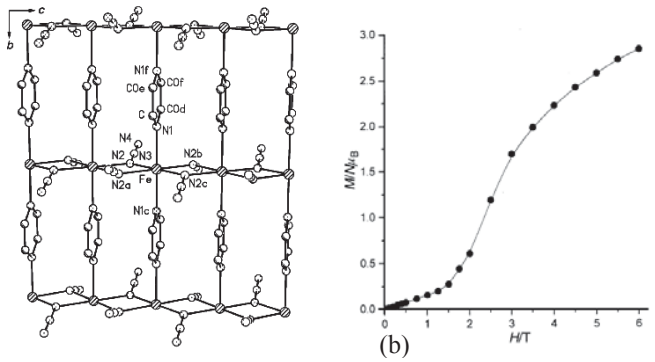

(a) (b)

Figure 83 2D layer structure of $[Fe(N_3)_2(pyz)]_n$ (a) and isothermal magnetization plot at 1.8 K.[26]

This topic focused on the versatile 2-aminopyrazine (ampyz) spacer as organic coligand in magnetic azido complex system. Ampyz spacer contains many interaction sites; coordination sites at N atoms on pyrazine ring, hydrogen donor site at amino group, and the intermolecular π–π stacking site through aromatic moieties, which has been used for constructing many coordination polymers.[34, 36, 37, 153, 154] Without the spin carriers, the structural diversity of zinc(II) azido complexes with ampyz has been recently obtained depending on the molar ratio of the starting components.[36] With this in mind, herein this topic shows that ampyz spacer well accommodates in the magnetic anisotropic Co^{II} azido system. Remarkably, new 2D layer $[Co(N_3)_2(ampyz)]_n$ (**V-3**) and 3D framework $[Co(N_3)_2(ampyz)]_n$ (**V-4**) of azido-bridged Co^{II} coordination networks with the identical molar ratio were well prepared in different preparative techniques and characterized structurally and magnetically. In addition both compounds similarly contain the 1D chain of alternately double EO and double EE azido-bridged Co^{II} ions, whereas the ampyz spacers in **V-3** and **V-4** are in dissimilar arrangements, *trans*- and *cis*-positions in octahedral Co^{II} ions for **V-3** and **V-4**, respectively. As it is known, only two azido Co^{II} chains with alternating double EE and double EO bridges have been reported in the literature.[121, 155] Although **V-3** and **V-4** are similar in local coordination environments but somewhat different in structural symmetries, dimensionalities and bridging parameters, consequently, their magnetic behaviors at low temperature reveal the significant disparities. The magnetic investigation of **V-3** shows the coexistence of big spin canting angle and metamagnetism having magnetic ordering at 10 K, whereas the magnetic behavior of **V-4** simply exhibits

spin-canted antiferromagnetism below T_N of 16 K. These behaviors allow us to perform the magnetic investigation and discussion.

3.4.2.1 General observations and spectroscopic characterizations

The different preparative methods of $Co(NO_3)_2 \cdot 6H_2O$, azide anion and ampyz in a 1:2:2 molar ratio in a mixture of ethanol and aqueous media yielded two cobalt(II) coordination polymers containing ampyz spacer together with the alternating double EO and double EE azido bridging mode which show the different dimensionalities. The layered diffusion reaction in ambient temperature gave the orange rectangular crystals of **V-3** showing the high symmetric 2D square-grid structure of $[Co(N_3)_2(ampyz)]_n$ whereas the hydrothermal reaction at 90 °C for 1 day yielded the red-orange polygonal crystals of **V-4** showing 3D framework of $[Co(N_3)_2(ampyz)]_n$. These experiments do not only demonstrate the significant role of the primary units, the excellent azido bridges and versatile ampyz spacer for building both structures, but also demonstrate the important influence of reaction's conditions on the structural topologies and dimensionalities. The physical purities of crystalline phase of bulk products were confirmed by XRPD technique comparing with their simulated XRD patterns from the single-crystal data.

The IR spectra of both compounds are quite similar (Figure 84). Compounds **V-3** and **V-4** containing both μ_2-1,1 and μ_2-1,3 bridging azides, show two very strong bands due to $\nu_{as}(N_3^-)$ modes at 2100 and 2080 cm^{-1} for **V-3** and 2105 and 2068 cm^{-1} for **V-4** indicating the presence of two different azido groups. The weak band at ≈1320 cm^{-1} is $\nu_s(N_3^-)$ for the EO bridge. This band is not active for the symmetrical EE bridge.[118] Two narrow weak bands in the regions 3400–3300 cm^{-1} can be assigned to ν(N–H) of the primary amine in the ampyz ligand.

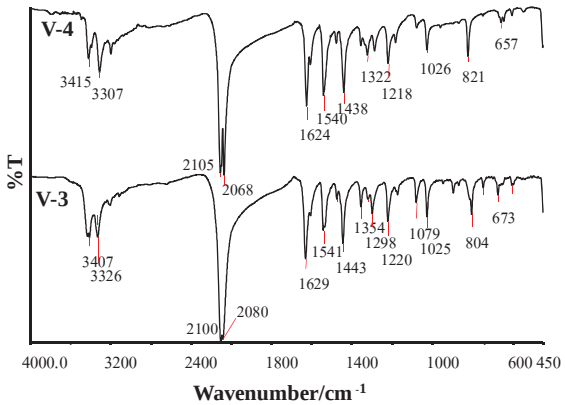

Figure 84 IR spectra of **V-3** and **V-4**.

The solid-state UV-vis diffuse reflectance spectra of both compounds (Figure 85) agree with the typical *d-d* transition of high-spin Co^{II} in octahedral geometry with two observed bands at 20000–18000 and less than 9500 cm^{-1}, which are assigned to the $^4T_{1g} \rightarrow {}^4T_{1g}(P)$ and $^4T_{1g} \rightarrow {}^4T_{2g}$

transitions, respectively. The weak band at *ca*. 15000 cm^{-1} which is assigned to the $^4T_{1g} \rightarrow {}^4A_{2g}$ transition is not well resolved. The growing bands which appear higher than 22000 cm^{-1} are due to charge transfer transition and internal transition within ampyz.[93]

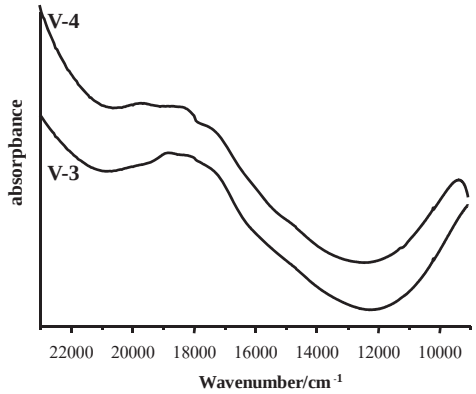

Figure 85 UV-Vis diffuse reflectance spectra of **V-3** and **V-4**.

3.4.2.2 Description of crystal structures

2D layer of $[Co(N_3)_2(ampyz)]_n$ (V-3)

Compound **V-3** was crystallized in orthorhombic crystal system with high centrosymmetric space group, *Immm*. The coordination environment of the Co^{II} center is shown in Figure 86. The Co1 atom, EE azido atoms N6, N7 and EO azido N3 atom all lie on a crystallographically *ac* mirror plane. In addition there are three other vertical mirror planes. The first *bc* mirror plane lies on EO azido N3, N4 and N5 atoms. Second is another *bc* mirror plane lying on EE azido atom N7 and the third is *ab* mirror plane lying on pyrazine N1 and Co1 atoms. There is only one crystallographically independent Co^{II} ion, which has slightly elongated octahedron comprised of two N atoms from bridging ampyz in the axial sites (2.193(4) Å) and four N atoms from two EE and two EO azide ions located in the equatorial positions (2.141(5)–2.116(4) Å).

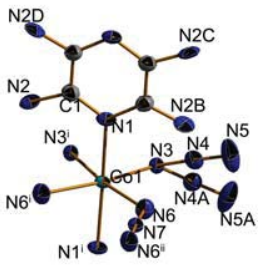

Figure 86 Crystal structure and atom labeling scheme of **V-3**, (i) *x*, –*y*, 2–*z*; (ii) –*x*, –*y*, *z*. The ellipsoids are shown at 50% probability level. All disordered positions of amino group and N atoms of EO-azide are shown.

The adjacent Co^{II} ions are related by those crystallographic mirror planes and inversion center and linked alternately by double EE and double EO azido bridges, giving rise to a neutral 1D perfect linear chain along *a* axis (Figure 87) with the Co···Co separations of 5.157(2) and 3.283(1) Å, respectively, where the sum of these values equals to the crystallographic *a* parameter of 8.440(2) Å. In double EO bridged $Co(\mu_2\text{–}1,1\ N_3)_2Co$ moiety, the Co1–N3–Co1A–N3A ring is strictly planar due to the existence of the inversion center and mirror planes with the Co1–N3–Co1A angle of 101.7(3)°, as is usually observed for this kind of azido bridge.[156] The disordered EO azido bridge, which is nearly linear (∠N3–N4–N5 = 178.1°), slightly deviates (up and down) from that plane. For double EE mode, the $Co(\mu_2\text{–}1,3\ N_3)_2Co$ moiety forms the perfect planarity because the crystallographic *ac* mirror plane is placed on this ring. As a result, a dihedral angle δ between the N6N7N6aN6cN7bN6b mean plane and the CoN6N6b plane is 0°, as shown in Figure 88. The symmetric Co1N6N7 angle is 129.3(5)°. It is the uncommon observation of the complete planar for the $M(\mu_2\text{–}1,3\ N_3)_2M$ moiety in the alternating chain of double EE and double EO azido bridges, where the chair conformation is usually observed.[117, 123] As it is known, the lowest δ value is 1.82° which is found in $[Mn(TaiEt)(N_3)_2]_n$ (TaiEt = 1-ethyl-2-(ρ-tolylazo)imidazole).[117]

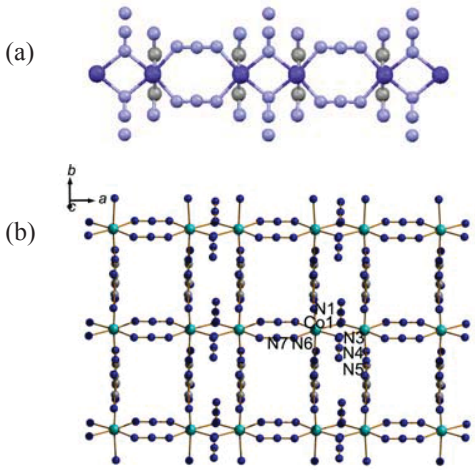

Figure 87 Azido Co^{II} neutral linear chain with the alternating double EE and double EO azido bridges along *a* axis (a). 2D layer of **V-3** in *ab* plane (b). All H atoms are omitted for clarity.

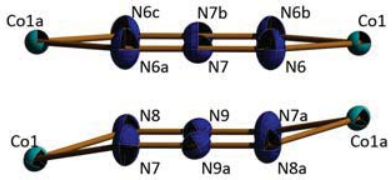

Figure 88 The different conformations of the double EE azido bridged $Co(\mu_2\text{–}1,3\ N_3)_2Co$ ring, complete planarity in **V-3** (top) and chair conformation in **V-4** (bottom).

The ampyz acts as a *N,N′*-ditopic connector in *trans* position, bridging this neutral azido cobalt(II) chain along *b* axis and building the 2D square-grid sheet of **V-3**, as shown in Figure 87. The intralayer π-π stacking interactions among ampyz spacers stabilize the layer of **V-3** with the separations of 3.502(4) and 4.938(4) Å. The Co···Co separation *via* ampyz spacer equals to the crystallographic *b* parameter of 7.1808(12) Å. Moreover, the adjacent 2D sheets of **V-3** are assembled by interlayer hydrogen bonding between the amine H of ampyz and N6 atom of EE azido bridge [N2H···$N6^{i}$ = 2.39 Å (157°), N2···$N6^{i}$ = 3.205(14) Å, (i) =1/2–*x*, 1/2–*y*, 1/2+*z*], yielding a 3D framework of **V-3** with the closest interlayer Co···Co separation of 7.8453(9) Å, as shown in Figure 89.

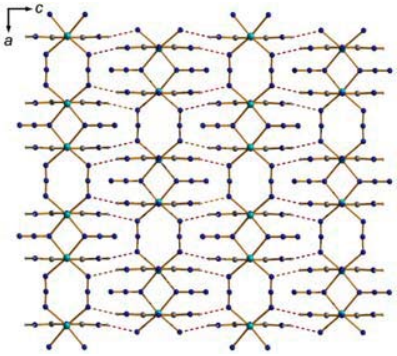

Figure 89 Formation of 3D framework of **V-3** in *ac* plane formed by hydrogen bonds between the neighboring layers. The dotted line represents the interlayer N2–H2B···N6 hydrogen bond.

3D layer of $[Co(N_3)_2(ampyz)]_n$ (V-4)

The crystal structure of **V-4** is depicted in Figure 90. Compound **V-4** shows 3D framework which is isostructural to the reported zinc(II) compound $[Zn(N_3)_2(ampyz)]_n$.[36] There is one crystallographically independent Co^{II} ion, which is octahedral CoN_6 chromophore comprised of two N atoms from two bridging ampyz ligands in *cis*-position and four N atoms from two EE and two EO bridging azide ions.. 3D framework of **V-4** also consists of an azido cobalt(II) neutral zigzag chain with the alternating double EE and double EO azido bridges along *a* axis but *N,N′*-ditopic ampyz spacers link adjacent Co^{II} ions in *cis*-arrangement. The angle of Co···Co···Co in the zigzag chain is 116.62(8)° and the Co···Co separation *via* ampyz spacers are 7.1119(14) and 7.6013(14) Å (Figure 91). The hydrogen bonds between the amine H of *cis*-ampyz spacers and N atoms of azido bridges additionally stabilize the entire framework [N3H···$N4^{i}$ = 2.48 Å (138°), N3···$N4^{i}$ = 3.174(3) Å; N3H···$N7^{ii}$ = 2.57 Å (124°), N3···$N4^{ii}$ = 3.130(3) Å; and N3H···$N8^{iii}$ = 2.31 Å (171°), N3···$N8^{iii}$ = 3.165(3) Å, (i) = 1/2+*x*, 1/2–*y*, –1/2+*z*, (ii) = 1/2–*x*, –1/2+*y*, 1/2–*z*, (iii) = –1/2+*x*, 1/2–*y*, 1/2+*z*.]. The adjacent Co^{II} ions in an azido chain are related by inversion centers and linked alternately by double EE and double EO azido bridges with the Co···Co

distances of 5.3279(10) Å and 3.2438(6) Å, respectively. In double EO bridging mode, the Co1–N4–Co1A–N4A ring is strictly planar due to the existence of the inversion center with the Co1–N4–Co1A angle of 98.90(7)°. The EO azido bridge is nearly linear (∠N4–N5–N6 = 178.1(3)°) and deviate up and down 43.8° from the plane of Co_2N_2. For double EE bridging mode, the EE bridges adopt a chair conformation for the Co(μ_2–1,3 N_3)$_2$Co unit with the dihedral angle δ of 12.57(6)°, as shown in Figure 5.24. The Co$\bar{1}$N$\bar{8}$N9 and Co$\bar{1}$N$\bar{7}$N9B angles are 124.3(2)° and 139.3(2)°, respectively.

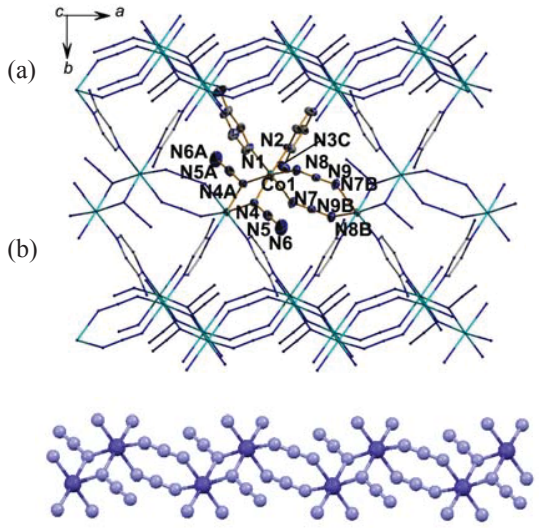

Figure 90 3D framework with atom labeling scheme of **V-4** in *ab* plane (a). The ellipsoids are shown at 50% probability level. Atoms labeled with the notation ‘‘A’’, ‘‘B’’ and “C” are symmetry-generated equivalents, (A) –*x*, 1–*y*, 1–*z*; (B) 1–*x*, 1–*y*, 1–*z*; (C) 1/2+*x*, 1/2–*y*, 1/2+*z*. Azido Co^{II} neutral linear chain with the alternating double EE and double EO azido bridges along *a* axis (b).

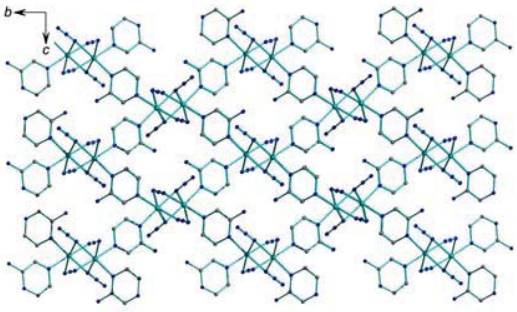

Figure 91 Another view of 3D structure of **V-4** in *bc* plane.

3.4.2.3 Long-range magnetic ordering behaviors

The magnetic susceptibility of a polycrystalline sample of **V-3** at 2-310 K is shown in Figure 92. At 310 K, the $\chi_m T$ value is 2.98 cm^3 K mol^{-1}, which is significantly higher than the spin-only value of 1.87 cm^3 K mol^{-1} expected for $S = 3/2$ ion, owing to the significant orbital contribution of high-spin Co^{II} in an octahedral surrounding. Upon cooling, the $\chi_m T$ value decreases slowly, attains a minimum value of 2.21 cm^3 K mol^{-1} at 70 K and then shows an abrupt increase to a maximum value of 4.64 cm^3 K mol^{-1} at 18 K. This behavior indicates that a small spontaneous magnetization emerges in an antiferromagnetic system, owing to spin canting in which the predominantly antiferromagnetic coupled spins from different sublattices are not perfectly antiparallel, but canting to each other, and the resulting net moments are correlated in a weak ferromagnetic fashion.[108, 111, 144] Upon further cooling to 2 K, $\chi_m T$ decreases gradually down to 0.70 cm^3 K mol^{-1}, suggesting antiferromagnetic interactions among the neighboring azido Co^{II} chains or the magnetization saturation.

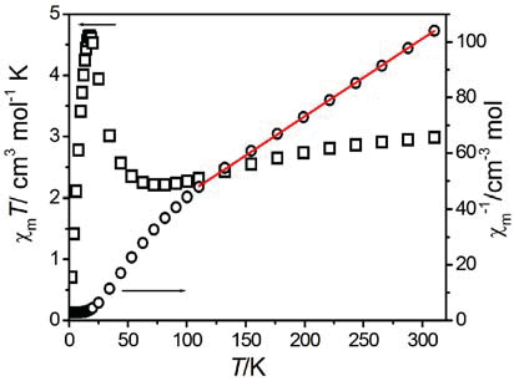

Figure 92 Temperature dependence of $\chi_m T$ (□)and χ_m^{-1} (○) of **V-3** from 2 to 310 K at $H = 10$ kOe. The solid lines correspond to the best fit to the Curie-Weiss law.

The χ_m^{-1} values above 100 K were fitted with the Curie-Weiss law $\chi = C/(T-\theta)$ with a Curie constant $C = 3.58(2)$ cm^3 K mol^{-1} and a Weiss constant $\theta = -61.8(13)$ K. The C is in the usual range of octahedral high-spin Co^{II} ions.[102, 111, 126] The negative θ value can be attributed to both significant spin-orbit coupling of the octahedral Co^{II} ions with a $^4T_{1g}$ ground term and the presence of antiferromagnetic coupling between the Co^{II} centers through the $\mu_{1,3}$-azido bridging ligands. Owing to the lack of a theoretical model for the alternating chain of exchange interactions of octahedral Co^{II} with large spin-orbit coupling effects, the exchange parameters could not be estimated.

To characterize the low-temperature behaviors of **V-3**, the temperature dependencies of field-cooled (FC) and zero-field-cooled (ZFC) magnetization were performed under a field of 100 Oe upon warming from 2 K, as shown in Figure 93. The ZFC and FC plots present a cusp at around 11 K and show a disagreement below 10 K, suggesting the onset of long-range antiferromagnetic ordering

and hysteretic long-range magnetic order, respectively. The temperature dependence of the *ac* susceptibility measured in a field of 3 Oe shows the same features (Figure 94). The maximum of χ' observed at 11 K, in agreement with the above results, confirming the occurrence of phase transition. The absence of an out-of-phase signal (χ'') around this temperature points to a long-range antiferromagnetic order. However, the χ'' value shows nonzero signal below 10 K which is the signature of a magnetized state, thus indicating that a partly canted antiferromagnetic structure exists below this temperature.[157-159]

The temperature dependence of the FC magnetization of **V-3** at various fields is depicted in Figure 93, inset. The application of different magnetic fields in the range of 100–3000 Oe showed a strong field dependence of the magnetic susceptibility below T_N. For applying fields below 500 Oe, the curves show a swell at around 11 K, indicating the antiferromagnetic ordered state. In lower temperature region, the magnetizations increase due to small spontaneous magnetization of canted antiferromagnetism. However, applying magnetic field above 800 Oe is sufficient to overcome these interactions. The cusp disappears and the magnetization tends to saturate at higher filed. These trends suggest a field-induced magnetic phase transition from an antiferromagnetic to a ferromagnetic-like state.[135, 160, 161]

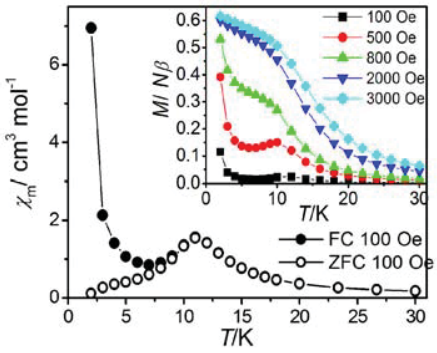

Figure 93 The ZFC and FC magnetization of **V-3** at H = 100 Oe from 2 to 30 K. The inset shows the FC magnetization plot of **V-3** below 30 K at various fields.

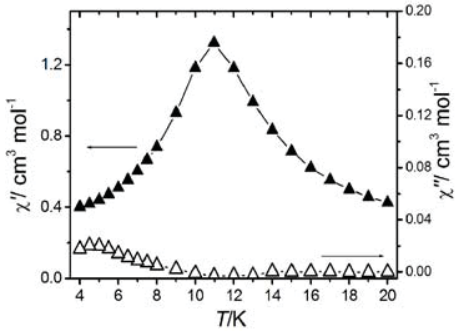

Figure 94 Temperature dependence of the *ac* susceptibility for **V-3** at H_{dc} = 0 Oe, H_{ac} = 3 Oe, with frequency of 997 Hz.

In addition, the spin canting and metamagnetic-like behaviors were confirmed by the hysteresis loop measurements at 2 K in an external field of 0–5 T, as given in Figure 95. The initial $M(H)$ plot shows a characteristic sigmoidal form (Figure 95, inset), which is a typical feature of a metamagnetic behavior.[26, 135, 160, 161] The critical field H_c is ≈ 600 Oe, estimated as the field at which a maximum $\partial M/\partial H$ value is reached. At H < 600 Oe, a linear increase in $M(H)$ is associated with antiferromagnetic interactions, and then above the critical field, the magnetization is drastically increased to H = 5 T without saturation and exhibits a magnetization value of 0.79 $N\beta$, that is far from the theoretical saturation magnetization of Co^{II} ion (M_s = 2.16 $N\beta$, S' = 1/2, g' = 4.33 for octahedral Co^{II} at 2 K),[59, 106] suggesting the overall antiferromagnetic coupling between Co^{II} ions. Clearly, a higher field is required to reach saturation to a ferromagnetic phase. Upon decreasing the applied field, the magnetization curve decreases along a different route and exhibits a slightly sigmoid-shaped hysteresis loop with coercive field of ≈ 350 Oe and remanent magnetization M_r of ≈ 0.29 $N\beta$. These behaviors confirm the occurrence of spontaneous magnetization of **V-3** which is in agreement with the observed coexistence of spin-canted antiferromagnetism and metamagnetism. The canting angle (α) is estimated to be about 7.7° based on the equation $\alpha = \sin^{-1}M_r/M_s$, where M_s the theoretical saturation magnetization of Co^{II} ion at 2 K.

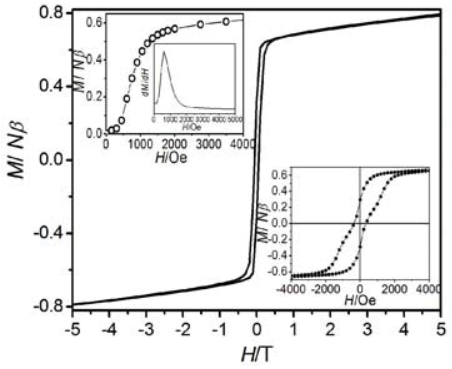

Figure 95 Field dependence of the magnetization for **V-3** at 2 K. The insets show the initial plot in a low field (left) and the hysteresis loop (right).

Temperature dependence of the magnetic susceptibility of **V-4** at 2-310 K under the field of 10 kOe is presented in Figure 96. The $\chi_m T$ value of 2.86 cm^3 K mol^{-1} at 310 K is much higher than the spin-only value of high-spin Co^{II} ions, owing to the orbital contributions of octahedral Co^{II} ions. Upon cooling the temperature, the $\chi_m T$ values decrease gradually and show the cusp around 15 K with the $\chi_m T$ value of 0.57 cm^3 K mol^{-1}, after that the $\chi_m T$ values drop sharply down to 0.09 cm^3 K mol^{-1} at 2 K. The plot of $\chi_m T$ *vs*. T at small fields in the temperature range of 2-30 K is depicted in Figure 96, inset. Below 16 K, the abrupt increases in $\chi_m T$ values are observed under the field below 100 Oe, the susceptibility becomes

field dependent. At small field of 10 Oe, $\chi_m T$ shows an abrupt increase to a maximum value of 9.86 cm^3 K mol^{-1} at 12 K before decreasing in the lowest temperature region. The upturn of $\chi_m T$ below 16 K suggests uncompensated magnetic moments of the system arising from spin canting of the antiferromagnetically coupled Co^{II} ions.[117, 121] The data above 150 K obeys the Curie-Weiss law with a Curie constant C = 3.99(6) cm^3 K mol^{-1} and a Weiss constant $\theta = -119(5)$ K. The C is much larger than the expected spin-only value, which indicates the significant orbital contribution of Co^{II} in an octahedral surrounding.[109] The large negative θ value suggests the strong spin-orbital coupling of Co^{II} ions in an octahedral field and the antiferromagnetic coupling between Co^{II} ions within 3D framework of **V-4**.

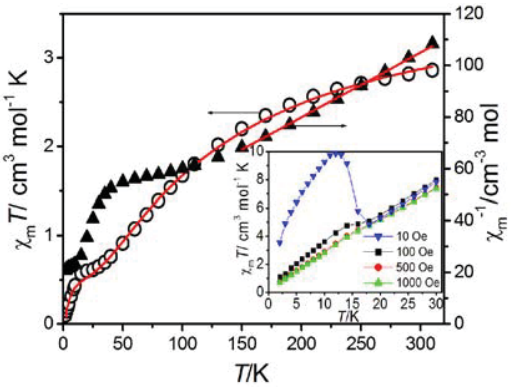

Figure 96 Temperature dependence of $\chi_m T$ (○) and χ_m^{-1} (▲) of **V-4** from 2 to 310 K at H = 10 kOe. The solid lines correspond to the best fit (see the text). The inset shows the $\chi_m T$ *vs*. T plot of **V-4** below 30 K at small fields.

To estimate both magnetic exchange interactions and the spin-orbit coupling effect in the temperature range of 2-310 K for low-dimensional Co^{II} systems, the simple phenomenological equation (5.2) is used. The fitted parameters are $A + B$ = 3.90 cm^3 K mol^{-1}, practically equivalent to the Curie constant obtained from the Curie-Weiss law in the high temperature range, 3.99 cm^3 K mol^{-1}. The E_1/k is +112(8) K which is of the same magnitude as those reported for Co^{II} complexes (the order of +100 K).[136, 137, 139-141] For the antiferromagnetic coupling E_2/k = +4.4(2) K, corresponding to J = –8.8 K, according to the Ising chain approximation, $\chi_m T \propto \exp(+J/2kT)$. It is noticeable that the small E_2/k value is very close to those reported value for compound **V-2** (E_2/k = +4.1(2) K), which contains the same alternating double EO and double EE azido-Co^{II} chain. It is indication of the overall antiferromagnetic coupling within the 1D azido-Co^{II} chain. However, the E_1/k value of **V-4** is much higher than that of **V-2** (E_1/k = +61(2) K) implying that **V-4** presents the stronger spin-orbit coupling of Co^{II} ions in an octahedral field, corresponding to the observation of higher Curie and Weiss constants of **V-4**.

As a further proof for the presence of the spin canting, the temperature dependencies of the ZFC and the FC magnetization were measured at a low field of 10 Oe, as shown in Figure 97, inset. The obvious divergence of the ZFC and FC plots below 16 K indicates the onset of a magnetized state, which is compatible with the maxima in χ' and the nonzero χ'' signal at 16 K in *ac* susceptibility at 997 Hz, indicative of a long-range magnetic ordering (Figures 98). The isothermal magnetization with a field up to 5 T at 2 K is depicted in Figure 97. The initial increase of magnetization shows a positive curvature to 0.198 $N\beta$ at 5 T, far from the theoretical saturation magnetization of Co^{II} ion and no saturation is observed, which is indicative of the overall antiferromagnetic coupling between Co^{II} ions. A hysteresis loop of **V-4** is clearly observed when the field is less than 1 T, giving a coercive field of ≈ 450 Oe and remanent magnetization of ≈ 0.004 $N\beta$. These results indicate that the spin canting effect between overall antiferromagnetically coupled Co^{II} ions leads to residual spins. The canting angle (α) is estimated to be about 0.11° based on the equation $\alpha = \sin^{-1}M_r/M_s$ (M_s = 2.16 $N\beta$ for octahedral Co^{II} at 2 K).

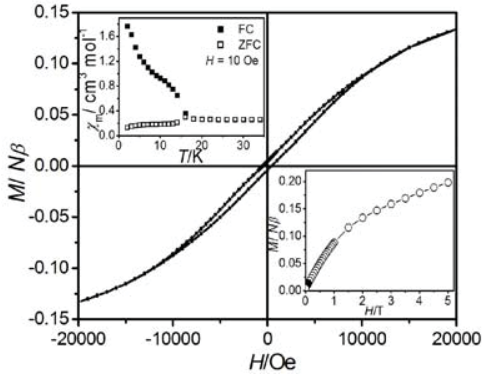

Figure 97 Hysteresis curve of **V-4** at 2 K. The insets show the field dependence of initial magnetization (right) and the ZFC-FC plots of **V-4** at 10 Oe (left).

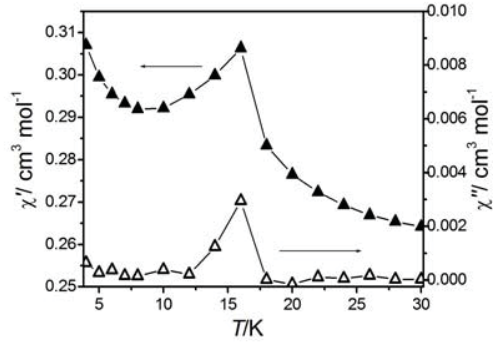

Figure 98 Temperature dependence of the *ac* susceptibility for **V-4** at H_{dc} = 0 Oe, H_{ac} = 3 Oe, with frequency of 997 Hz.

Remarkably, 2D layer of **V-3** exhibits the coexistence of big canting angle and metamagnetic phenomena whereas 3D framework of **V-4** only displays the canted antiferromagnetism with smaller canting angle. As it is known that two mechanisms lead to spin canting behavior (equation 1.16): (i) single-ion magnetic anisotropy and (ii) antisymmetric exchange interaction.[59, 106] However, the spin canted structures are not compatible with both crystal structures of **V-3** and **V-4** because of the presence of an inversion center between the bridged Co^{II} sites, which forbids the occurrence of antisymmetric interactions. It is noticeable that the canted antifferomagnets in the presence of an inversion center between metal sites have been often observed in corresponding complexes that contain the 1D chain of alternating double EO and double EE azido-bridged metal(II) ions. Generally, these complexes were crystallized in low crystal systems (monoclinic and triclinic lattices) and display inversion center between metal sites. The 1D chain complexes with *cis*-bidentate chelating coligands are widely found in this magnetic system while the 2D layer and 3D framework structures are rarely observed. The isotropic Mn^{II} complexes usually exhibit the overall antiferromagnetic interaction within the 1D alternating ferromagnetic and antiferromagnetic chains and their magnetostructural correlations have been investigated entirely.[117, 118, 123, 141] Whereas the metamagnetism and weak ferromagnetism due to canted antifferomagnetic system are usually observed in anisotropic ones (Co^{II}, Fe^{II} and Ni^{II} complexes).[121, 122, 155] However some spin canting of 1D Mn^{II} complexes were also reported, which are due to the possible distortion in the crystal structure at low temperature. [117, 120, 141] Consequently, the observation of spin canting for **V-3** and **V-4** should be attributed to the competition of ferromagnetic and antiferromagnetic interactions within intrachain of the alternating double EO and double EE azido bridging mode together with a relevant single-ion anisotropy of octahedral cobalt(II) ions and a possible structure phase transition at low temperature.[117, 120-122, 155]

Obviously from the structural data, compound **V-3** which was crystallized in orthorhombic system with high centrosymmetric space group *Immm*, presented the disordered amino group on ampyz moiety and disordered terminal EO azido bridge arising from related crystallographic mirror planes and inversion center. It supposes that these disordered positions and inversion centers between the Co^{II} sites somewhere are possibly demolished at very low temperature and develop to the exact atomic location in the crystal lattice with the lower space group. Therefore, the antisymmetric coupling for **V-3** possibly exists at low temperature together with the single-ion anisotropy of octahedral Co^{II} ion yielding big canting angle for **V-3**, as similarly observed in other reported weak ferromagnets with large canting angles (Table 5.7). Moreover the interchain and the interlayer weak antiferromagnetic coupling of **V-3** which originate from *trans*-ampyz bridging shortly between the azido Co^{II} chain and the interlayer hydrogen bonding between NH_2 on ampyz and symmetric double EE azido bridges, would justify for the observed maximum of susceptibility at H_c < 600 Oe. In a magnetic field below 600 Oe, the residual magnetic moments due to spin canting on the chains are weak antiferromagnetically coupled to each other (Figure 5.31, inset). In stronger fields above 600 Oe, the amplitude of the applied magnetic field can

overcome the interchain and interlayer weak antiferromagnetic coupling leading to the observed metamagnetic-like behavior of **V-3**. However, because of the great spin-orbit coupling of Co^{II} ions, the magnetic interaction might be more complicated. Generally, the coexistence of spin canting and metamagnetism is found in the system consisting of a large anisotropy, which leads to a significant spin canting through increasing the possibility of antisymmetric exchange and may induces a metamagnetic transition in the presence of competing interactions within the structure.[157, 159, 162-166]

It is worthwhile to compare the magnetic properties of **V-2, V-3** and **V-4** with the reported Co^{II} complexes containing similar alternating double EO and double EE azido bridging mode, as shown in Table 1. The comparison demonstrates that all compounds are hard magnets at 2 K ($H_c \approx$ 300-500 Oe) and only compound **V-3** which is in the highest-symmetry space group, shows the coexistence of big spin canting angle and metamagnetism whereas the others display very small spin canting angle. This unusual feature of **V-3** could be attributed to the abovementioned significant antisymmetric exchange interaction between Co^{II} ions and the single-ion anisotropy of Co^{II} ion. In addition, the interlayer hydrogen bonding between NH_2 of ampyz and symmetric double EE azido bridges in **V-3** which are not found in other structures, might play the important role on the presence of the field-induce metamagnetic phase transition.

Table 1 Structural and magnetic data for Co^{II} complexes containing the alternating double EO and double EE azido bridging mode.

Compound [a]	$[Co(dpa)(N_3)_2]_n$	**V-2**	**V-3**	**V-4**
Dimension	1D	2D	2D	3D
Co-ligand	*cis*-chelating	*trans*-bridging	*trans*-bridging	*cis*-bridging
Crystal system	monoclinic	triclinic	orthorhombic	monoclinic
Space group	$P2_1/n$	$\bar{P}1$	*Immm*	$P2_1/n$
$\tilde{Co}\tilde{N}Co$ (deg)	103.7	102.25(14)	101.7(3)	98.90(7)
δ (deg) [b]	36.0	33.8(1)	0	12.57(6)
Co···Co (Å) [c]	9.294	8.322(2)	7.1808(12)	7.1119(14)
Magnetic behavior	Canted AF	Canted AF	Canted AF, metamagnetism	Canted AF
θ (K)	–40.0[e]	–58(2)[d]	–61.8(13)[d]	–119(5)[d]
T_N (K)	12.4	12	10	16
M_r ($N\beta$) [f]	0.002	0.002	0.29	0.004
H_c (Oe) [g]	500	300	350	450
α (deg) [h]	0.05	0.05	7.7	0.11
Ref.	[121]	this work	this work	this work

[a] Abbreviations: 2,2′-bpe = 1,2-bis(2-pyridyl)ethylene and dpa = 2,2′-dipyridylamine. [b] The dihedral angle between the mean plane of $Co(\mu_2\text{–}1,3\ N_3)_2Co$ and the Co-N-N plane. [c] The shortest Co···Co distance among alternating double EO and double EE azido-Co^{II} chains. [d] The best fit to Curie-Weiss law above 150 K. [e] The best fit to Curie-Weiss law above 210 K. [f] Remanent magnetization at 2 K. [g] Coercive field at 2 K. [h] Canting angle based on the equation $\alpha = \sin^{-1}M_r/M_s$ ($M_s = 2.16\ N\beta$).

In comparison with **V-3**, compound **V-4** and the others which were crystallized in lower crystal systems, reveal very small canting angles. This result indicates that the major magnetic anisotropy of octahedral Co^{II} ion in **V-4** plays a key role on spin canting as well as a minor magnitude of antisymmetric coupling between Co^{II} ions which possibly arises from a distortion in the crystal framework, suppressing the inversion center at low temperature. Abovementioned compound **V-4** shows the very close antiferromagnetic coupling E_2/k value to that reported for **V-2** but the Weiss constant and E_1/k value are much higher, which point to the very strong spin-orbital coupling of octahedral Co^{II} ions of **V-4**. This extra inherent anisotropy of the Co^{II} ions for **V-4** might provide an additional contribution to a larger degree of spin canting, resulting to the observation of the higher M_r and the larger canting angle when comparing with **V-2** and $[Co(dpa)(N_3)_2]_n$. The T_N of **V-4** is slightly higher than other complexes owing to the closest Co···Co distance among the magnetic chains in 3D covalent framework of **V-4**.

4. Conclusions

The introduction of the amine group to the pyz ring in Cu^{II} carboxylate systems contributes to the structural networks mostly by amending from higher dimension to lower dimension when comparing with pyz spacer, as found in $[Cu(HCO_2)_2(pyz)]_n$[31] revealing a 3D framework, whereas compound **III-1** shows a 2D wavy network. The structure is attributed to the more pronounced steric effect in ampyz which possibly causes the carboxylate group to organize itself to reduce the steric effect, as found in **III-5**. Here malonate acts as tridentate ligand bridging between Cu^{II} centers to build a 2D stairlike layer, instead of acting as tetradentate bridging three Cu centers to build 3D framework, like in the pyz system.[29] However, the ampyz spacer in addition effectively provides other weaker interactions, such as hydrogen bonding and π-π stacking in which it is not only stabilizing within the coordination network but also contributing the stability of whole supramolecular lattice structure which is not observed in pyz system. For instance, compound **III-4** reveals a 2D sheet which is composed of double-stranded chains acting as SBU, connected by ampyz spacers, whereas it is not found in those of the Cu^{II}-pyz systems. For **III-2** and **III-3**, the structures exhibit a 2D sheet stabilized *via* the hydrogen bonding between polymeric chains. Magnetic properties of **III-1** and **III-5** reveal weak ferromagnetic and weak antiferromagnetic spin exchange interactions between adjacent Cu^{II} ions *via* μ_2-*syn-anti* carboxylates and μ_2-ampyz with the spin exchange parameters of J_{inter}/k = +6.9 K and J_{intra}/k = –2.3 K, for **III-1** and J_{inter}/k = +7.4 K and J_{intra}/k = –2.2 K for **III-5**, respectively. Magnetic behaviors of **III-2-4** exhibit very strong antiferromagnetic interactions *via* four μ_2-*syn-syn* carboxylates bridging between Cu^{II} ions which is well-known for the classical paddle-wheel Cu^{II} complexes.

Furthermore, by using versatile ligand ampyz in sulfate system, three metal supramolecular assemblies with a lack of coordination bridges **IV-1-3** and a Cd^{II} coordination polymer **IV-4** were successfully

synthesized. The Cd^{II} ion (ionic radius = 124 pm for 8-coordination)[167] has a larger accessible space for arranging the bridging ampyz and bridging sulfato group leading to the 2D coordination network. In contrast, the smaller Co^{II} (ionic radius = 75 pm for 6-coordination)[168] and Fe^{II} (ionic radius = 78 pm for 6-coordination)[168] ions give isostructural assemblies of monomeric complexes which contain intermolecular π-π stacking and hydrogen bonding interactions stabilizing the whole structures. The water desorption/resorption processes trigger the reversible crystal-to-amorphous transformation with chromotropism for compounds **IV-1-3**. Although the lack of coordination bridge maintaining the skeleton of the framework structures in **IV-1-3**, the original crystalline phases are recovered from collapsed amorphous structures by the restoration of water molecules. On the other hand, the coordination bridges in **IV-4** play an important role for preserving the crystallinity in dehydrated phase thus the reversible structural phase transformation in **IV-4** is observed. The selective methanol accommodation with chromotropism in dehydrated **IV-1A** is observed which could be attributed to the proper size of methanol and weak host-guest interactions causing the changes of the *d*-orbital energy in distorted octahedral geometry. However the **IV-1A·MeOH** is unstable in air. The original crystalline phase **IV-1″** is easily recovered after the evaporation of methanol at room temperature which is indication of high selective recognition of **IV-1A** to water molecules. This work is beneficial to expand the field of the crystal engineering by controlling the weak interaction of coordination moieties.

In case of 2D-1D Co(II) 3,5-pyridinedicarboxylate frameworks, compounds $[Co(pydc)(H_2O)_2]_n$ (**IV-5**) and $[Co(pydc)(H_2O)_4]_n(H_2O)_n$ (**IV-6**) have been successfully synthesized with 2D and 1D structural arrangement. The pydc acts as a tridentate ligand bridging between Co centers to build a 2D layer in **IV-5**, and a didentate bridging fashion to form 1D zig-zag chain in **IV-6**. Moreover, the pydc spacer in addition provides other weaker interactions, such as hydrogen bonding and π-π stacking in which it is not only stabilizing within the coordination network but also contributing the stability of whole framework structure. We have been able to demonstrate that the water molecules in both compounds can be reversibly exchanged along with the change in color of the sample. The reversibility of the solid transformation has been supported by spectroscopic techniques, elemental analysis, TGA and XRPD and shows that **IV-5** and **IV-6** exhibit water induced crystal-to-amorphous transformation with chromotropism. Furthermore, upon reintroduce of the water molecules, the original structure of **IV-6** could be generated from the dehydrated forms of both **IV-5** and **IV-6**. A striking contrast for this system is that the 2D honeycome-like layer structure of **IV-5** can be transformed readily to the 1D zig-zag chain of **IV-6**, but not vice versa. The results suggest that **IV-6** is thermodynamically more stable than **IV-5** and the water molecules function as template molecules. They are essential for inducing the zig-zag chain structure when exposed to the enrichment water vapor and the weak interactions (hydrogen bonds and π-π stacking) pay an important role in the reversible phase transformation. Therefore, the conspicuous response of the dehydrated and

rehydrated samples to the presence of water suggests that these compounds could be employed as humidity sensors.

In the last complex system, two novel cobalt(II) azido inorganic-organic hybrid materials containing 2,2′-bpe have been obtained. The 2,2′-bpe can serve as either terminal coligand in monodentate coordination in **V-1** or ditopic bridging spacer in *trans* position in **V-2** with which molecular magnets of different lattice dimensionalities were developed. The 1D chain of **V-1** contains the rare mixing geometries of Co^{II} ions in a unique $[-5-5-6-]_n$ sequence of coordination number bridged by double EO mode of azide. The adjacent chains are assembled by C–H···π interaction and the intermolecular hydrogen bonds, stabilizing 2D sheet of **V-1**. The magnetic behavior of **V-1** reveals the metamagnetic transition which may be due to the presence of weak interchain antiferromagnetic interactions among the strong ferromagnetism of double EO Co^{II} azido chains. In contrast, compound **V-2** is 2D wavy coordination polymer containing the alternating double EO and double EE bridging modes of azides and exhibits a weak ferromagnetism due to spin canting. In case of the versatile ampyz spacer, two high dimensional cobalt(II) azido inorganic-organic hybrid frameworks, which contain similarly alternating double EO and double EE azido-bridged Co^{II} chain were obtained from the different preparative methods. The high symmetric square-grid structure of **V-3** from layer diffusion method which consists of *trans*-ampyz bridging between octahedral Co^{II} centers in axial positions, presents the coexistence of a big spin canting angle and metamagnetism below 10 K. The canting angle is estimated to be 7.7° and the critical field for metamagnetic phase transition is ≈ 600 Oe at 2 K. The interlayer hydrogen bonding between amino group of ampyz spacer and symmetric double EE azido bridges plays an important role on the field-induce metamagnetic phase transition. The spin canting of **V-3** could be attributed to the significant antisymmetric exchange arising from the structure phase transition at low temperature and the great role of magnetic anisotropy of Co^{II} ion. Whereas 3D framework containing *cis*-ampyz bridging among Co^{II} centers of **V-4** was synthesized from hydrothermal technique. It was crystallized in lower space group and exhibited only small spin-canted antiferromagnetism below 16 K. It is suggests that the large magnetic anisotropy in **V-4** might contribute a spin canting together with small antisymmetric coupling between Co^{II} ions, arising from a distortion in the crystal net at low temperature, which is frequently found in the related complexes containing the same bridging mode of azide. These results will provide the merit for future investigations and demonstrate the importance of the crystal engineering of inorganic-organic hybrid framework in the field of molecular-based magnetic materials.

5. References

[1] H. K. Chae, D. Y. Siberio-Pérez, Y. G. J. Kim, M. Eddaoudi, A. J. Matzger, M. O'Keeffe, O. M. Yaghi, *Nature* **2004**, *427*, 523.

[2] X.-Y. Wang, Z.-M. Wang, S. Gao, *Chem. Commun.* **2008**, 281.

[3] Y. G. Huang, D. Q. Yuan, L. Pan, F. L. Jiang, M. Y. Wu, X. D. Zhang, W. Wei, Q. Gao, Y. L. Jeong, J. Li, M. C. Hong, *Inorg. Chem.* **2007**, *46*, 9609.

[4] C. J. Kepert, *Chem. Commun.* **2006**, 695.
[5] I. G. Georgiev, L. R. MacGillivray, *Chem. Soc. Rev.* **2007**, *36*, 1239.
[6] Y. Li, R. T. Yang, *J. Am. Chem. Soc.* **2006**, *128*, 8136.
[7] J. Yuasa, S. Fukuzumi, *J. Am. Chem. Soc.* **2008**, *130*, 566.
[8] W. G. Lu, J. Z. Gu, L. Jiang, M. Y. Tan, T. B. Lu, *Cryst. Growth Des.* **2008**, *8*, 192.
[9] M. Frisch, C. L. Cahill, *Cryst. Growth Des.* **2008**, *8*, 2921.
[10] H. Li, M. Eddaoudi, M. O'Keeffe, O. M. Yaghi, *Nature* **1999**, *402*, 276.
[11] O. R. Evans, W. Lin, *Acc. Chem. Res.* **2002**, *35*, 511.
[12] O. M. Yaghi, M. O'Keeffe, N. W. Ockwig, H. K. Chae, M. Eddaoudi, J. Kim, *Nature* **2003**, *423*, 705.
[13] C. Janiak, *Dalton Trans.* **2003**, 2781.
[14] A. K. Cheetham, C. N. R. Rao, R. K. Feller, *Chem. Commun.* **2006**, 4780.
[15] M. Mikuriya, D. Yoshioka, M. Handa, *Coord. Chem. Rev.* **2006**, *250*, 2194.
[16] Z. Wang, B. Zhang, Y. Zhang, M. Kurmoo, T. Liu, S. Gao, H. Kobayashi, *Polyhedron* **2007**, *26*, 2207.
[17] M. Melnik, *Coord. Chem. Rev.* **1982**, *42*, 259.
[18] J. Su, Y. Wang, S. Yang, G. Li, F. Liao, J. Lin, *Inorg. Chem.* **2007**, *46*, 8403.
[19] W. A. Wojtczak, M. J. Hampden-Smith, E. N. Duesler, *Inorg. Chem.* **1998**, *37*, 1781.
[20] D. K. Towle, S. K. Hoffmann, W. E. Hatfield, P. Singh, P. Chaudhuri, *Inorg. Chem.* **1988**, *27*, 394.
[21] H. Adams, S. Clunas, D. E. Fenton, T. J. Gregson, P. E. McHugh, S. E. Spey, *Inorg. Chem. Commun.* **2002**, *5*, 211.
[22] J. Boonmak, S. Youngme, T. Chotkhun, C. Engkagul, N. Chaichit, G. A. v. Albada, J. Reedijk, *Inorg. Chem. Commun.* **2008**, *11*, 1231.
[23] S. Youngme, A. Cheansirisomboon, C. Danvirutai, C. Pakawatchai, N. Chaichit, C. Engkagul, G. A. van Albada, J. S. Costa, J. Reedijk, *Polyhedron* **2008**, *27*, 1875.
[24] M. Du, X. J. Jiang, X. J. Zhao, *Inorg. Chem.* **2007**, *46*, 3984.
[25] S. Kitagawa, T. Okubo, S. Kawata, M. Kondo, M. Katada, H. Kobayashi, *Inorg. Chem.* **1995**, *34*, 4790.
[26] X. Hao, Y. Wei, S. Zhang, *Chem. Commun.* **2000**, 2271.
[27] G. Bhosekar, I. Jess, C. Näther, *Inorg. Chem.* **2006**, *45*, 6508.
[28] J. L. Manson, T. Lancaster, J. A. Schlueter, S. J. Blundell, M. L. Brooks, F. L. Pratt, C. L. Nygren, H. J. Koo, D. Dai, M. H. Whangbo, *Inorg. Chem.* **2007**, *46*, 213.
[29] Y. Rodríguez-Martín, M. Hernández-Molina, F. S. Delgado, J. Pasán, C. Ruiz-Pérez, J. Sanchiz, F. Lloret, M. Julve, *CrystEngComm* **2002**, *4*, 440.
[30] T. F. Liu, H. L. Sun, S. Gao, S. W. Zhang, T. C. Lau, *Inorg. Chem.* **2003**, *42*, 4792.
[31] J. L. Manson, J. G. Lecher, J. Gu, U. Geiser, J. A. Schlueter, R. Henning, X. Wang, A. J. Schultz, H. J. Koo, M. H. Whangbo, *Dalton Trans* **2003**, 2905.
[32] H. Mao, C. Zhang, G. Li, H. Zhang, H. Hou, L. Li, Q. Wu, Y. Zhu, E. Wanga, *Dalton Trans.* **2004**, 3918.
[33] F. S. Delgado, J. Sanchiz, C. Ruiz-Perez, F. Lloret, M. Julve, *CrystEngComm* **2003**, *5*, 280.
[34] J. L. Manson, J. A. Schlueter, U. Geiser, M. B. Stone, D. H. Reich, *Polyhedron* **2001**, *20*, 1423.
[35] S. Pagola, R. D. Pike, K. DeKrafft, T. A. Tronic, *Acta Crystallogr.* **2008**, *C64*, m134.
[36] M. A. S. Goher, F. A. Mautner, B. Sodin, B. Bitschnau, *J. Mol. Struct.* **2008**, *879*, 96.
[37] T. A. Tronic, K. E. DeKrafft, J. L. Mi, A. N. Ley, R. D. Pike, *Inorg. Chem.* **2007**, *46*, 8897.
[38] F. S. Delgado, F. Lahoz, F. Lloret, M. Julve, C. Ruiz-Perez, *Cryst. Growth Des.* **2008**, *8*, 3219.
[39] R. Vaidhyanathan, S. Natarajan, C. N. R. Rao, *Cryst. Growth Des.* **2003**, *3*, 47.
[40] M. R. Montney, S. M. Krishnan, N. M. Patel, R. M. Supkowski, R. L. Laduca, *Cryst. Growth Des.* **2007**, *7*, 1145.
[41] F. S. Delgado, J. Sanchiz, C. Ruiz-Perez, F. Lloret, M. Julve, *Inorg. Chem.* **2003**, *42*, 5938.
[42] S. Youngme, A. Cheansirisomboon, C. Danvirutai, C. Pakawatchai, N. Chaichit, *Inorg. Chem. Commun.* **2008**, *11*, 57.
[43] B. J. Hathaway, G. Wilkinson, R. D. Gill, J. A. McCleverty, *Comprehensive coordination chemistry*, Pergamon Oxford, **1987**.
[44] A. W. Addison, T. N. Rao, J. Reedijk, J. Van Rijn, G. C. Verschoor, *J. Chem. Soc., Dalton Trans.* **1984**, 1349.

[45] C. Janiak, *J. Am. Soc., Dalton Trans.* **2000**, 3885.
[46] J. S. Valentine, A. J. Silverstein, Z. G. Soos, *J. Am. Chem. Soc.* **1974**, *96*, 97.
[47] A. Das, I. Todorov, S. K. Dey, S. Mitra, *Inorg. Chim. Acta* **2006**, *359*, 2041.
[48] M. Masahiro, A. Hiroshi, H. Makoto, *Mol. Cryst. Liq. Cryst. Sci. Technol* **2002**, *379*, 205.
[49] C. Z. Zhang, H. Y. Mao, Y. L. Wang, H. Y. Zhang, J. C. Tao, *J. Phys. Chem. Solids* **2007**, *68*, 236.
[50] S. Youngme, C. Chailuecha, G. A. Van Albada, C. Pakawatchai, N. Chaichit, J. Reedijk, *Inorg. Chim. Acta* **2004**, *357*, 2532.
[51] S. Youngme, C. Chailuecha, G. A. Van Albada, C. Pakawatchai, N. Chaichit, J. Reedijk, *Inorg. Chim. Acta* **2005**, *358*, 1068.
[52] C. Chailuecha, S. Youngme, C. Pakawatchai, N. Chaichit, G. A. van Albada, J. Reedijk, *Inorg. Chim. Acta* **2006**, *359*, 4168.
[53] S. Youngme, J. Phatchimkun, N. Wannarit, N. Chaichit, S. Meejoo, G. A. van Albada, J. Reedijk, *Polyhedron* **2008**, *27*, 304.
[54] B. KozlevcŒar, I. Leban, M. PetricŒ, S. Petricek, O. Roubeau, J. Reedijk, P. Segedin, *Inorg. Chim. Acta* **2004**, *357*, 4220.
[55] B. KozlevcŒar, I. Leban, M. PetricŒ, S. Petricek, O. Roubeau, J. Reedijk, P. Segedin, *Inorg. Chim. Acta* **2004**, *357*, 4220.
[56] M. Murugesu, R. Clerac, B. Pilawa, A. Mandel, C. E. Anson, A. K. Powell, *Inor. Chim. Acta* **2002**, *337*, 328.
[57] B. Li, X. Wang, Y. Zhang, S. Gao, Y. Zhang, *Inor. Chim. Acta* **2005**, *358*, 3519.
[58] E. Colacio, M. Ghazi, R. Kiveka, J. M. Moreno, *Inorg. Chem.* **2000**, *39*, 2882.
[59] O. Kahn, *Molecular magnetism*, VCM Publishers, USA, **1993**.
[60] S. Kitagawa, K. Uemura, *Chem. Soc. Rev.* **2005**, *34*, 109.
[61] S. Kitagawa, R. Kitaura, S.-i. Noro, *Angew. Chem. Int. Ed.* **2004**, *43*, 2334.
[62] C. J. Kepert, T. J. Prior, M. J. Rosseinsky, *J. Am. Chem. Soc.* **2000**, *122*, 5158.
[63] N. Yanai, W. Kaneko, K. Yoneda, M. Ohba, S. Kitagawa, *J. Am. Chem. Soc.* **2007**, *129*, 3496.
[64] S. I. Ohkoshi, K. I. Arai, Y. Sato, K. Hashimoto, *Nat. Mater.* **2004**, *3*, 857.
[65] S. Hasegawa, S. Horike, R. Matsuda, S. Furukawa, K. Mochizuki, Y. Kinoshita, S. Kitagawa, *J. Am. Chem. Soc.* **2007**, *129*, 2607.
[66] M. R. Kishan, J. Tian, P. K. Thallapally, C. A. Fernandez, S. J. Dalgarno, J. E. Warren, B. P. McGrail, J. L. Atwood, *Chem. Commun.* **2010**, *46*, 538.
[67] D. J. Collins, H. C. Zhou, *J. Mater. Chem.* **2007**, *17*, 3154.
[68] M. Edgar, R. Mitchell, A. M. Z. Slawin, P. Lightfoot, P. A. Wright, *Chem. Eur. J.* **2001**, *7*, 5168.
[69] J. J. Vittal, X. Yang, *Cryst. Growth Des.* **2002**, *2*, 259.
[70] X. Yang, D. Wu, J. D. Ranford, J. J. Vittal, *Cryst. Growth Des.* **2005**, *5*, 41.
[71] K. S. Min, M. P. Suh, *Chem. Eur. J.* **2001**, *7*, 303.
[72] L. Zhao, B. H. Northrop, P. J. Stang, *J. Am. Chem. Soc.* **2008**, *130*, 11886.
[73] C. L. Chen, A. M. Beatty, *J. Am. Chem. Soc.* **2008**, *130*, 17222.
[74] S. A. Dalrymple, G. K. H. Shimizu, *Chem. Commun.* **2006**, 956.
[75] S. A. Dalrymple, G. K. H. Shimizu, *J. Am. Chem. Soc.* **2007**, *129*, 12114.
[76] K. Uemura, S. Kitagawa, K. Fukui, K. Saito, *J. Am. Chem. Soc.* **2004**, *126*, 3817.
[77] C. L. Chen, A. M. Goforth, M. D. Smith, C. Y. Su, H. C. Zur Loye, *Inorg. Chem.* **2005**, *44*, 8762.
[78] M. D. Stephenson, M. J. Hardie, *CrystEngComm* **2007**, *9*, 496.
[79] B. Moulton, M. J. Zaworotko, *Chem. Rev.* **2001**, *101*, 1629.
[80] N. L. Rosi, M. Eddaoudi, J. Kim, M. O'Keeffe, O. M. Yaghi, *CrystEngComm* **2002**, *4*, 401.
[81] M. J. Rosseinsky, *Microporous and Mesoporous Mater.* **2004**, *73*, 15.
[82] K. Biradha, M. Sarkar, L. Rajput, *Chem. Commun.* **2006**, 4169.
[83] C. L. Cahill, D. T. De Lill, M. Frisch, *CrystEngComm* **2007**, *9*, 15.
[84] C. N. R. Rao, J. N. Behera, M. Dan, *Chem. Soc. Rev.* **2006**, *35*, 375.
[85] D. Bradshaw, J. E. Warren, M. J. Rosseinsky, *Science* **2007**, *315*, 977.
[86] J. Lu, C. Yu, T. Niu, T. Paliwala, G. Crisci, F. Somosa, A. J. Jacobson, *Inorg. Chem.* **1998**, *37*, 4637.
[87] K. Uemura, A. Maeda, H. Kita, *Polyhedron* **2008**, *27*, 2939.

[88] P. Amo-Ochoa, G. Givaja, P. J. S. Miguel, O. Castillo, F. Zamora, *Inorg. Chem. Commun.* **2007**, *10*, 921.
[89] Y. L. Yao, L. Xue, Y. X. Che, J. M. Zheng, *Cryst. Growth Des.* **2008**, *8*, 1801.
[90] L. Carlucci, G. Ciani, D. M. Proserpio, S. Rizzato, *CrystEngComm* **2003**, *5*, 190.
[91] J. R. Allan, A. D. Paton, K. Turvey, H. J. Bowley, D. L. Gerrard, *Inorg. Chim. Acta* **1987**, *134*, 259.
[92] K. Nakamoto, *Infrared and raman spectra of inorganic and coordination compounds*, 5 ed., Wiley, New York, **1997**.
[93] A. B. P. Lever, *Inorganic electronic spectroscopy*, 2 ed., Elsevier, The Netherlands, **1984**.
[94] R. Wang, L. Han, F. Jiang, Y. Zhou, D. Yuan, M. Hong, *Cryst. Growth Des.* **2005**, *5*, 129.
[95] N. Zheng, J. Zhang, X. Bu, P. Feng, *Cryst. Growth Des.* **2007**, *7*, 2576.
[96] H. D. Guo, X. M. Guo, S. R. Batten, J. F. Song, S. Y. Song, S. Dang, G. L. Zheng, J. K. Tang, H. J. Zhang, *Cryst. Growth Des.* **2009**, *9*, 1394.
[97] J. K. Shiba, R. Bau, *Inorg. Chem.* **1978**, *17*, 3484.
[98] H. T. Zhang, Y. Z. Li, H. Q. Wang, E. N. Nfor, X. Z. You, *CrystEngComm* **2005**, *7*, 578.
[99] S. J. Fu, C. Y. Cheng, K. J. Lin, *Cryst. Growth Des.* **2007**, *7*, 1381.
[100] C. L. Chen, A. M. Goforth, M. D. Smith, C. Y. Su, H. C. Zur Loye, *Angew. Chem. Int. Ed.* **2005**, *44*, 6673.
[101] L. G. Beauvais, M. P. Shores, J. R. Long, *J. Am. Chem. Soc.* **2000**, *122*, 2763.
[102] M. Kurmoo, *Chem. Soc. Rev.* **2009**, *38*, 1353.
[103] Y.-F. Zeng, X. Hu, F.-C. Liu, X.-H. Bu, *Chem. Soc. Rev.* **2009**, *38*, 469.
[104] J. Ribas, A. Escuer, M. Monfort, R. Vicente, R. Cortés, L. Lezama, T. f. Rojo, *Coord. Chem. Rev.* **1999**, *193-195*, 1027.
[105] A. Escuer, G. Aromí, *Eur. J. Inorg. Chem.* **2006**, 4721.
[106] R. L. Carlin, *Magnetochemistry*, Springer-Verlag, Germany, **1986**.
[107] T. F. Liu, D. Fu, S. Gao, Y. Z. Zhang, H. L. Sun, G. Su, Y. J. Liu, *J. Am. Chem. Soc* **2003**, *125*, 13976.
[108] G. En-Qing, L. Pei-Pei, W. Yan-Qin, Y. Qi, W. Qing-Lun, *Chem. Eur. J.* **2009**, *15*, 1217.
[109] R.-Y. Li, X.-Y. Wang, T. Liu, H.-B. Xu, F. Zhao, Z.-M. Wang, S. Gao, *Inorg. Chem.* **2008**, *47*, 8134.
[110] H. Chang Seop, K. Ja-eung, S. Sang-Kil, L. Yoon Sup, K. Yaung-Soo, D. Youngkyu, *Chem. Eur. J.* **2001**, *7*, 4243.
[111] F. A. Mautner, L. Öhrström, B. Sodin, R. Vicente, *Inorg. Chem.* **2009**, *48*, 6280.
[112] X.-Y. Wang, Z.-M. Wang, S. Gao, *Inorg. Chem.* **2008**, *47*, 5720.
[113] M. L. Hernández, M. G. Barandika, M. K. Urtiaga, R. Cortés, L. Lezama, M. I. Arriortua, *J. Chem. Soc., Dalton Trans.* **2000**, 79.
[114] A. K. Ghosh, D. Ghoshal, E. Zangrando, J. Ribas, N. Ray Chaudhuri, *Inorg. Chem.* **2005**, *44*, 1786.
[115] S. Konar, E. Zangrando, M. G. B. Drew, T. Mallah, J. Ribas, N. Ray Chaudhuri, *Inorg. Chem.* **2003**, *42*, 5966.
[116] S. Hao-Ling, W. Zhe-Ming, G. Song, *Chem. Eur. J.* **2009**, *15*, 1757.
[117] R. Umasankar, J. Sk, G. Barindra Kumar, M. Montserrat, R. Joan, M. Golam, L. Tian -Huey, S. Chittaranjan, *Eur. J. Inorg. Chem.* **2004**, *2004*, 250.
[118] R. Cortés, M. Drillon, X. Solans, L. Lezama, T. Rojo, *Inorg. Chem.* **1997**, *36*, 677.
[119] L. Cai-Ming, G. Song, Z. De-Qing, H. Yong-Hong, X. Ren-Gen, L. Zhi-Liang, J. Feng-Chi, Z. Dao-Ben, *Angew. Chem. Int. Ed.* **2004**, *43*, 990.
[120] J.-Y. Zhang, C.-M. Liu, D.-Q. Zhang, S. Gao, D.-B. Zhu, *Inorg. Chem. Commun.* **2007**, *10*, 897.
[121] X.-T. Wang, X.-H. Wang, Z.-M. Wang, S. Gao, *Inorg. Chem.* **2009**, *48*, 1301.
[122] G. Viau, M. G. Lombardi, G. D. Munno, M. Julve, F. Lloret, J. Faus, A. Caneschic, J. M. Clemente-Juana, *Chem. Commun.* **1997**, 1195.
[123] E.-Q. Gao, S.-Q. Bai, Y.-F. Yue, Z.-M. Wang, C.-H. Yan, *Inorg. Chem.* **2003**, *42*, 3642.
[124] J. L. Manson, A. M. Arif, J. S. Miller, *Chem. Commun.* **1999**, 1479.
[125] J. Ribas, M. Monfort, C. Diaz, C. Bastos, X. Solans, *Inorg. Chem.* **1994**, *33*, 484.
[126] H. S. Yoo, J. Kim, N. Yang, E. K. Koh, J.-G. Park, C. S. Hong, *Inorg. Chem.* **2007**, *46*, 9054.
[127] X. Lin, J. Tao, R. B. Huang, L. S. Zheng, *Inorg. Chem. Commun.* **2009**, *12*, 154.
[128] S.-Q. Bai, E.-Q. Gao, Z. He, C.-J. Fang, Y.-F. Yue, C.-H. Yan, *Eur. J. Inorg. Chem.* **2006**, 407.
[129] T. Yang, J. Ju, G. Li, S. Yang, J. Sun, F. Liao, J. Lin, J. Sasaki, N. Toyota, *Inorg. Chem* **2007**, *46*, 2342.

[130] A. Das, G. M. Rosair, M. S. El Fallah, J. Ribas, S. Mitra, *Inorg. Chem* **2006**, *45*, 3301.
[131] L. K. Thompson, S. S. Tandon, F. Lloret, J. Cano, M. Julve, *Inorg. Chem* **1997**, *36*, 3301.
[132] L. M. Toma, F. S. Delgado, C. Ruiz-Perez, R. Carrasco, J. Cano, F. Lloret, M. Julve, *Dalton Trans.* **2004**, 2836.
[133] J. H. Yoon, H. C. Kim, C. S. Hong, *Inorg. Chem.* **2005**, *44*, 7714.
[134] P. Lama, A. Aijaz, E. Carolina Sanudo, P. K. Bharadwaj, *Cryst. Growth Des.*, *10*, 283.
[135] W.-W. Sun, C.-Y. Tian, X.-H. Jing, Y.-Q. Wang, E.-Q. Gao, *Chem. Commun.* **2009**, 4741.
[136] J. M. Rueff, N. Masciocchi, P. Rabu, A. Sironi, A. Skoulios, *Eur. J. Inorg. Chem.* **2001**, 2843.
[137] J. M. Rueff, N. Masciocchi, P. Rabu, A. Sironi, A. Skoulios, *Chem.Eur. J.* **2002**, *8*, 1813.
[138] S. C. Manna, S. Konar, E. Zangrando, K.-i. Okamoto, J. Ribas, N. R. Chaudhuri, *Eur. J. Inorg. Chem.* **2005**, 4646.
[139] T. D. Keene, M. B. Hursthouse, D. J. Price, *Cryst. Growth Des.* **2009**, *9*, 2604.
[140] F.-C. Liu, Y.-F. Zeng, J. Jiao, X.-H. Bu, J. Ribas, S. R. Batten, *Inorg. Chem.* **2006**, *45*, 2776.
[141] M. Villanueva, J. Mesa, M. K. Urtiaga, R. Cortés, L. Lezama, M. a. I. Arriortua, T. Rojo, *Eur. J. Inorg. Chem.* **2001**, 1581.
[142] J. S. Miller, *Inorg. Chem.* **2000**, *39*, 4392.
[143] P. Dechambenoit, J. R. Long, *Chem. Soc. Rev.* **2011**, *40*, 3249.
[144] D.-F. Weng, Z.-M. Wang, S. Gao, *Chem. Soc. Rev.* **2011**, *40*, 3157.
[145] M. A. M. Abu-Youssef, A. Escuer, D. Gatteschi, M. A. S. Goher, F. A. Mautner, R. Vicente, *Inorg. Chem.* **1999**, *38*, 5716.
[146] F.-C. Liu, Y.-F. Zeng, J.-P. Zhao, B.-W. Hu, X.-H. Bu, J. Ribas, J. Cano, *Inorg. Chem.* **2007**, *46*, 1520.
[147] S. Martín, M. G. Barandika, L. Lezama, J. L. Pizarro, Z. E. Serna, J. I. R. d. Larramendi, M. I. Arriortua, T. Rojo, R. Cortés, *Inorg. Chem.* **2001**, *40*, 4109.
[148] M. A. M. Abu-Youssef, M. Drillon, A. Escuer, M. A. S. Goher, F. A. Mautner, R. Vicente, *Inorg. Chem.* **2000**, *39*, 5022.
[149] C. Adhikarya, S. Koner, *Coord. Chem. Rev* **2010**, *254*, 2933.
[150] M. A. M. Abu-Youssef, A. Escuer, F. A. Mautnerc, L. Öhrström, *Dalton Trans.* **2008**, 3553.
[151] A. a. A. Massoud, M. A. M. Abu-Youssef, J. P. Vejpravová, V. Langera, L. Öhrström, *CrystEngComm* **2009**, *11*, 223.
[152] W. Dong, Y. Ouyang, D.-Z. Liao, S.-P. Yan, P. Cheng, Z.-H. Jiang, *Inor. Chim. Acta* **2006**, *359*, 3363.
[153] J. Boonmak, S. Youngme, N. Chaichit, G. A. van Albada, J. Reedijk, *Cryst. Growth Des.* **2009**, *9*, 3318.
[154] J. Boonmak, M. Nakano, N. Chaichit, C. Pakawatchai, S. Youngme, *Dalton Trans.* **2010**, *39*, 8161.
[155] J. Boonmak, M. Nakano, S. Youngme, *Dalton Trans.* **2011**, *40*, 1254.
[156] X.-Y. Wang, L. Wang, Z.-M. Wang, S. Gao, *J. Am. Chem. Soc* **2006**, *128*, 674.
[157] M.-H. Zeng, W.-X. Zhang, X.-Z. Sun, X.-M. Chen, *Angew. Chem. Int. Ed.* **2005**, *44*, 3079.
[158] Z.-L. Huang, M. Drillon, N. Masciocchi, A. Sironi, J.-T. Zhao, P. Rabu, P. Panissod, *Chem. Mater.* **2000**, *12*, 2805.
[159] B.-P. Yang, A. V. Prosvirin, Y.-Q. Guo, J.-G. Mao, *Inorg. Chem.* **2008**, *47*, 1453.
[160] S. M. Winter, K. Cvrkalj, P. A. Dube, C. M. Robertson, M. R. Probert, J. A. K. Howard, R. T. Oakley, *Chem. Commun.* **2009**, 7309.
[161] J. Pasán, J. n. Sanchiz, C. Ruiz-Pérez, J. Campo, F. Lloret, M. Julve, *Chem. Commun.* **2006**, 2857.
[162] X.-Y. Wang, L. Wang, Z.-M. Wang, G. Su, S. Gao, *Chem. Mater.* **2005**, *17*, 6369.
[163] K. Mitsumoto, T. Shiga, M. Nakano, M. Nihei, H. Nishikawa, H. Oshio, *Eur. J. Inorg. Chem.* **2008**, 4851.
[164] H. H. Ko, J. H. Lim, H. C. Kim, C. S. Hong, *Inorg. Chem.* **2006**, *45*, 8847.
[165] H.-P. Jia, W. Li, Z.-F. Ju, J. Zhang, *Chem. Commun.* **2008**, 371.
[166] S. M. Humphrey, P. T. Wood, *J. Am. Chem. Soc* **2004**, *126*, 13236.

OUTPUT OF THE RESEARCH

Ph.D Students:

1) Dr. Pongthipun Phuengphai (2007-2010)**:** "Design of Metal Organic Frameworks (MOFs) and Their Functions Towards Catalysis and Anion-exchange" Doctor of Philosophy Thesis in Chemistry, Graduate School, Khon Kaen University.
2) Dr. Jaursup Boonmak. (2006-2011): "Structural Diversity, Dynamic Structural Transformations and Magnetic Properties of Inorganic-Organic Hybrid Frameworks" Doctor of Philosophy Thesis in Chemistry, Graduate School, Khon Kaen University.

Publication papers:

1) J. Boonmak, S. Youngme, N. Chaichit, G.A. van Albada, and J. Reedijk, "Series of copper(II) coordination polymers containing aminopyrazine and different carboxylato bridges: Syntheses, structures and magnetic properties", ***Cryst. Growth des.,*** 2009, **9**, 3318-3326.
2) P. Phuengphai**,** S. Youngme**,** P. Kongsaeree**,** C. Pakawatchai**,** N. Chaichit**,** S. J. Teat**,** P. Gamez and J. Reedijk**, "**Drastic steric effects from, respectively, a hydrogen, a methyl and an ethyl group on the coordination network of a zinc(II)-4,4 '-bipyridine-carboxylato ternary system", ***CrystEngComm,*** 2009, **11**, 1723-1732.
3) C. Ramon, I. rio de P.R. Moreira, S. Youngme, K. Siriwong, N. Wannarit and F. Illas, "Toward the Design of Ferromagnetic Molecular Complexes: Magnetostructural Correlations in Ferromagnetic Triply Bridged Dinuclear Cu(II) Compounds Containing Carboxylato and Hydroxo Bridges" ***Inorg. Chem.***, 2010, **49**, 285-294**.**
4) Cheansirisomboon, S. Youngme, C. Pakawatchai and N. Chaichit, "Synthesis and crystal structure of two new dinuclear oxalato-bridged copper(II) complexes containing bis(2-pyridyl)amine as a ligand", ***Mendeleev Commun.***, 2010, **20**, 109–110.
5) J. Boonmak, M. Nakano, N. Chaichit, C. Pakawatchai, and S.Youngme, "Water-induced reversible structural phase transformation with chromotropism in metal supramolecular frameworks containing aminopyrazine and sulfate anions", ***Dalton Trans***., 2010, **39**, 8161 – 8167.
6) P. Phuengphai, S. Youngme, P. Gamez and J. Reedijk, "Catalytic properties of a series of coordination networks: cyanosilylation of aldehydes catalyzed by Zn(II)-4,4′-bpy-carboxylato complexes*", **Dalton Trans**,* 2010, **39** (34), 7936-7942.
7) N. Wannarit, N. Chaichit, C. Pakawatchai, and S. Youngme, "New trinuclear carbonato-bridged copper(II) complexes:synthesis, crystal structure, and spectroscopic properties" ***Russ. J. Coord. Chem.,*** 2010, **36**, (10), 778–785.
8) J. Boonmak, M. Nakano, S. Youngme, "Structural diversity and magnetic properties in 1D and 2D azido-bridged cobalt(II) complexes with 1,2-bis(2-pyridyl)ethylene" ***Dalton Trans.,*** 2011, **40**, 1254-1260.

9) J. Boonmak, M. Nakano, N. Chaichit, C. Pakawatchai, S. Youngme, "Spin Canting and Metamagnetism in 2D and 3D Cobalt(II) Coordination Networks with Alternating Double End-On and Double End-to-End Azido Bridges" ***Inorg. Chem.,*** 2011, **50**, 7324-7333.

10) N. Wannarit, K. Siriwong, N. Chaichit, S. Youngme, R. Costa, I.P.R. Moreira, F. Illas, "New series of triply-bridged dinuclear Cu(II) compounds: synthesis, crystal structure, magnetic properties and theoretical study" ***Inorg. Chem.,*** 2011, **50** (21), 10648–10659.

11) N. Wannarit, K. Siriwong, N. Chaichit, S. Youngme, " Multiple-Layer Heterometallic MnII-AgI Coordination Polymers Constructed from $[AgI_2(CN)_3]^-$ and $[AgI(CN)_2]^-$ Units " ***Transition Met. Chem.***, 2012, **37**, 79-84.

12) P. Phuengphai, S. Youngme, I. Mutikainen, P. Gamez, J. Reedijk, "A series of related 2D coordination polymers based on [copper(II)-4,4′-bpy-carboxylato] building blocks" ***Polyhedral***, 2012, **42**, 10-17.

Honor and Awards:

1) S. Youngme, CST Distinguished Chemist Award 2010 (Inorganic Chemistry)
2) S. Youngme, Excellent Researcher Award 2010: Gold Metal Researcher Award
3) P. Phuengphai , Professor Dr. Thab Neelanithi's Foundation Distinguished Dissertation Award in 2010
4) P. Phuengphai, Surindra Rajabhat University Researcher Distinguished Achievement Award in 2010
5) P. Phuengphai, Dissertation Graduate student Distinguished KKU Thesis Award in 2011
6) J. Boonmak, Merck-CST Distinguished Dissertation Award 2011 by The Chemical Society of Thailand under the Patronage of Her Royal Highness Princess Chulabhorn Mahidol.
7) J. Boonmak, Student Best Poster Award in the 12th International Conference on Molecule-Based Magnets, Beijing, China.
8) A. Cheansirisomboon "IUPAC Young Chemist Awards" supported by IUPAC, RSC and Bangkok Bank at 14th Asian Chemical Congress (ACC), Bangkok, Thailand.
9) N. Wannarit, The Best Outstanding Poster Presentation Award at PERCH-CIC congress VII, Pattaya, Chonburi, Thailand..

Presentations:

1) S. Youngme "Design of metal organic frameworks and their functions towards catalysis, anion-exchange and dynamic structural transformation"***Invited as a keynote lecture*** *at* at **Pure and**

Applied Chemistry International Conference(PACCON), Bangkok, Thailand. 5-7 January 2011.

2) S. Youngme "Frameworks of Zn^{II}-4,4′-bipyridine-carboxylate and M^{II}-2-aminopyrazine-sulfate (M^{II} = Co, Fe and Cd) and their functions toward catalysis, anion-exchange and dynamic behaviors" ***Invited as a keynote lecture*** *at* at 37th Congress on Science and Technology of Thailand, Bangkok, Thailand. 10-12 October 2011.
3) S. Youngme "Frameworks of Zn^{II}-4,4′-bipyridine-carboxylate and M^{II}-2-aminopyrazine-sulfate (M^{II} = Co, Fe and Cd) and their functions toward catalysis, anion-exchange and dynamic behaviors" ***Invited as a keynote lecture*** *at* at 3rd Asian Conference on Coordination Chemistry (3rd ACCC), New Delhi, India. 17-20 October 2011.
4) S. Youngme "Metal-Organic Frameworks and their Functional Toward Anion-exchange, Catalysis, Magnetism and Dynamic structural Transformation with Chromotropism" ***Invited as a keynote lecture*** *at* at The 4th International Conference on Science and Technology for Sustainable Development of the Greater Mekong Sub-region (4th STGMS), at Pullman Khon Kaen Raja Orchid Hotel, Khon Kaen, Thailand. 23-24 January 2012
5) P. Phuengphai, S. Youngme, J. Reedijk "Framework Engineering of Zn(II)/4,4'-bipy Porous Coordination Polymers and Carboxylate-regulator: Synthesis, Structures and Thermal properties" ***Poster presented*** *at the 33th Congress on Science and Technology of Thailand* ***(STT-33)***, 18-20 October 2007. Nakorn Sri Thammarat, Thailand.
6) P. Phuengphai, J. Reedijk and S. Youngme, "Framework Engineering of Zn(II)/4,4'-bpy Porous Coordination Polymers and Carboxylate-regulator; Synthesis, structures and thermal properties" ***Poster presented*** *at* The Royal Golden Jubilee Ph.d Program RGJ-Ph.D. Congress IX (RGJ-Ph.D IX), April 4-6, 2008, Jomtien Palm Beach Hotel and Resort, Chonburi, Thailand.
7) P. Phuengphai, S. Youngme, P. Gamez and J. Reedijk "Framework Engineering of Zn(II)/4,4'-bipy Porous Coordination Polymers and Carboxylate-regulator: Synthesis, Structures and Thermal properties". ***Poster presented*** *at the Holland Research School of Molecular Chemistry (HRSMC)*, 27 November 2008, Vrije University, Amsterdam, the Netherlands.
8) P. Phuengphai, S. Youngme, P. Gamez and J. Reedijk "Framework Engineering of Zn(II)/4,4'-bipy Porous Coordination Polymers and Carboxylate-regulator: Synthesis, Structures and Thermal properties" ***Oral presented*** *at the 10th Netherlands Catalysis and Chemistry Conference (NCCC)*, 2-4 March 2009, Noordwijkerhout, the Netherlands.
9) P. Phuengphai, S. Youngme, P. Gamez and J. Reedijk "Framework Engineering of Zn(II)/4,4'-bipy Porous Coordination Polymers and Carboxylate-regulator: Synthesis, Structures and Thermal properties" ***Poster presented*** *at the 1st Hybrid Materials Conference*, 14-19 March 2009, Tours, France.

10) P. Phuengphai, S. Youngme, P. Kongsaeree, C. Pakawatchai, N. Chaichit, S. J. Teat, P. Gamez and J. Reedijk, "Drastic steric effects from, respectively, a hydrogen, a methyl and an ethyl group on the coordination network of a zinc(II)–4,4'-bipyridine–carboxylato ternary system" ***Oral presented*** at *at the 33th Congress on Science and Technology of Thailand* ***(STT-35)***, 14-17 October 2009. Cholburi, Thailand.
11) P. Phuengphai, S. Youngme, P. Kongsaeree, C. Pakawatchai, N. Chaichit, S. J. Teat, P. Gamez and J. Reedijk, "Drastic steric effects from, respectively, a hydrogen, a methyl and an ethyl group on the coordination network of a zinc(II)–4,4'-bipyridine–carboxylato ternary system" ***Poster presented*** *the 2nd Asian Conference on Coordination Chemistry (2nd ACCC),* 1-4 November 2009. Nanjing University, Nanjing, China.
12) P. Phuengphai, S. Youngme, P. Gamez and J. Reedijk, "Anion Exchange and Catalytic Properties of a Series of Coordination Networks: Cyanosilylation of Aldehydes Catalyzed by Zn(II)-4,4'-bpy-carboxylato Complexes" ***Oral presented*** *the 2nd Pure and Applied Chemistry International Conference (2nd PACCON),* 21-23 January 2010. Ubonratchatani University, Ubonratchatani, Thailand.
13) P. Phuengphai, S. Youngme, P. Gamez and J. Reedijk, "Design of Metal Organic Frameworks (MOFs) and Their Functions Towards Catalysis and Anion-exchange" ***Oral presented*** *the 2nd Acadamic Conference (2nd SIFF),* 14-24 January 2010. Surindra Rajabhat University, Surin, Thailand.
14) J. Boonmak, "Structural diversity, dynamic structural transformations and magnetic properties of inorganic-organic hybrid frameworks containing aminopyrazine spacer" ***Invited lecture*** *at CST award in Pure and Applied Chemistry International Conferences 2012 (PACCON 2012),* Chiang Mai, Thailand. January 11-13, 2012
15) J. Boonmak, M. Nakano, N. Chaichit, C. Pakawatchai, S. Youngme, "Spin canting and metamagnetism in 2D and 3D cobalt(II) coordination networks with alternating double end-on and double end-to-end azido bridges" ***Poster*** *presented at 14th Asian Chemical Congress (14ACC),* Bangkok, Thailand. September 5-8, 2011.
16) J. Boonmak, M. Nakano, N. Chaichit, C. Pakawatchai, S. Youngme, "Water-induced reversible structural phase transformation with chromotropism in metal supramolecular frameworks containing aminopyrazine and sulfate anions" ***Oral*** *presentation at NanoThailand 2010*, Thailand Science Park Convention Center (NSTDA) Pathumthani, Thailand. November 8 – 20, 2010.
17) J. Boonmak, M. Nakano, S. Youngme, "Structural diversity and magnetic properties in 1D and 2D azido-bridged Co(II) complexes with 1,2-bis(2-pyridyl)ethylene" ***Poster*** *presented at The Inaugural CU-IMS Joint Symposium: The Overseas Sokendai Lecture in Bangkok 2010*, Department of Chemistry, Faculty of Science, Chulalongkorn University. October 19–21, 2010.

18) J. Boonmak, M. Nakano, S. Youngme, "Structural diversity and magnetic properties in 1D and 2D azido-bridged Co(II) complexes with 1,2-bis(2-pyridyl)ethylene" ***Poster*** *presented at The 12th International Conference on Molecule-Based Magnets (ICMM12th),* Beijing, China. October 8-12, 2010.

19) J. Boonmak, N. Chaichit, C. Pakawatchai, G.A. van Albada, J. Reedijk, S. Youngme " Series of Copper(II) Coordination Polymers Containing Aminopyrazine and Different Carboxylato Bridges: Syntheses, Structures and Magnetic Properties" ***Poster*** *presented at The 59th Symposium on Coordination Chemistry of Japan (JSCC59),* Bunkyo-machi, Nagasaki-city, Nagasaki University, Japan. Sep. 25–27 2009.

20) J. Boonmak, N. Chaichit, C. Pakawatchai, M. Nakano, S. Seki, S. Youngme "Syntheses, Crystal Structures, and Magnetic Studies of Cobalt(II) Azido Coordination Networks Containing *N,N'*-Ditopic Spacers" ***Oral*** *presentation at JENESYS Programme 2009 General Meeting and Mini Symposium*, Institute for molecular science, Okazaki, Japan. July 31, 2009.

21) J. Boonmak, N. Chaichit, C. Pakawatchai, G.A. van Albada, J. Reedijk, S. Youngme "A Series of Copper(II) Coordination Polymers Containing Aminopyrazine and Different Carboxylato Bridges: Syntheses, Structures and Magnetic Properties" ***Poster*** *presented at the 6th PERCH-CIC Congress,* Chonburi, Thailand. 3–6 May 2009.

22) J. Boonmak, N. Chaichit, S. Youngme, "Metal-directed supramolecular assemblies and coordination polymer based on aminopyrazine with sulfate anions" ***Poster*** *presentation at RGJ-Ph.D. Congress X*, Jomtien Palm Beach Hotel&Resort, Pattaya, Chonburi, Thailand, Apr. 3 – 5, 2009.

23) J. Boonmak,N. Chaichit, S. Youngme "Copper coordination polymers containing aminopyrazine with various carboxylato bridges" ***Oral*** *presentation at 34th Congress on Science and Technology of Thailand*, Queen Sirikit National Convention Center, Bangkok, Thailand. Oct. 31 – Nov.2, 2008.

24) N. Wannarit, S. Youngme**,** K. Siriwong, R. Costa, I.P.R. Moreira, and F. Illas "Magnetostructural correlations in ferromagnetic triply bridged dinuclear Cu(II) compounds containing carboxylato and hydroxo bridges Inorganic chemistry". ***Poster*** *presented* at PERCH-CIC congress VII, Pattaya, Chonburi, Thailand. 4-7 May 2011.

25) N. Wannarit, S. Youngme**,** K. Siriwong, R. Costa, I.P.R. Moreira, and F. Illas "Toward the Design of Ferromagnetic Molecular Complexes: Magnetostructural correlations in ferromagnetic triply bridged dinuclear Cu(II) compounds containing carboxylato and hydroxo bridges Inorganic chemistry". ***Poster*** *presented* at 14th Asian Chemical Congress (ACC), Bangkok, Thailand. 5-8 September 2011.